Glacier Surface Melt Modelling: Extending an Enhanced Temperature-Index Model to Fit the Surface Melt Under a Geotextile Cover

GEO 511 Master's Thesis

Author
Bogdan Dukic
13-701-297

Supervised by
Prof. Dr. Andreas Vieli

Faculty representative
Prof. Dr. Andreas Vieli

27.09.2023
Department of Geography, University of Zurich

Table of Contents

Abstract

In the context of global climate change, most glaciers on Earth are losing more mass through melt every year. The loss of glacier ice can lead to various problems on different scales. One crucial form of ice loss is surface melt. Understanding ice melt dynamics is important to be able to quantify the problems resulting from ice loss. Local ice melt mitigation strategies involve covering glaciers with specific materials. One among those materials is non-woven geotextile. Its effect on glacier ice surface melt has been researched only to some degree. This thesis aims to close the gap between glacier ice surface modelling and the cover of glacier ice with non-woven geotextile. On the Morteratsch glacier in southeastern Switzerland, data was gathered over a time period of two weeks. Based on that data, a slightly adapted and, for this thesis, improved version of an already existent empirical glacier surface melt model was generated and calibrated within MS Excel. Aside from the empirical model, a physical model was generated in the same software. Due to some limitations, the second model is not fully physical and therefore it had to be calibrated as well. After the successful calibration of the physical model, a calibration of the terms in the physical model was done to scale down to different energy terms responsible for surface melt to fit the measured melt under the covered ice. Based on those newly calibrated factors, a translation method from the physical back to the empirical model was proposed. That newly resulting model is an extension of the prior empirical model. The newly formulated model was extended in time to be validated with various approaches. While the conceptual approach to formulating such a model is viable, it is argued that the actual approach was hindered due to some shortcomings. At the end, the viability of such glacier cover projects is discussed briefly to contextualize the attempted formulation of the extended glacier surface melt model under the conditions of two layers of non-woven geotextile on a glacier.

List of Figures

List of Tables

Acknowledgments

1. Introduction

1.1 Scientific Background

1.1.1 Climate Change & Glacier Melt

Climate change has impacted humans, other living creatures, and nature as a whole negatively. That also includes the cryosphere. Glaciers and their ice loss can be named as one example feature which is, according to the IPCC, caused by climate change with high confidence. Glacier ice loss takes place in the form of glacier melt which is described as a process where solid ice is turned into liquid water (Silwal *et al.*, 2023). It is also considered by the IPCC that humans are very likely the most central reason for glacier retreat through the melt. Consequently, it is likely that resources dependent on glacier ice melt such as freshwater, especially during periods of low precipitation (medium confidence) will become scarcer (UNEP, 2023). Especially in more arid mountainous regions such as the Andes, glaciers and their continuous melt guarantee the availability of fresh water for various purposes on which numerous humans depend (Fuchs, Asoaka and Kazama, 2013). However, not just the water resulting from ice melt can be considered as a resource in the context of glaciers and resources. Aside from the usage of water for hydropower and irrigation systems, glacier ice can be considered as a resource for cooling. Further, glaciers serve as a tourist attraction on which locals might depend financially, simply as an attraction or for the use of skiing slopes (Fuchs, Asoaka and Kamaza, 2013; Senese et al., 2020; Oerlemans, Haag and Keller, 2017). Specifically in the context of skiing slopes, glacier ice loss can lead to the abandonment of ski tracks (Olefs and Fischer, 2008). Aside from glaciers being considered solely a resource, they can also be regarded as an asset. In the context of natural hazards, glaciers are more likely to cause damage while losing ice mass through loss of slope stability and consequent rock fall, glacier lake outburst floods or even ice avalanches through ice instability (Oerlemans *et al.*, 1998). Even far away, glacier ice loss has an immense impact on human lives through the rise of the sea level (MacDougall, Wheler and Flowers, 2011). In an even broader context, or rather on a different spatial scale, glacier ice holds a crucial influence on hydrology and meteorology (Hock, 2005). Numerous other authors state a combination of the aforementioned implications of glacier ice loss and its effects on humans (Zekollari, Fürst and Huybrechts, 2014; Oerlemans, Haag and Keller, 2017; Silwal *et al.*, 2023).

For these reasons, there is a great interest in being able to estimate glacier melt. In the context of estimation, it was already proposed back in the 18th century that glacier melt and climate are interconnected. About a century later, further insights came that temperature is relevant to glacier melt. At the beginning of the 20th century, it was also recognized that solar radiation was the most crucial driver, while wind plays an important role as well (Hock, 2005). These were among the foundations for glacier melt estimations. Melt, however, affects glaciers in various ways and in different time scales. Surface melt followed by run-off is immediate while the shape of the glacier as well as its area and volume can be perceived as somewhat more delayed (Oerlemans *et al.*, 1998).

1.1.2 Glacier Surface Melt Models

When it comes to surface melt specifically, which can be described as a melt based on the glacier-atmosphere interface, modelling can be distinguished into two main approaches (Pellicciotti *et al.*, 2014). These are physically based or index-based (Pellicciotti *et al.*, 2014). The index-based models can be understood as simplifications of the physical models (Pellicciotti *et al.*, 2005). The index-based models are generally based solely on air temperature as input data to calculate the surface melt since they are based on the assumption that air temperature above for instance 0° C causes ice melt (Carenzo *et al.*, 2009). The physical models on the other hand require much more input data such as "… relative humidity, wind speed and direction, incoming and reflected shortwave radiation and incoming and outgoing longwave radiation, as well as knowledge of the surface properties such as

aerodynamic surface roughness.". To bridge the gap between those two modelling approaches, intermediate models have been suggested to increase the model accuracy of index-based models while still keeping a low data requirement (Pelicciotti *et al.*, 2014).

For simplification purposes, abbreviations will be used for the various models and model types. For the first distinguishment, the physical models, also known as energy balance models, will be abbreviated with "EBM". As for the index-based models, which are also known as temperature index models, those will be abbreviated with "TIM" (MacDougall, Wheler and Flowers, 2011).

1.1.2.1 Temperature Index Models

When it comes to the TIMs, even though the original one, also called the classical temperature index model "CTIM", requires only temperature as input data, more distinguished versions of it exist today. One TIM version, which was defined back in 1999 by Hock which can be abbreviated as HTIM, includes a distinction between snow and ice as potential melt surfaces as well as a "… potential direct shortwave radiation.". However, that potential direct shortwave radiation is a variable dependent on numerous factors. Another difficulty arises with this version as the model structure implies the multiplication of temperature-dependent terms and radiation-dependent terms (Pelicciotti *et al.*, 2005; MacDougall, Wheler and Flowers, 2011).

Perhaps the most renowned adaptation of the TIM is by Pelicciotti et al. from 2005. It is arguably one of the most crucial works in that field when it comes to glacier surface melt modelling as numerous others have cited the named journal article (Carenzo et al., 2009, 2016; MacDougall and Flowers, 2011; Fuchs, Asoaka and Kazama, 2013; Pelicciotti et al., 2014; Matthews et al., 2015; Zekollari et al., 2022; Silwal et al., 2023). This is abbreviated in literature as PTIM (MacDougall, Wheler and Flowers, 2011). However, in this thesis, this version will be abbreviated as ePDH. The abbreviation stands for "enhanced positive degree-hour". Reasons for that are that for one, TIMs can also be considered degree models (Hock, 2005) and that an adapted version of that specific one will be crucial for this thesis. Further, the variation is hourly and not daily as in the positive degree-day (PDD). But to be able to understand the adaptation from the original, the suggested abbreviation makes more sense. There will be more on that in the methodology chapter.

While the HTIM includes solar radiation as one of the factors relevant for melt, it is more of a conceptual inclusion. The PTIM includes solar radiation as data in the model. Thus, compared to the initial TIM which only requires temperature as data input, the PTIM requires solar radiation as well. Thus, model complexity and data requirements rise (Pelicciotti *et al.*, 2005; MacDougall, Wheler and Flowers, 2011). When it comes to performance, PTIM outperforms other TIMs since it accounts for, but separates temperature-dependent melt factors from temperature-independent ones thus reducing the modelled effect on glacier ice melt solely by temperature (Pelicciotti *et al.*, 2005).

Further fine-tuning attempts of various TIMs have been done such as versions of the HTIM being adapted to various weather types to make the melt factors more flexible (Matthews *et al.*, 2015), a comparative study of the three mentioned TIMs (CTIM, HTIM, PTIM or ePDD) (Silwal *et al.*, 2023), an adaptation of the eTIM to account for debris cover on glaciers (Carenzo *et al.*, 2016) or the potential to transfer the model parameters in space and time (Carenzo *et al.*, 2009) among others. Overall, one can conclude that TIMs are defined in various ways depending on data availability, required complexity, and required level of abstraction of reality.

1.1.2.2 Energy Balance Models

Moving away from the index or degree-based models, this section introduces the counterpart to it, the physical energy balance models. It is noteworthy that, these models are also called surface mass balance models occasionally (Zekollari, Fürst and Huybrechts, 2014).

The main difference between the aforementioned TIMs and EBMs as mentioned before is the amount of data required to model the surface melt. However, with more data, there is also a potential to be more accurate with the modelling of the surface melt (Zekollari, Fürst and Huybrechts, 2014). One might wonder why research does not always depend on EBMs if their results are potentially more accurate if the only increasing cost is more data. In reality, data availability to that extent is rare, and even if so, then only available for shorter time periods. Plus, if one wants to acquire all the required data, it is connected to a lot of equipment, maintenance, and potential malfunctioning of the instruments which can be regarded as further costs. To reduce those costs to some degree, the use of EBMs occasionally tends to use other data available such as meteorological data. Even though this represents a simplification, the results have been satisfying (Hock, 2005).

The structure of EBMs varies to some degree as it did for the TIMs. However, there tends to be a consensus on the base of it. The potential total melt energy in the system of a glacier surface consists of the following components: incoming shortwave radiation, outgoing shortwave radiation, incoming longwave radiation, outgoing longwave radiation, sensible heat flux, and the latent heat flux (Hock, 2005; Oerlemans, 2000). The energy available for glacier ice/snow melt can then also be translated into a water equivalent (Hock, 2005).

Other sources of energy may include rain (Hock, 2005; MacDougall and Flowers, 2011) or subsurface absorption or release of energy when snow or ice changes temperature (MacDougall and Flowers, 2011; MacDougall, Wheler and Flowers, 2011). Simplifications of the model are also possible such as connecting the longwave radiation and the turbulent heat fluxes (sensible and latent), since those are all temperature-dependent (Zekollari, Fürst and Huybrechts, 2014).

1.1.3 Melt Reduction Strategies

Being aware of the possibilities to model glacier surface melt is important. However, just knowing the amount of melting ice to a specific degree of accuracy will not save the glaciers from melting away. All the aforementioned problems such as water scarcity, diminishing tourism, natural hazards, rising sea levels, or the impact on hydrology and meteorology remain. Thus, it is crucial to also research approaches to mitigate glacier melt. Aside from reducing greenhouse gas emissions (UNEP, 2023), artificial mitigation strategies constitute a potential approach to mitigating glacier ice loss. Such approaches are taken and the overall effect of it is being researched. This involves mainly different types of cover on a glacier such as "… foam, sawdust, wood chips, and textiles…" (Xie *et al.*, 2023). Those covers are applied to glaciers and/or snowpacks during the season when no snowfall is expected and removed for snowfall season to enable snow to accumulate on the surfaces (Huss *et al.*, 2021). Other materials involve artificial snow (Oerlemans, Haag and Keller, 2017) or nanofiber sheets (Liu *et al.*, 2022). Various approaches to evaluate the effect exist. While numerous studies evaluate the results in situ, where the covering materials are set up (Oerlemans, Haag and Keller, 2017; Senese *et al.*, 2020; Huss *et al.*, 2021; Liu *et al.*, 2022; Xie *et al.*, 2023), some approaches take the covering materials to the laboratory to examine their overall melt reduction effect (Skogsberg and Lundberg, 2005).

Among the more prominent and more researched materials to cover glaciers for such a cause are sawdust, and even more so geotextiles (Skogsberg and Lundberg, 2005; Senese *et al.*, 2020; Huss *et al.*, 2021; Liu *et al.*, 2022; Xie *et al.*, 2023). Especially, the geotextile has received more attention in recent years.

Considering that shortwave radiation was found to be the most important driver of ice melt (Hock, 2005), most of those fabrics are aimed at either increasing the albedo or reducing the thermal conductivity and thus the transfer of energy available for melt (Senese *et al.*, 2020; Huss *et al.*, 2021). Reduction effects varied between 15 % and 96 % (Olefs and Fischer, 2008; Huss *et al.*, 2021; Xie *et al.*,

2023). The lowest melt reduction results were documented in China compared to the other studies in other regions (Parbak Mountains or Alps) (Xie *et al.*, 2023).

Yet, while the results seem promising, there are major setbacks to this approach which is the reason why not all glaciers are covered yet by now. The reason behind that is feasibility and involves financial aspects, accessibility of glaciers, material stability issues, and further (Senese *et al.*, 2020; Liu *et al.*, 2022; Xie *et al.*, 2023). Why feasibility is an issue, is addressed in chapter 5.6 of this thesis.

1.2 Rationale & Research Questions

1.2.1 Research Gap

After having looked at the connection between climate change and glacier ice loss, the implications for humans and nature, methods and approaches to model glacier ice melt as well as human-made mitigation strategies against glacier ice melt, this section emphasizes on an existent research gap which constitutes the rationale for this thesis.

While there are mitigation approaches against glacier ice melt as well as evaluations of their efficiency, all those evaluations were in-situ based, meaning that the cover materials had to be set up and left in place for some time, before one was able to estimate the overall reduction effect on ice melt (Skogsberg and Lundberg, 2005; Oerlemans, Haag and Keller, 2017; Senese *et al.*, 2020; Huss *et al.*, 2021; Liu *et al.*, 2022; Xie *et al.*, 2023). So far, no model exists to model and thus estimate glacier ice melt for cases when glaciers are covered with a specific material aside from one exception. That exception consists of a natural debris cover being accounted for by a TIM with an extension for the debris cover (Carenzo *et al.*, 2016). Aside from that, no model to estimate glacier ice melt under conditions of human-made covers on the glaciers is known. This constitutes an arguably immense gap since these kinds of cover projects can be very expensive, especially for the prominent case of geotextile (Senese *et al.*, 2020; Xie *et al.*, 2023). Not knowing the efficiency of such a cover on a specific glacier connected with the huge costs leaves an immense hurdle for policymakers to initialize such glacier ice protection projects, so it is argued. Having a model, a tool so to speak, to estimate the efficiency of cover projects would make them more transparent. So, the willingness to invest money into this kind of plans might be increased.

1.2.2 Research Questions and Hypotheses

To start closing the existing research gap, this thesis aims to formulate a model to estimate glacier surface melt when the glacier is covered with geotextile. For that purpose, the ePDH model serves as a base (Pellicciotti *et al.*, 2005). The reason to use ePDH for that purpose instead of some sort of an EBM is that the ePDH has much smaller data requirements and complexity (Pellicciotti *et al.*, 2005, 2014; Matthews *et al.*, 2015; Zekollari *et al.*, 2022). This would guarantee at least some transparency and an easier understanding of the model for non-academic users who might not have profound expertise in glacier surface melt modelling. Consequently, potential use would increase. The concrete intention is to scale down the two terms in the ePDH, namely the shortwave radiation factor and the positive degree hours temperature factor to fit the melt of glacier ice under geotextile cover (Pellicciotti *et al.*, 2005).

The following two research questions were formulated:

1. How much can glacier ice melt be reduced when covering the glacier ice with two layers of non-woven geotextile?

2. How much do the shortwave radiation factor and the positive degree hours temperature factor in the ePDH need to be reduced respectively to correspond to the actual melt of glacier ice under two layers of geotextile for a point scale location?

Concerning the two research questions, for each one a hypothesis was formulated:

1. The geotextile will achieve an estimated reduction of glacier ice melt of between 50 % and 70 % as compared to the surrounding clean ice (Senese *et al.*, 2020; Huss *et al.*, 2021; Liu *et al.*, 2022; Xie *et al.*, 2023)**.**

2. The shortwave radiation factor will have to be reduced more than the positive degree hours melt factor since shortwave radiation is the biggest source of energy for melt on a glacier and with the cover, the albedo is being increased and the possibility for shortwave light to reach the ice directly is being reduced.

2. Study Site

The site at which the data was acquired, is the Morteratsch glacier, or in the local Romansh language, Vadret da Morteratsch. It is located in the south-east of Switzerland in the upper part of the Engadin valley. It is situated on a northern slope and thus is flowing mostly in a south-north direction. The glacier itself is embedded within a glacier complex with the same name. That complex consists of the Morteratsch Glacier and the Pers glacier (Romansh: Vadret Pers). Before 2015, those two glaciers were connected. After 2015, they were disconnected and therefore act independently (Zekollari and Huybrechts, 2018).

The geometry and mass balance of the Morteratsch glacier complex used to be complicated due to a confluence of multiple glaciers (Klok and Oerlemans, 2002). However, since the glaciers are more distinct by now, it might open up more distinct results as well.
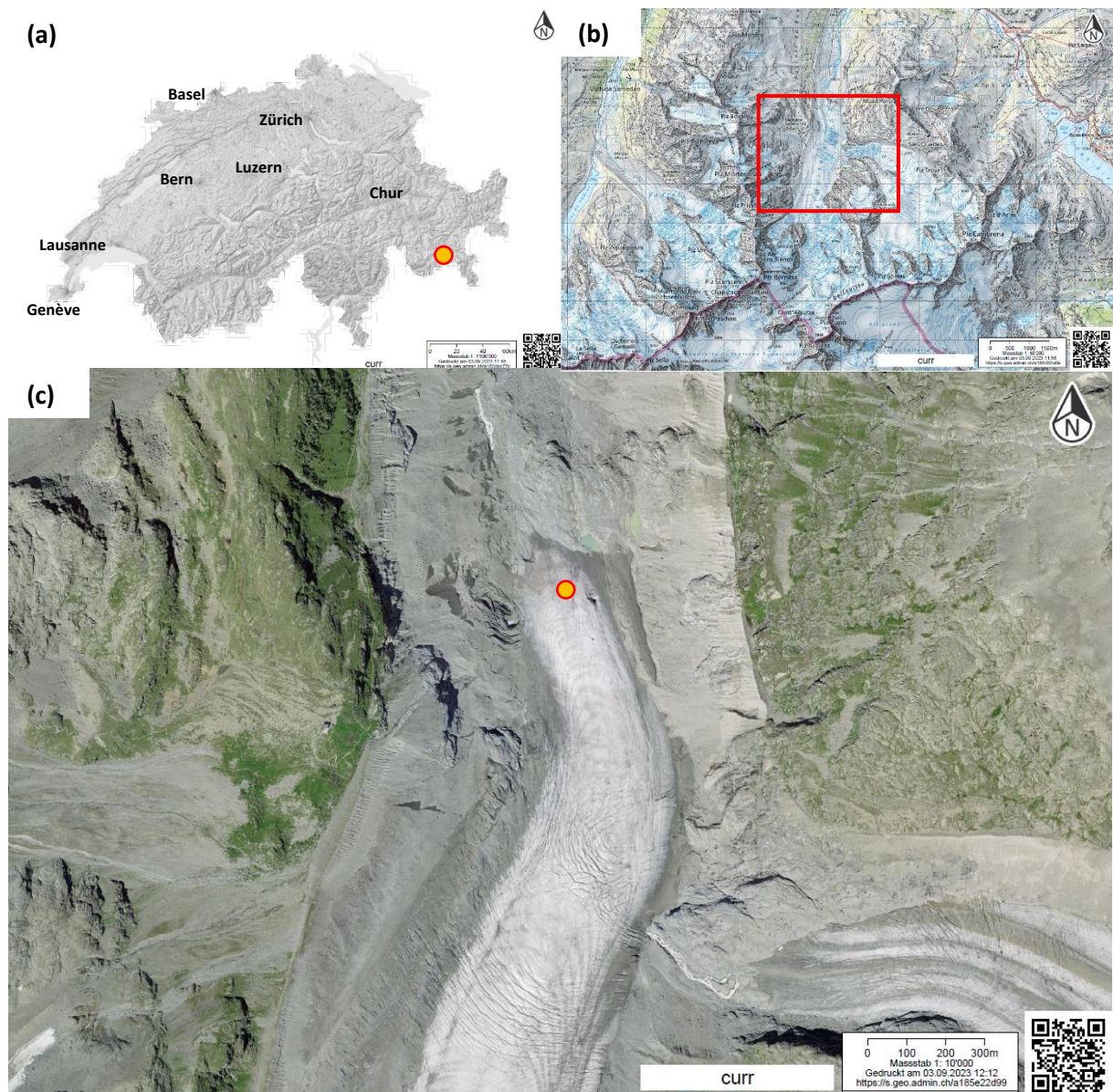
Figure 1: (a) Grey-shaded relief map of Switzerland and the location of the Morteratsch glacier in the orange dot, (b) map of the location of the glacier with a red rectangle showing the location of (c), an arial image of the glacier with an orange dot showing the location of the deployment.

The approximate location of the study site is about N: 4625124, E: 00955977 (LV95). The elevation is at about 2'160 m.a.s.l. The slope gradient is at about 10° and exposition is at about 340° (N:0°, E:90°, S:180°, W:270°). Different factors influenced the choice of location. Accessibility was important as well as security. Going longer distances on the glacier reduces the accessibility and increases the risk of crevasses. Next, that area was rather flat, therefore the covers could be placed easily and stood well on their spot. Further, at the end of the tongue, the glacier ablation is usually the biggest, which would enhance the difference in melt rates of covered and open areas thus also increasing the understanding of the processes at hand (Liu *et al.*, 2022). What is noteworthy, is that the ice at the time of measurement was rather dirty. It is assumed that this was dust that was blown onto the glacier from the Sahara which is not unusual for the valley of Engadin to occur. This is important since the surface properties have been changed which influences the surface melt. The dust density on the ice varied over time.

Figure 2: Picture of the glacier and the measurement deployment taken on 07.09.2022 at 10:20. The deposition of assumed Sahara dust is well visible.

3. Methodology

Since the entire methodology is a longer sequence of different steps to reach the results answering the two research questions, it is helpful to have an overview of the entire approach. The entire methodological approach to modelling is displayed in Figure 3. It is important to remember that there are various models which are capable of estimating glacier surface melt such as the ePDH or the physical and thus more complex EBM (Oerlemans, 2000; Hock, 2005; Pellicciotti *et al.*, 2005; Carenzo *et al.*, 2009; MacDougall, Wheler and Flowers, 2011; Fuchs, Asoaka and Kamaza, 2013) and that there is geotextile among the cover types to reduce glacier surface melt (Olefs and Fischer, 2008; Senese *et al.*, 2020; Liu *et al.*, 2022; Xie *et al.*, 2023).
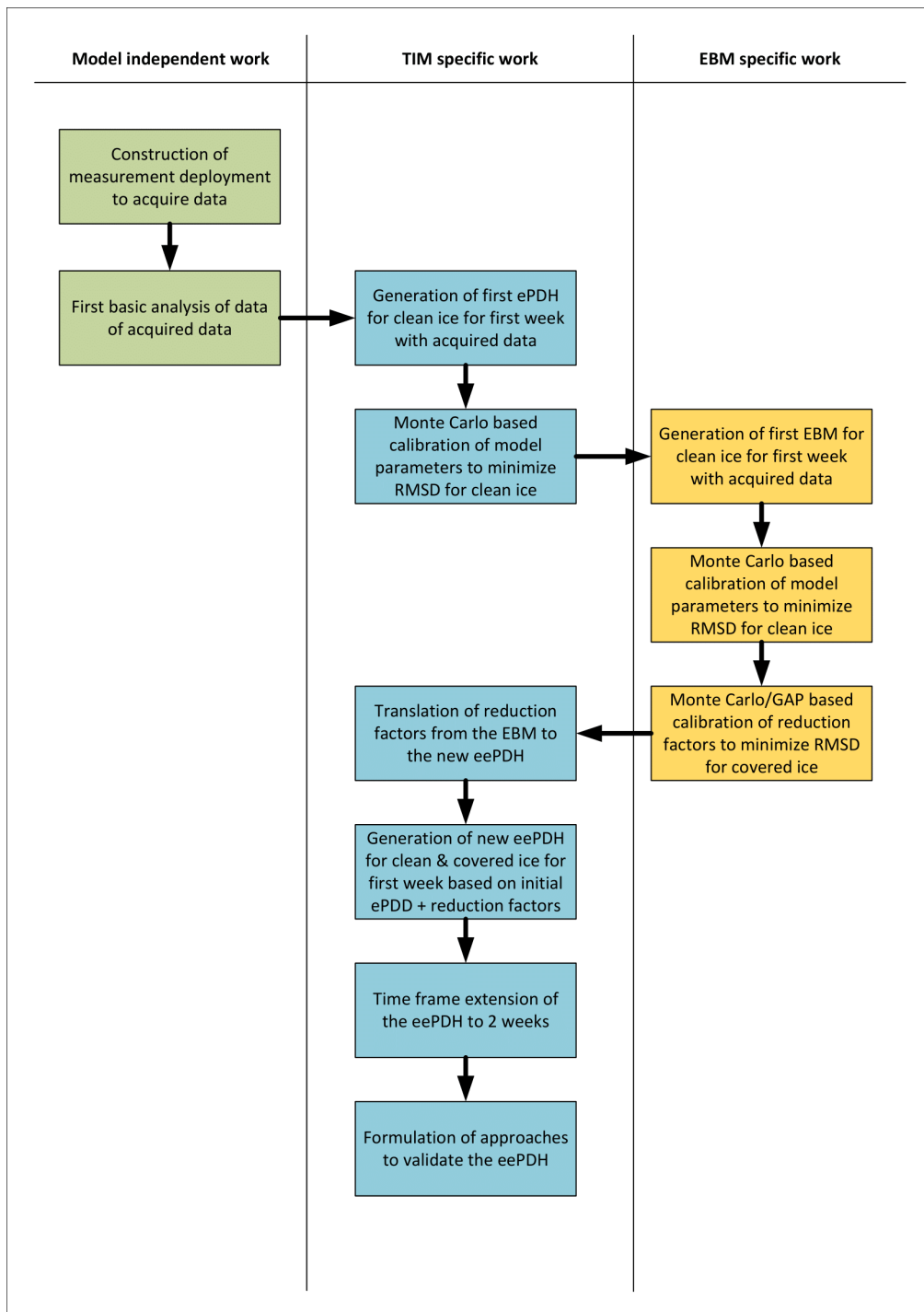
Figure 3: Display of the entire methodology of the modelling process.

9

3.1 Model Independent Work

3.1.1 Deployment and instruments

As displayed in Figure 3, the first step to answering the two research questions is to acquire the required data in the field of the study site. For that, an appropriate deployment is needed. This chapter introduces that deployment together with everything necessary to acquire the data needed. At the end of this subchapter, Figure 4 displays the entire deployment graphically.

Since the aim of this thesis is to find accurate factors to reduce the two terms in the ePDH when the glacier is covered with geotextile, the first thing required is geotextile to cover the glacier. For that purpose, a non-woven geotextile was used. Non-woven means that the production of the material is based on "… bonding materials together, either through chemical processes or heat, needle punching or other methods, which allows for better drainage." (Senese *et al.*, 2020). The source material of the cover is polypropylene. It was needle punctured and later processed with heat. The surface area-dependent weight varies between 144 and 198 g/cm2. More technical details can be found in the product's technical supplement (Geoproduct, 2021). Non-woven geotextile is more popular for the application of glacier cover as compared to the woven one due to "… excellent properties such as lightweight, low cost, corrosion resistance, anti-filtering, drainage, isolation, enhancement, and more." (Xie *et al.*, 2023).

In this deployment, this non-woven geotextile was used to cover two areas. One area covered one square meter (1 meter x 1 meter) while the other covered four square meters (2 meters x 2 meters). Both areas were covered with a double layer of geotextile since a double layer has a notable increase in the effect of reducing ice surface melt as compared to a single one. A third layer on the other hand would not increase the reduction effect much more (Olefs and Fischer, 2008). Each cover area got a letter assigned to it to be able to distinguish them. The one with one square meter area covered is "S" for the small cover, and the four square meter one is "B" for the big cover (this nomenclature will be kept throughout this entire thesis).

Since non-woven geotextile is capable of absorbing water which then potentially freezes, it has a good hold on the glacier. To further stabilize the cover though, rocks lying on the glacier were put on each of the corners of the covers (Senese *et al.*, 2020). It was attempted to take rocks with a brighter colour, since their assumed higher albedo would lead to them less heating up and thus having a smaller effect onto the cover through their also respectively smaller longwave eradiation. Depictions of the cover placements can be found in Figures 5 & 6.

Next, it is necessary to be able to quantify the surface melt on the glacier. To achieve this, ablation stakes were used. Those were put into drilled holes in the glacier before the official measurements began. To measure the surface melt of the ice with ablation stakes, one uses an ablation disk which is placed on the ground around an ablation stake until it is flat on the ground. Then, the distance from the ablation disk to the top of the respective ablation stake is measured. The more melt occurs with time, the greater that distance becomes (Olefs and Fischer, 2008; Senese *et al.*, 2020; Liu *et al.*, 2022).

A total of four ablation stakes were used in the deployment. One was put in the middle of S to measure the ablation under the geotextile. Three more were put into the surrounding clean ice. One was put about a 4m slope upwards from S, one was about 3m to the right of S when facing upwards the slope, and one was put about a 3m slope downwards from S. The stake at the cover is named S, when it comes to measured melt underneath the cover. The other three were named R1, R2 & and R3 respectively in that order and stand for references 1, 2, and 3.

Aside from the ablation stakes, temperature sensors were used in various locations of the already described parts of the deployment. Those temperature sensors are called iButtons. They were programmed to measure the temperature at an hourly rate at each full hour. There are three different locations at which those sensors were positioned. The first one is on B. On B, a total of nine iButtons were deployed. Those are distinguished by location and height above the surface. There was a total of three groups of them on B. The first group was located in the upper left corner of B when facing uphill. The second group was exactly in the centre of B. The final group was located in the middle of the lower part of B. Each of the groups of three iButtons were placed underneath radiation shields. There were seven radiation shield layers. The first iButton was taped underneath the 2nd shield, the second was taped underneath the 4th shield, and the final one underneath the 6th shield (always from seen from above) and a final layer of radiation shields was under the lowest iButton. The radiation shields again were placed on top of beverage cartons which were cut in half to elevate the iButtons from the surface of the ice. The beverage cartons were taped onto the geotextile cover from the inside of the pack to not influence the cover more than necessary. The reason for the elevation of the sensors further above the surface is that there is the assumption that all surplus energy (+0° C) present at the glacier surface is used to melt the glacier (Hock, 2005). The reason for deploying the iButtons is to see if there is a gradient above the cover in some way. More of that is displayed in Figure 5.

The next group of iButtons was placed above S. The concept of using three iButtons per radiation shield applies here in the same way as for B. The sole difference is only in how the radiation shield is fixed above the geotextile. As mentioned above, S has an ablation stake in the middle of it. The radiation shield was fixed on the stake, circa 15 cm above the surface. Figure 5 shows what it looked like. The reason for the placement of these iButtons is the same as for B.

The last group of iButtons was fixed onto stake S. It was done so with tape at distances of 10 cm. The first iButton was deep in the ice and the last one was closer to the surface. Measuring those temperatures was done to see if the temperature in the ice was effectively 0° C or if the stake had perhaps some warming effect which could further increase the melt.

The core part of the deployment consists of the automatic weather station, which in literature is abbreviated with AWS (Pellicciotti *et al.*, 2005; Carenzo *et al.*, 2009; MacDougall, Wheler and Flowers, 2011; Oerlemans, Haag and Keller, 2017; Senese *et al.*, 2020). In the case of this thesis, it will be abbreviated by solely WS, as for weather station.

The WS was positioned about 6 m downhill from B. The exact location of the WS was chosen for a few reasons. First, since the glacier is facing north and is located in the northern hemisphere, light from the sun also comes from a slightly southward direction. If the WS was placed uphill (further south), there would be a possibility that the WS casts a shadow onto the covers, thus falsifying the results to some degree. With that the chosen location, it could also be positioned closer to the rest of the deployment without any risks of casting a shadow on it. Finally, since the instruments are on a metal bar, they are some distance above the ground. With the station being further downhill, the instruments are about at the same height as the rest of the deployment initially, thus potentially reducing elevation-dependent differences in data.

The WS was equipped with a total of five instruments fixed onto a metal bar. Those involve the Davis Cup Anemometer (measuring wind speed, wind gusts and wind direction), 2 PYR Solar Radiation sensors, one facing straight to the sky, the other facing vertically down (measuring shortwave radiation from the sun and the reflected proportion from the ice), an ECRN-100 Precipitation gauge (measuring precipitation) and a VP-4 Humidity/Temp/Barometer (measuring relative humidity, air temperature and air pressure). With that, most of the data necessary for the generation of an EBM was present except for measurements of longwave radiation which was approximated as will be explained later

(Oerlemans, 2000; Hock, 2005; Pellicciotti *et al.*, 2005; MacDougall, Wheler and Flowers, 2011). The presence of required data applies even more so for the ePDH, which requires solely air temperature, incoming shortwave radiation, and surface albedo or reflected shortwave radiation (Pellicciotti *et al.*, 2005; Carenzo *et al.*, 2009; MacDougall, Wheler and Flowers, 2011). The measurements of all instruments from the WS were also programmed to work at an hourly rate for each full hour. A picture of the WS is shown in Figure 2.

This all defines the deployment, as it was set. It is noteworthy that all automatic measurements took place every full hour. This was done to be able to measure daily variations of the melt, which would increase the understanding of physical processes taking place as melt occurs under the cover, yet the amount of data would be manageable.

While part of the deployment, mainly the WS, was set up already on 05.09.2022, the official start of the entire deployment was on 06.09.2022 at 16:00. The final timestep of data acquisition was exactly two weeks later, on 20.09.2022 at 16:00. So, a total of two weeks of hourly data from the automatic measurement devices is available for this thesis.

A significant problem was discovered after returning to the site for the final measurements. The weather station was extremely tilted, rotated, and ran out of battery. Thus, the measurements only go until 16.09.2022. Thus, data for the second week, which was supposed to be used for validation of the modelling could not be done anymore with the data from the WS. Further, the covers were blown off to some degree. B was blown off and the radiation shields were not on the cover anymore. S was blown off heavily. There was especially barely any cover on the lower side. However, due to the ablation stake, the middle part was seemingly covered for most of the time.
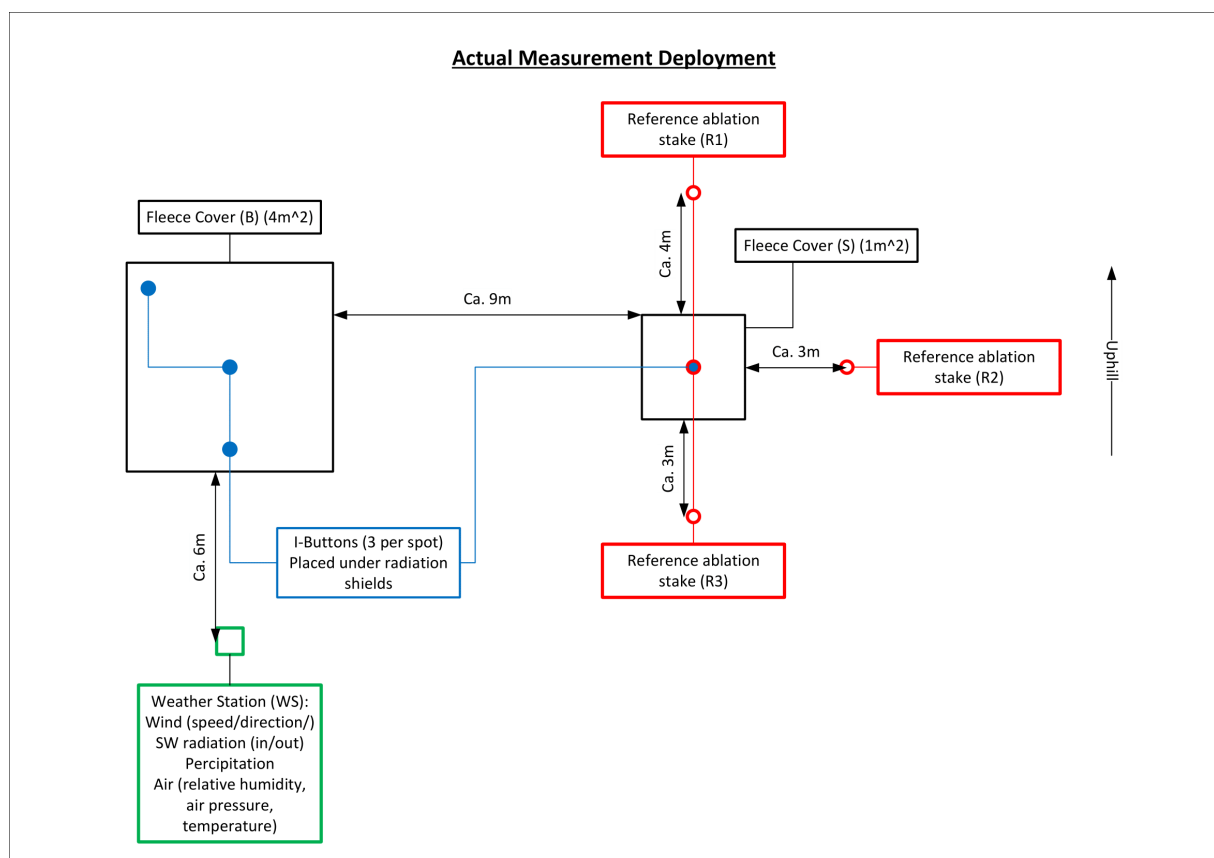
Figure 4: Graphic illustration of the deployment as described in chapter 3.1.
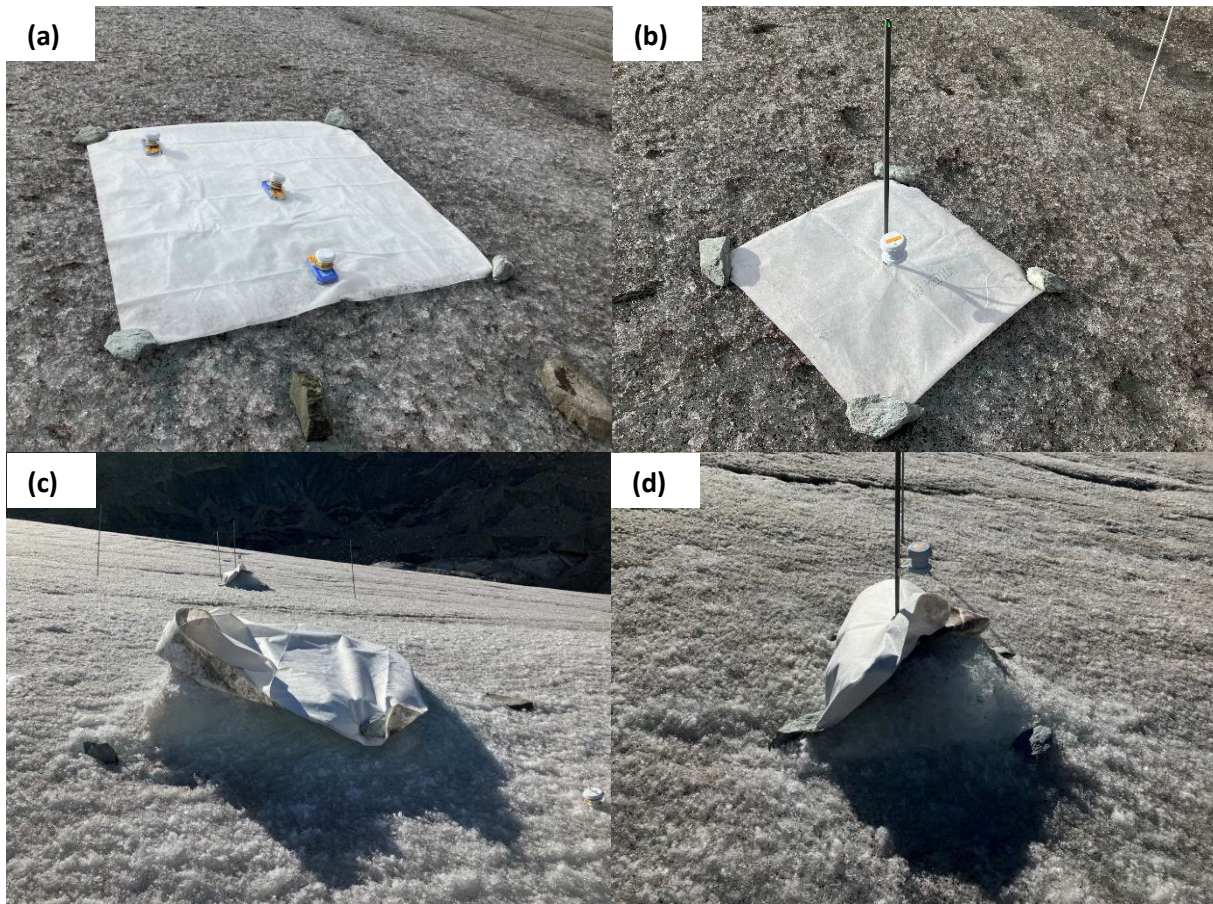
Figure 5: B (a) & S (b) moments after the geotextile covers were set up (07.09.2022, 10:20). (c) & (d) show the same two covers B & S after returning to the site for the final measurement (20.09.2022, 15:56).

For the second week of modelling, it was important to have air temperature and shortwave radiation. For this, data was used from another weather station. More on that will be explained later.

3.1.2 Manual Data Acquisition Through Field Work

This section involves the description of all the data acquired which was not possible to acquire with automatic devices. While building the deployment can also be considered manual work, the instruments used to record the data were automated in the previous section. This subchapter deals with data that could not be acquired by instruments measuring automatically throughout the entirety of the sampling period

The first part of manual measurements involves location measurements. Those are the coordinates (LV95), the altitude above sea level, the slope gradient, and the exposition aspect. This was done for WS, B, S, R1, R2 and R3 respectively. The coordinates as well as the elevation were measured with a handheld GPS. The slope gradient and the exposition aspect were measured with an inclinometer. All this data was measured at the beginning of the entirety of the two-week measurement period as well as at the end of it to double-check if the measurements taken were the same in the end. Each of the measurements was taken multiple times (between five and ten) and the median of the measurements was taken to make sure that simple measurement blunders were kept as low as possible (Pellicciotti *et al.*, 2005; Olefs and Fischer, 2008; Carenzo *et al.*, 2009; Senese *et al.*, 2020).

Aside from that, the ablation for all four ablation stakes had to be measured and noted (Pellicciotti *et al.*, 2005; Olefs and Fischer, 2008; Carenzo *et al.*, 2009; Senese *et al.*, 2020; Liu *et al.*, 2022; Xie *et al.*, 2023). Analogue to the location measurements, the ablation measurements were also taken multiple times and the median was taken to reduce measurement blunders. That is why the ablation disk was

13

always placed so that it was only touching the side of the stake which faced upslope. Then, the ruler was set to face 90° sideways from the upward slope and held as close as possible to the ablation stake side facing upwards to keep it as straight as can be. Measurements were taken at about 5-7 times per stake and measurement timeslot. Those measurements were taken twice a day, shortly after 10:00 and 16:00 for the first week aside from 06.09.2022 where it was done only in the afternoon after 16:00. In the last week it was done only for the final measurement on 20.09.2022 after 16:00.

The last of the manual measurements involves the albedo. This was measured with a handheld albedometer (Apogee Albedometer) for B, S, R1, R2, and R3. That device measures the incoming shortwave radiation in the sky as well as the reflected part of the shortwave radiation from the ground in the wavelengths of 0.35 – 2.8 μm. Based on that, it calculates the albedo which is defined as follows (Hock, 2005):

$$\alpha = \frac{SWout}{SWin} \tag{1}$$

Those measurements were taken multiple times as well. For each of the five measurement spots, the albedo was measured from four different sides (E, S, W, N) always in that order. Again, if the variability of the results was too high, another four measurements were taken. That was repeated until the results were somewhat stable. Thus, the number of measurements per location varied between four and twelve. Analogue to the ablation measurements, the albedo measurements were taken in the same session. The two main reasons for the variable measurements were clouds passing by reducing the *SWin* and *SWout* as well as the high sensitivity of the instrument being easily affected by the height above the ground and the angle of the instrument relative to the ice surface.

Figure 6: Measurements with the handheld albedometer. Photo by Anna Czerniejewska (20.09.2022, 16:11).

3.1.3 Primary Data Analysis

While working in the field, some unforeseen things occurred which diminished the completeness of the data. First is that there seemed to be loose contact between the cable for the Davis Cup and the WS core piece which saves the measured data. This was the case from 10.09.2022, 18:00 until 13.09.2022, 16:00. That issue was solved later by inserting wind data from the same hours of the day from the previous days. The wind data is thus not fully real. This will raise the uncertainty of the entire modelling to some degree. However, it is assumed that the influence should be minor since wind data is similar over the measured period throughout each day with some random fluctuations.

Aside from that, it was realized that the WS was tilted multiple times during the measurement period. The reason for that is believed to be the metal bar holding the instruments which got heated up due to the intense sunlight and thus melted the surrounding ice it was placed in. The tilt always went in the direction of the flow of the glacier (downwards). Because of that the WS had to be repositioned twice during the first week to guarantee it was standing upright. The first repositioning took place at 10.09.2023, 16:55, where it was repositioned about 1m to the right of the initial position as displayed in the deployment Figure 4 and the second one took place at 13.09.2022, 11:05 in between the initial and the last spot. At all times, the WS was facing in the same direction to keep disturbances at a minimum. The first repositioning of the WS could have been the reason as to why a loose contact resulted in the Davis Cup. Next, the precipitation measurement was off on two occasions. The first one was at the 09.09.2022 at 17:00. The measurement showed 6.8mm of precipitation. That was considered unrealistic since the surrounding hours had none. This is assumed to be a fault in the measurement and was thus corrected to 0mm manually. The next one was on 13.09.2022 for the hours of 11:00 and 12:00. It was sunny then with no rain. During that time, the WS had to be put into the third spot as mentioned above. While doing so, the measurement gauge for precipitation clicked a few times which is supposed to indicate rain. Thus, that wrong count was also set to 0 manually afterward.

Further, some minor statistical analysis was conducted. This involves especially the iButtons on B. As stated, those were placed to research if there is temperature variability above the geotextile surface for orientation as well as with altitude. This involves specifically analyses of variance (ANOVA) of temperatures within a single radiation shield as well as a single altitude layer. Results of that can be found in Appendix A.

3.2 ePDH-Dependent Work

3.2.1 Generation of the ePDH Model

As stated in the introduction, the core model to be used for this thesis is the ePDH. It is based on the classical TIM or CTIM. The CTIM is defined as follows (Pellicciotti *et al.*, 2005; MacDougall, Wheler and Flowers, 2011; Seguinot, 2013; Matthews *et al.*, 2015):

$$M = \begin{cases} MF * T : T > Tc \\ 0 : T \leq Tc \end{cases} \tag{2},$$

where *T* is the air temperature in °C and T_c is the limit air temperature, also in °C, above which melt is defined to take place. How much of it takes place, is dependent on the defined or calibrated melt factor (*MF*). If T_c is set to 0°C, then *MF* is also called degree-day factor (DDF). Thus, days, where the temperature is over T_c, are called positive degree days. The *MF* is distinguished between snow and ice (Matthews *et al.*, 2015). The DDF (*MF*) is defined as mm d^{-1} K^{-1} (Hock, 2005).

However, making glacier ice melt solely dependent on temperature was considered unrealistic and inaccurate as solar radiation plays a major role as well (Hock, 2005).

Thus, further and more distinct glacier surface melt modelling approaches based on the PDD were generated. One of the more prominent ones is the one by Hock (HTIM) which involves the inclusion of a "… clear-sky shortwave radiation to account for the spatial heterogeneity of radiation and melt conditions in complex terrain." (Hock, 2005). Thus, the new model is defined as follows:

$$M = \begin{cases} (MF + r * Ip) * T : T > Tc \\ 0 : T \leq Tc \end{cases} \tag{3},$$

where *T* is the air temperature in °C and T_c is the limit air temperature, also in °C, above which melt is defined to take place. r is the radiation melt factor dependent on the surface (snow or ice) and I_p is "… the potential shortwave radiation" (Pellicciotti *et al.*, 2005; MacDougall, Wheler and Flowers, 2011). That factor is dependent on the surrounding topography, the aspect and slope of the surface, and the position of the sun. It was found problematic in this approach that temperature and solar irradiation are multiplied which makes physically not much sense as those two are different physical properties and are therefore measured in different units of size (MacDougall, Wheler and Flowers, 2011.

Consequently, a further model was defined. This one was the enhanced temperature index model eTIM (Pellicciotti *et al.*, 2005), or the so-called PTIM (MacDougall, Wheler and Flowers, 2011). This one also has a component for shortwave radiation. However, if compared to the HTIM, shortwave radiation and temperature are separated and thus completely independent from one another. In the initial journal article, where this model was formulated, another version of it was also defined which is described there as the multiplicative version, again multiplying shortwave radiation and temperature as is the case for the HTIM. However, that one was not used for this thesis due to the reasoning of it not making much sense physically. The model is defined as follows:

$$M = \begin{cases} TF * T + SRF(1 - \alpha)G : T \cup G > 0 \\ 0 : T \leq 1 \cap G = 0 \end{cases} \tag{4},$$

where *T* is the temperature, *G* is the incoming shortwave radiation, α is the albedo, *TF* is an empirical factor which translates temperature to melt and *SRF* is an empirical factor which translates incoming shortwave radiation to melt. The albedo in the original paper is assumed to be correct for a daily frequency even though it is known that albedo can vary throughout the day. Further, it is assumed that melt occurs only at 1°C or higher. Finally, the data used in the initial proposition is on an hourly basis (Pellicciotti *et al.*, 2005; Carenzo *et al.*, 2016). G and α can both be measured or modelled values (Carenzo *et al.*, 2009). The boundary at which temperature melt occurs is not set in stone but has

rather to be defined or assumed by oneself. As compared to Pellicciotti and others in their 2005 article, one can also set the *TF* to 0°C (Fuchs, Asoaka and Kamaza, 2013)). For this thesis, the model, mostly as described in Equation 5 was used as the base. The required assumptions were set as follows. Shortwave radiation and temperature data were provided hourly by the WS (Matthews *et al.*, 2015). The albedo was calculated based on the measured incoming and reflected shortwave radiation by the WS and thus varied in time. The difference to the introduced model as in Equation 4 is that for this thesis, melt was assumed to occur at temperatures at 0°C or higher instead as compared to 1°C (Pellicciotti *et al.*, 2005). One more adaptation, however, is to be made for the *SW*. *SWin* is at a 100 % effect rate when it hits the surface vertically. However, since the surface angle at which the *SWin* hits the surface is dependent on the latitude of the location, the date, the slope angle, and exposition, it has to be multiplied by a factor of 0.8857066188 which is going to be called the inclination factor *Icf* (Olson, Rupper and Shean, 2019). That factor was calculated and is based on some assumptions for simplification. The exact calculation and reasoning can be found in Appendix D.

Since the critical temperature for melt is set to be at 0°C, one can also call that model an enhanced positive degree-day model, or short ePDD (Matthews *et al.*, 2015). However, since the data used has an hourly frequency, it would be even more accurate to call the model enhanced positive degree-hour model, or short ePDH. This is the terminology that will be used for this thesis' core model. The ePDH was defined as follows:

$$M = \begin{cases} TF * T + SRF(1 - \alpha)G * Icf : T \cup G > 0 \\ 0 : T \leq 1 \cap G = 0 \end{cases} \qquad (5)$$

3.2.2 Calibration of the ePDH

As stated in the previous subchapter, the ePDH has two empirical factors within the model. Those need to be calibrated to be able to model the ablation on the glacier appropriately. How does one know though if the model is accurate, and how is the accuracy of a model measured in the first place? This subchapter emphasizes these questions.

First, model performance has to be compared to something. That something is the field measurements themselves, as the model attempts to predict what was measured in the field. Other approaches involve comparison to a reality-close model result such as in the case of glacier surface melt modelling an EBM (MacDougall, Wheler and Flowers, 2011)). In the case of this thesis, there are field measurements to which the model can be compared to. Thus, the model calibration can be done by comparing model results to the field measurements. Of course, this thesis also makes use of an EBM. However, that one is based on numerous assumptions and simplifications and should thus not be used more often than necessary as it involves a sufficient presumed uncertainty.

The following question is how to compare a model to reality. In the case of reality in this context, there are ablation measurements that were taken twice a day (with the exception of the first and final day, where there was only one measurement respectively). Thus, the model and measurement outputs must be compared to each time slot. However, since the model is based on the measurements of the WS which were taken each full hour and the manual field measurement did not occur exactly at full hours, a slight adaptation of the data was necessary to be more accurate.

The field measurements always took place some minutes after a respective full hour (never more than 26 minutes after the closest full hour). Those measurements were then linearly interpolated to correspond to the approximate melt at the closest full hour. This was done via the following formula:

$$Mi = Ma - \frac{(Ma - Ml)}{(ta - tl)} * \frac{(ta - tf)}{1440} \qquad (6),$$

where M_i is the interpolated melt to the closest full hour, M_a is the measured melt, M_l is the previous actual measured melt, t_a is the actual time, it is the previous actual time and t_f is the time of the previous full hour. This was done with an accuracy level of a single minute. That is why 1'440 is in the second denominator as it corresponds to the number of minutes in an entire day.

With that, there are modelled and measured melts that are comparable to the same minute. However, comparing them is difficult without a score as to how similar they are. There are many different scores which measure model efficiency such as the Nash-Sutcliffe efficiency criterion (Hock, 2005; Pellicciotti et al., 2005; Carenzo et al., 2009, 2016; MacDougall, Wheler and Flowers, 2011; Seibert and Vis, 2012; Fuchs, Asoaka and Kamaza, 2013; Pool, Vis and Seibert, 2021)), the perhaps even more sophisticated Kling-Gupta efficiency criterion (Gupta *et al.*, 2009; Knoben, Freer and Woods, 2019; Pool, Vis and Seibert, 2021), or the arguably more intuitive root mean square error (RMSE) (MacDougall, Wheler and Flowers, 2011; Fuchs, Asoaka and Kamaza, 2013; Carenzo *et al.*, 2016; Pool, Vis and Seibert, 2021). In the case of this thesis, the RMSE was used, but instead, it was called root mean square deviation (*RMSD*). This is solely a nomenclature difference, but at the core, *RMSD* and RMSE are exactly the same thing. The reason for that choice of the *RMSD* is its simplicity of it which makes it easier understandable, transparent, and therefore, also more accessible. In the context of the scientific method, it is important to keep the method reproducible. This is especially considered important for this thesis since it attempts to create an extension of a model never attempted before. The *RMSD* was not just used to calibrate the ePDH, but also the EBM as well as the eePDH. The *RMSD* is defined as follows:

the
$$RMSD = \sqrt{\frac{\sum_{t=1}^{T}(Msi-Mri)^2}{n}}$$
(7),

where Ms_i is the modelled value, Mr_i is the observed value and n is the number of comparisons taken (MacDougall, Wheler and Flowers, 2011). In the case of this thesis for the ePDH, the observed value is the respective mean value of the three reference stakes R1, R2, and R3. That mean is summarised as Rx.

Now, since the tool to define the efficiency of the model is set, the next step is to calibrate the two model parameters at hand. This is done while attempting to keep the *RMSD* as low as possible since, based on the *RMSD* equation, the smaller the *RMSD*, the smaller the overall difference between model and reality. The two empirical factors from Equation 5 have to be defined in such a way as to minimize the *RMSD*. While one could attempt to calibrate this model by hand, it could take a very long time to find a satisfying calibration since there are two factors. Due to combinatorics, calibration difficulty increases immensely with the rising number of factors to be calibrated. Thus, the Monte-Carlo simulation approach was chosen (MC). MC is a brute force approach where a predefined number of iterations of random numbers, in this case, between 0 and 1 are being inserted for the two parameters at hand and for each combination of the inserted values for the two parameters, the *RMSD* is calculated and saved in a sheet as well as the two respective numbers for the parameters (Seibert and Vis, 2012). Then, one can sort the list to find the parameter values which lead to the lowest *RMSD* and insert those into the ePDH. MC was always used for calibration of any sort with *RMSD* as an efficiency criterion, aside from one example where an additional procedure, next to MC, was used as well. Applying to MC and other sorts of simulations for calibration, there was always a total of 100'000 simulations per calibration approach for the entirety of this thesis.

While calibrating the ePDH, a sensitivity analysis for the two parameters was conducted. It is important to understand that here a global sensitivity approach was taken which focuses on the variability of the model output based on the model input parameters, while a local one would focus on the derivative of the model output (Saltelli and Bolado, 1998). Calibration of parameters varies globally depending

on the specific location (Silwal *et al.*, 2023). Aside from the location, in the fixed study site for this thesis, a superficial model parameter sensitivity was generated to display how swiftly the model efficiency criterion increases with continuously growing or shrinking parameter value. An increase in this context means an increase in the *RMSD* which is optimally kept as low as possible as compared to other criterions such as the Nash-Sutcliffe efficiency criterion (NSE) (Pellicciotti *et al.*, 2005). This is a shallow approach to an overall sensitivity analysis as longer times (multiple years) as well as different, but geographically close glaciers should be compared among the years to assess model parameter sensitivity thoroughly (MacDougall, Wheler and Flowers, 2011). However, in the scope of this thesis, that was not possible to do. Thus, a simple graphical comparison of the model parameters' sensitivities was generated.

One important aspect, which has not been addressed so far, is the software used to model the ePDH and analogue for later the EBM as well as the eePDH. All the modelling was done with Microsoft Excel (Version 2308) from the Microsoft Office Professional Plus 2016 package. Among the reasons why Excel was chosen, is that it is a software that is present on most devices and is thus also easily available in the field (Brock and Arnold, 2000). Aside from that, it is a personal preference due to familiarity with the software. Additionally, manipulating data and accessing single data fields is convenient and easily manageable. The last point became useful in the context of missing wind data, which was previously mentioned.

3.3 EBM-Dependent Work

3.3.1 Generation of the EBM

Before getting into the model structure of the EBM, it is important to stress that for the EBM and analogically for the ePDH, there is a major assumption: It is assumed than there is no time delay between melt and the lowering of the surface (Pellicciotti *et al.*, 2005).

The model structure of the EBM is complex. It is a more distinct and physical version of the ePDH, just like the ePDH, the EBM has a clear distinction between temperature-independent and temperature-dependent variables. The EBM distinguishes the temperature-dependent energy sources clearly (Pellicciotti *et al.*, 2005). The most frequent and core structure of the EBM can be described as follows:

$$Rs = SW + LW + Qsens + Qlat \tag{8},$$

where R_s is the modelled energy available for melt, *SW* is the sum of shortwave radiation, *LW* is the sum of longwave radiation, Q_{sens} and Q_{lat} are turbulent heat fluxes, namely the sensible heat flux and the latent heat flux (Brock and Arnold, 2000; Zekollari, Fürst and Huybrechts, 2014; Senese *et al.*, 2020). Further terms that can be added to the EBM, depending on the underlying assumptions, level of detail, and hypotheses at hand, which involve subsurface heat flux (Hock, 2005; MacDougall and Flowers, 2011; MacDougall, Wheler and Flowers, 2011)or sensible heat added by precipitation in the form of rain (Hock, 2005; MacDougall and Flowers, 2011). In the case of this thesis, the model was defined as follows:

$$Rs = SW + LW + Qsens + Qlat + Qrain \tag{9},$$

where all terms are equal as in Equation 7 with the addition of the sensible heat through rainfall. It is noteworthy that for *SW* and *LW*, these are directional, meaning that there are waves that reach the glacier from somewhere outside the system of the glacier surface and are considered a positive energy input into the system. And then there are waves being either reflected (in the case of shortwave radiation) to some degree by the glacier or being emitted by the glacier itself (in the case of longwave radiation) which are considered a loss of energy and thus defined as a negative energy flux (Hock, 2005; MacDougall and Flowers, 2011; MacDougall, Wheler and Flowers, 2011; Senese *et al.*, 2020). The available energy for ice melt water equivalent can be translated into ice melt via the following formula:

$$M = \frac{Rs}{\rho w * Lf} \tag{10},$$

where *M* is ice melt, ρ_w is the density of water (1'000 kg m^{-3}) and L_f is the latent heat for fusion (3.34 $*10^5$ J kg^{-1}) (Hock, 2005; MacDougall, Wheler and Flowers, 2011; Carenzo *et al.*, 2016; Senese *et al.*, 2020). By multiplying *M* by 100, the result equals to cm s^{-1} melt, and by multiplying it with 3600, you get the result in cm h^{-1} which is the most convenient and thus in this case used measure of melt. However, one major difference exists between the approaches cited in the literature and the one in this thesis. For the purpose of how much ice melted, irrelevant of the respective water equivalent, since the methodology does not involve measuring water levels or discharge, it is more advantageous to model solely the ice that melted away. For that purpose, instead of using ρ_w, this approach uses the density of ice ρ_i instead (910 kg m^{-3}).

Next, to get an idea of what the core model Equation 8 consists of, the following paragraphs will go into detail on every one of the terms in the model.

Starting off with the *SW*, as it was explained above for the ePDH, there is *SWin* and a part of it is reflected by the glacier depending on the reflectance, or α. When talking about the *SWin*, this applies

to solely the direct one. However, there is a diffuse one as well which can be quantified through different approaches (Brock and Arnold, 2000; MacDougall, Wheler and Flowers, 2011).This diffuse part can be disregarded in its quantification since in the case of this thesis, the WS measured all *SWin* indifferent of its source as long as it came from above. Thus, in this EBM, there is no distinction between direct and diffuse *SWin*.

The outgoing *SW* can be either measured or estimated by using α of ice as a factor. Snow albedo can be disregarded for this approach since no snow was involved in the entire measurement and deployment (Brock and Arnold, 2000; Hock, 2005; Pellicciotti *et al.*, 2005; MacDougall and Flowers, 2011; MacDougall, Wheler and Flowers, 2011; Zekollari, Fürst and Huybrechts, 2014). Usually, models use albedo to calculate the *SW* due to scarce data availability. However, since the WS of the used deployment measured the *SWin* and the *SWout*, it makes more sense to use these data since it is already available (Pellicciotti *et al.*, 2005). Further, using a fixed α makes the model less accurate since α varies with melt rate and thus with time (Hock, 2005). Thus, the *SW* part of the entire EBM is pretty simple to define.

$$SW = SWin - SWout \tag{11}$$

The inclination factor *Icf* applies to the *SWin* in the EBM as it does for the ePDH. Therefore, it is also added to the *SW* part of the EBM as a factor.

$$SW = Icf * SWin - SWout \tag{12}$$

The next term in the EBM is the *LW*. The *LW*, as is the case for the *SW*, has an incoming as well as an outgoing sub-term (Brock and Arnold, 2000; Hock, 2005; MacDougall and Flowers, 2011; MacDougall, Wheler and Flowers, 2011). Approaches to model or measure *LW* differ. For all modelled and not directly measured approaches, the emissivity ε of the sky and the glacier itself, the Stefan-Boltzmann constant σ (W m^{-2} K^{-4}), and the temperatures of air and the ice respectively (ice = 273.15 K) are constitutive. If respective instruments are available, the *LWin* and *LWout* can both be measured as is the case for *SWin* and *SWout* (Senese *et al.*, 2020). When modelling *LW* though, the core of complexity for *LW* is the ε of the sky as well as the one of ice. Relevant literature states that ε is dependent on knowledge of the number of clear sky time, the time of clouded sky, the cloud types, and the surrounding terrain (Brock and Arnold, 2000). Further approaches involve empirically determined parameters to model *LWin* especially (Hock, 2005). In the case of this thesis, simplifications based on assumptions had to be made to be able to model *LW*. First, modelling ε seemed rather difficult. Attempts to model *LWin* especially would have been connected to a lot of guessing and thus an immense increase in uncertainty. For ε of ice, it might have been possible, yet difficult to model *LWout* appropriately. And since, as stated in the first chapter of this thesis, *SW* is the main driver for glacier melt in the Alps, a simplification of *LW* seemed not just viable, but necessary and legitimate since it would most likely not shake the model to its core (Hock, 2005). Thus, the following equation was set to model *LW*:

$$LW = LWin - LWout = \sigma Tair^4 - \varepsilon\sigma Tice^4 \tag{13}$$

As is evident in Equation 11, *LWin* has no ε. This is due to the assumption that there is an average relation between the emissivity of air and the emissivity of ice. Thus, the ε in *LWout* is a relational emissivity factor describing the average relation of the emissivity of the sky and the ice. That ε is a parameter for the entire EBM and can thus vary. A further assumption was made that the ε cannot be smaller than 0.95. This means that the average emissivity relation between sky and ice cannot vary more than the ε_{ice} being 0.95 times the ε_{sky}.

The next part of the EBM are the turbulent heat fluxes, including Q_{sens} and Q_{lat}. It is somewhat difficult to describe both as they constitute complex physical processes. When it comes to estimating or modelling them, various approaches are possible. One is the Eddy correlation approach for Q_{sens} which is somewhat simple in structure but is highly dependent on useful deployment of instruments and the correct functioning of instruments which in glacial landscapes is risky due to the harsh environment and unstable weather conditions. Thus, the more sophisticated approaches via the bulk-transfer procedure are suggested (Munro, 1989). The bulk-transfer procedure was used by numerous others, some in a simpler fashion (Oerlemans, 2000), and others in a more complex way. For the more complex approaches, the surface roughness was modelled as well since that is a major component of the turbulent heat fluxes (Brock and Arnold, 2000; Hock, 2005; Pellicciotti et al., 2005; MacDougall and Flowers, 2011; MacDougall, Wheler and Flowers, 2011. For this thesis, the part of modelling surface roughness was simplified, since that part of modelling is rather complex and would arguably increase uncertainty further since lots of assumptions would need to be made due to missing data or measurements. Instead, the entire surface roughness calculation and everything that is involved in it, such as the von Kármán constant, is being simplified by the bulk-transfer coefficient C_{trans}. Since this is an empirical approach to the EBM, the coefficient needs to be fitted to the observations in the field, so the EBM can have the best possible fit. What is important to understand, is that C_{trans} is kept constant for this model. However, in reality, it can vary as for instance the coefficient decreases with Increasing temperature (Braithwaite, 2009). Further, the specific heat of air at constant pressure c_p was also assumed to be constant to keep it simpler. Thus, simplified formulas for the turbulent heat fluxes are as follows:

$$Qsens = \rho air * cp * Ctrans * u * Tair \tag{14},$$

$$Qlat = \rho air * \omega air * \lambda * Ctrans * u * (eair - esurf) * \frac{\rho air}{Pair} \tag{15},$$

where ρ_{air} is the density of air (1.26kg m^{-3}), c_p is the specific heat capacity of air (1003.5 J kg^{-1} K^{-1}), C_{trans} is aforementioned bulk-transfer coefficient, u is the wind speed (m s^{-1}), T_{air} is the air temperature (°C), ω_{air} is the ratio of the molecular weight of water vapour to air (0.622), λ is the latent heat of vaporization (2.5*10^{5}J kg^{-1}), e_{air} is the vapour pressure at the WS in an altitude of somewhere around $1 - 1.5$m above the surface (Pa), e_{surf} is the vapour pressure at the glacier surface (611Pa) and P_{air} is the atmospheric air pressure at sea level (101.325*10^{3}Pa) (Brock and Arnold, 2000). What is clear from these equations, is that both turbulent heat fluxes are dependent on wind speed and air temperature, air temperature directly for Q_{sens} and indirectly through ρ_{air} and e_{air}. This is important to remember in the context of the physics when the glacier is covered with two layers of non-woven geotextile. Conditions of wind speed and temperature might be completely different in that case when compared to clean ice.

Finally, the turbulent heat from rain will be described for this EBM. It is stated that rain plays only a minor role in the entire EBM, which is why it is frequently neglected. The energy available for melt coming from rain is defined as follows:

$$Qrain = \rho w * cw * R * (Train - Tice) \tag{16},$$

where ρ_w is the density of water (1'000 kg m^{-3}), c_w is the specific heat of water (4.2kJ kg^{-1} K^{-1}), R is rainfall rate (mm h^{-1}), T_{rain} is the temperature of the rain (°C) and T_{ice} is the temperature of ice (0°C) (Hock, 2005). It is noteworthy that there was no possibility to measure the temperature of the rain. Because of that, it was assumed that the rain had the exact same temperature as the air. Thus, the used equation for this EBM becomes:

$$Qrain = \rho w * cw * R * (Tair - Tice) \tag{17}$$

3.3.2 EBM Calibration

As stated in Chapter 3.2.2 Calibration, the same procedure applies analogue to the EBM calibration. That involves the linear time adaptation of the observed mean value Rx to the closest full hour as described in Equation 5, the efficiency criterion based on modelled EBM values and the adapted Rx values based on the *RMSD* as defined in Equation 6, the brute force Monte-Carlo simulation approach with 100'000 iterations as well as the sensitivity analysis of the two model parameters.

3.3.3 Downscaling of EBM from Clean Ice to Covered Ice

After having calibrated the EBM for clean ice as successfully as possible under the given conditions, the next step in the procedure is to scale the EBM down to the melt of the glacier ice under the cover. The EBM being a physical model represents all the, according to this thesis, relevant physical processes responsible for melting, which are not so small that they could be neglected. Now, under the circumstances of covers on the glacier, the conditions and thus the sources of energy start to differ. As stated further above, only one study is known that attempted to model glacier melt under different conditions due to cover, but that one was natural debris cover and not a human-made engineering-based cover. However, that one research added factors to the model to scale it down based on statistical analysis to calibrate the two lag factors (Carenzo *et al.*, 2016).

In this thesis, to get an appropriate down-scaling of the factors of the EBM to represent glacier ice melt under two-layered non-woven geotextile, two common, automated calibration approaches are being used. One was already introduced earlier and applies here again, namely the Monte-Carlo simulations, again including 100'000 iterations. The other, perhaps brute force approach, but slightly more sophisticated, is the so-called genetic algorithm and Powell optimization, or short GAP. The GAP also applies lots of numbers onto the to-be-calibrated terms, but it does so in a more iterative way. As compared to the MC, for the GAP three numbers need to be predefined by the user. The first one is the number of groups, the second one is the number of iterations per group and the third is the reduction factor per group change (Seibert and Vis, 2012). As this appears rather abstract, it will be exemplified with the specifically chosen numbers for this thesis. The first number is the number of groups which was defined as 5. The second one is the number of iterations which was defined as 20'000. Now, 20'000 multiplied by 5 equals 100'000 which is the same number of iterations as was done with the MC. When using GAP with the specific numbers so far, the procedure starts the same way as MC for the first 20'000 iterations. After that, it switches to the second group. And while doing so, the third predefined number, in this case 0.1 or 10 %, comes into play. With the first group of iterations completed, the algorithm checks for the best score so far, in this case, the lowest *RMSD*. It remembers the factors that achieved the lowest *RMSD* score. For the next group of iterations (20'000), the random numbers cannot vary between 0 and 1 anymore, but only ± half of the third predefined number, namely 5 %. So, for the next group of iterations, the range at which the algorithm can search for an even better result according to the *RMSD* score is narrower. That process is repeated again for the following groups, meaning that for the third group, the possible range is ± 0.5 %, for the fourth group analogue ±0.05 %, and for the fifth and final group ±0.005 %. Thus, this algorithm searches for the optimal score in a more sophisticated procedure than the MC. It has thus the potential to be more accurate. However, there is the risk, depending on the model and its complexity that it finds only a local optimum and missing the global optimum since it finds a somewhat reasonable result.

The top 40 results (smallest *RMSD* scores) of each the MC and the GAP can be found in Appendix E and F. They give an overview of what the results look like and how much they vary.

3.4 eePDH-Dependent Work

3.4.1 Translation of Reduction Factors from EBM to eePDH

The approach of translating the most optimal downscaling results from the EBM to the extended ePDH, or short eePDH, is based on one single and specific realization. That constitutes the most crucial step in the modelling and thus answering of the second research question. The realization was already stated in the subchapter 1.1.2. This is that index-based models can be understood as simplifications of the physical models (Pellicciotti *et al.*, 2005). Based on this assumption, the translation of the EBM-based downscaling to the eePDH downscaling can be achieved via a set of already-known equations and the manipulation of those. And that is what will be explained in this subchapter.

As was displayed in the previous subchapters, there are different models that model glacier surface melt. The ones used for this thesis are the EBM and the ePDH. Those can be found in Equations 5 and a combination of 8 and 9. Further, it has to be noted that Equation 5 as the ePDH was not based on albedo itself directly, but on the incoming and outgoing shortwave radiation measured by the WS. Additionally, it can be stated that for the first week of measurements, no temperature ≤ 0°C above the glacier surface was recorded by any measurement device. Therefore, in the context of the first week, the model equation for the ePDH can be specified as follows:

$$M = Icf * SWRF * (SWin - SWout) + TF * T \tag{18}$$

Regarding the melt of the EBM, it can be described as a combination of Equations 8 and 9 which results in the following equation:

$$M = \frac{SW + LW + Qsens + Qlat + Qrain}{\rho w * Lf} \tag{19}$$

If one assumes that both models have the capability to model the melt exactly, the *M* in the last two equations should be the same. It is argued that the assumption is valid since both models the ablation of glacier surface ice melt. Next, it was already addressed that both models have temperature-dependent and independent terms represented in them (Pellicciotti *et al.*, 2005). Thus, the argument can be made that the, at least, temperature-independent terms in both models should equate to the same amount of melt on the glacier. Therefore, the following equation based on these assumptions can be made.

$$\frac{Icf * (SWin - SWout)}{\rho w * Lf} = Icf * SWRF * (SWin - SWout) \tag{20}$$

Equation 20 is in a sense fully correct yet. Since, in the context of this thesis, both models output their results in cm/h, for the left part of the previous equation, which is the EBM-based one, the result is multiplied by 100 and another time by 3'600, since the result as it stands on the left part of Equation 19, is given in m/s. To get to cm/h, the multiplication of these two numbers gives the correct result in the right quantity. Resulting, the correct equation is:

$$\frac{36 * 10^5 * Icf * (SWin - SWout)}{\rho w * Lf} = Icf * SWRF * (SWin - SWout) \tag{21}$$

Since the scaling down of the EBM to fit the melt for covered glacier ice was done for each of the terms in the EBM, this also applies to *SW*, which is the left part of Equation 20. Adding that scaling down factor to it to fit the measured melt would result in also having to add the same factor for the ePDH-based right side of the equation.

$$f1 * \frac{36 * 10^5 * ICF * (SWin - SWout)}{\rho w * Lf} = f1 * Icf * SWRF * (SWin - SWout) \tag{22},$$

where *f1* is the downscaling factor for *SW* resulting from either MC or GAP in the context of downscaling the EBM to fit the measured melt for the cover. With that, the factor for the temperature-independent part of the model is given.

As for the temperature-dependent part of the EBM, the approach described so far is not applicable. The reason for that is that compared to the temperature-independent part of the EBM, the connection of the required values is not linear, which especially applies to turbulent heat fluxes (Munro, 1989; Brock and Arnold, 2000; MacDougall and Flowers, 2011; MacDougall, Wheler and Flowers, 2011). Thus, translating a total of four factors from the EBM (*LW*, Q_{sens}, Q_{lat}, Q_{rain}) is not possible in this direct way. And until one has more detailed and quantified insight into the processes taking place under such a cover, translating the factors resulting from simulations leaves only room for speculation. The approach in this thesis is to assign a new factor to the temperature-dependent term in the ePDH by MC. In this case, there is only one factor that can be varied, which is the defined as *ft* for the temperature-dependent part of the ePDH.

Admittedly, this assigning approach seems arbitrary. However, with no further insights into the surface energy balance underneath such a cover, it is necessary to not make assumptions. The physics underneath the cover remains unclear and requires further research, perhaps under lab conditions. In the chapter results, it will become evident that this MC-based estimate gave a satisfying result. Although one could think that this was solely due to chance, the results of the approach should be able to perhaps at least reduce that assumption.

3.4.2 Generation of the eePDH

Based on the already existent ePDH, an extension of the enhanced positive degree-hours model was generated. It includes the aforementioned and defined two factors *f1* and *ft*. Aside from that, another brute force approach based on MC was done in an attempt to find alternative solutions to *f1* and *ft*. Consequently, the model involves the measurements of the average of the reference stakes for melt, summarized as *Rx*, the measurements of the stake in the *S* cover, the initial model of the ePDH, the eePDH with reduction factors *f1* and *ft* based on the EBM approach and later MC approach as well as the eePDH with reduction factors *f1* and *ft* based on solely MC. All of that is still done in the context of model calibration. Thus, it was done for the first week only. And that also constitutes the end of the model calibration. The novel eePDH is defined as follows:

$$M = \begin{cases} ft * TF * T + SRF * (SWin - SWout) * ICF * f1 : T \cup G > 0 \\ 0 : T \leq 0 \cap G = 0 \end{cases} \tag{23}$$

3.4.3 Extension of the Calibrated eePDH to the Second Week

Just having calibrated a model which, under the given circumstances seems to perform well, does not necessarily mean that it does so always. A model is an attempt to represent reality. Consequently, the model should also attempt to perform not only for the limited time used for calibration (Lee *et al.*, 2019). To validate model performance, it is crucial to use data for validation which is independent from the data used for calibration (Matthews *et al.*, 2015). In the case of this thesis, the second week was reserved for that, specifically the final measurement on 20.09.2022 at 16:04.

The data requirements involve temperature data as well as incoming shortwave radiation data as is visible from Equations 4 and 23. It was mentioned earlier that the weather station faced numerous issues during the second week where no visits were made to the site except for the one for the final measurement. Thus, there is data insecurity and data incompleteness. To bridge this gap, data from a nearby weather station was used. It is namely the MeteoSwiss station in Samedan (Lat/Long: 46°32'/ 9°53') (1'708 m.a.s.l.). In the research on the Morteratsch glacier, data from that weather station was

used previously and proved to be useful (Zekollari, Fürst and Huybrechts, 2014; Zekollari and Huybrechts, 2018). Data accessed from that weather station involved *SWin* and air temperature from 06.09.2022 at 00:00 until 20.09.2022 at 23:00 (MeteoSchweiz, 2022).

Since that weather station is more than 10km away from the deployment as well as at a different altitude, the air temperature data specifically was extrapolated to be closer to reality. For that, the already acquired data from the WS was put next to the data from the weather station in Samedan. The average difference in air temperature was calculated. That result was taken and subtracted from the air temperature data from the weather station in Samedan for the second week. The decision to take the data for the second week entirely from the weather station in Samedan is to keep the transparency higher and to not mix data within the validation period. Further, it can be argued that with the data coming from another weather station, the independence of data is even stronger.

No adaptations were made to the *SWin* data. It was simply used for the second week. Yet, after getting familiar with the data and comparing the data to the first week of the WS *SWin* data, it became evident that there was plenty more *SWin* in Samedan than on the glacier within the first week. The first *SWin* in Samedan was usually recorded at about 06:00 while on the glacier, the first *SWin* in the morning was usually measured at 08:00. Next, the total measured *SWin* for the first week in Samedan exceeds the *SWin* from the WS by close to 25 %. It is to be expected that the weather station in Samedan has higher values since it is located in the middle of a widely open valley while the WS is surrounded by high and close-by mountain peaks casting shadows. The decision was made not to adapt *SWin* for mainly one reason. Attempting to reduce *SWin* without any knowledge or insight into the exact reasons would only increase uncertainty in the modelling procedure.

Overall, the necessary use of other data to be able to model the second week to be able to validate model performance increases uncertainty in the model. One has to be aware of the circumstances and used data while interpreting and validating the results of this model.

3.4.4 Further Approaches to Validate the Model at Hand

With the extension of the model onto the second week and an efficiency criterion (*RMSD*), one could arguably already validate the model performance. However, having only one rather unsophisticated criterion, which was used in this thesis, might not give insights into how to improve the model further. Therefore, this section focuses on methods to further meaningfulness of the model validation.

Regarding the *RMSD*, that efficiency criterion was used or mentioned in variable studies and models to evaluate model performance (Brock and Arnold, 2000; MacDougall and Flowers, 2011; MacDougall, Wheler and Flowers, 2011; Carenzo *et al.*, 2016; Pool, Vis and Seibert, 2021). Making use of it due to its simplicity makes sense. However, an *RMSD* alone is not capable of explaining why and under what aspects the model performance is weaker.

There exist, however, other criterions which possess a higher degree of explanation towards a model performance. Among the most well-known is arguably the Nash-Sutcliffe efficiency criterion, or short *NSE* as it is used in numerous studies as a criterion for model performance (Hock, 2005; Pellicciotti *et al.*, 2005; MacDougall, Wheler and Flowers, 2011; Carenzo *et al.*, 2016; Silwal *et al.*, 2023). The *NSE*, also frequently called *R²*, is defined as follows:

$$NSE = 1 - \frac{\sum_{t=1}^{N}[qobs(t) - qsin(t)]^2}{\sum_{t=1}^{N}[qobs(t) - \bar{q}obs]^2} \tag{24},$$

where *qobs(t)* is the observed/measured value, in our case the measured melt, at a defined time step, *qsim(t)* is the simulated melt value at a defined timestep and *q̄obs(t)* is the mean measured melt over the entire measurement period (Pellicciotti *et al.*, 2005; Gupta *et al.*, 2009; Cooper, 2010; MacDougall,

Wheler and Flowers, 2011; Knoben, Freer and Woods, 2019). The *NSE* is a normalized measure that goes from 1 (ideal model) to -∞. It compares the mean square error of the model to the variability of the observed values. That is to be understood as a ratio of the specific model to the simplest model imaginable, namely a model that expects an average value. However, using an average as a model predictor can potentially not to be meaningful depending on the model at hand. (Cooper, 2010). It can be argued though that for a novel approach as is the case for this thesis, including the somewhat reduced complexity of the EBM, the *NSE* can still serve as a means to get an overview of the model performance.

Apart from the *NSE*, there are other criterions that can be used as well. Another prominent one that has an improved perspective on the model predictions is the Kling-Gupta efficiency criterion, or short *KGE* (Knoben, Freer and Woods, 2019). The KGE is defined as follows:

$$KGE = 1 - \sqrt{(r-1)^2 + \left(\frac{\sigma sim}{\sigma obs}\right)^2 + \left(\frac{\mu sim}{\mu obs}\right)^2} \qquad (25),$$

where *r* is the linear correlation coefficient between the simulated and observed values, σ are the standard deviations of the simulations or observations respectively and μ are the means of the simulations and observations respectively (Knoben, Freer and Woods, 2019). It is argued that, in a sense, model calibration can be regarded "… as a full multiple-criteria optimization problem resulting in a 'Pareto set' of non-dominated solutions." (Gupta *et al.*, 2009). Thus, compared to the *NSE*, the *KGE* does not solely account for deviations from the mean, but also differences in correlation and standard deviation. With that, it has more power to explain model performance and therefore, more meaningfulness.

Regarding the direct comparison of the criterions, since the *RMSD*, the *NSE,* and the *KGE* describe completely different things, they are not directly comparable (Knoben, Freer and Woods, 2019).

When it comes to defining observations, the approaches vary. Of course, one might think first that observations are what is measured in the field. However, measurements in the field are not always possible to be taken at the rate required to fit the modelled rate with rare exceptions to that (Brock and Arnold, 2000). However, for most cases, the initial melt model, as some sort of TIM, is compared to the physical and sophisticated EBM (Hock, 2005; Pellicciotti *et al.*, 2005; MacDougall and Flowers, 2011; MacDougall, Wheler and Flowers, 2011). For this thesis specifically, none of the above was possible. A third approach was taken. Field measurements were used as a base. However, since those were taken only twice a day at best, they do not have the same measurement frequency as the frequency of the eePDH of once every hour. The field measurements were then interpolated linearly based on the current measured melt rate and the one before. The exact procedure can be expressed with the following formula:

$$Mi = (M(t) - M(t-1))/t(d) \qquad (26),$$

where M_i is the interpolated melt, M_t is the melt at the actual or next measured time step, M_{t-1} is the melt measured at the previous time step and t_d is the time difference in hours between M_t and M_{t-1}. The reason for this approach, which generalized the data (and is thus admittedly not very accurate), is that the WS did not manage to measure the required data until the end of the measurement period. And even if it did, the data might have been deviated due to a given tilt of the WS and consequently inaccurate data. Taking data from another WS for this cause would not have been a viable solution since very local processes such as wind cannot be measured by a weather station far away. Model output based on such data thus cannot be considered viable. The uncertainty is assumed to be too great. Finally, the EBM was based on assumption and thus partly empirical. Taking empirical values as "observed values" did not seem very fitting.

4. Results

4.1 Model Independent Work

Starting off with the deployment location and geographical properties, Table 1 shows the measurements that were taken with a handheld GPS device and an inclinometer (compass included).

Table 1: Description of the field site's specific locations for each measurement location (N: & E: (LV95), elevation, slope inclination, and exposition).

Location:	N:	E:	Elevation:	Inclination:	Exposition:
WS	4625125	00955975	2109	9°	341°
B	4625123	00955976	2168	8°	348°
S	4625123	00955969	2168	8°	334°
R1	4625122	00955969	2169	8°	330°
R2	4625120	00955973	2169	9°	334°
R3	4625123	00955969	2168	7°	332°

The measurements look trustworthy with a few exceptions. The blue marked cells (N: & E:) for S and R3 have the exact same values, even after multiple attempts to measure them. Diffraction-, reflection- and scattering effects of electromagnetic waves in the case of having rock faces, mountains, and mountain edges can be expected effects that may disturb the signal. This might also be the reason why even after multiple attempts, the elevation for the WS location was continuously 60m too low. However, the elevation seems to be about right for most measurements which can also be perhaps assessed by eye if compared to the location of a previously present automated weather station (Oerlemans, 2000; Oerlemans, Haag and Keller, 2017).

The mentioned disturbing effects of GPS measurement become clear when taking a look at the control measurements taken after two weeks of measurements on the glacier.

Table 2: Same measurements as in Table 1 two weeks later (except for exposition), just after the final automated measurements.

Location:	N:	E:	Elevation:	Inclination:
WS:	4625124	00955977	2141	12°
B:	4625121	00955979	2151	11°
S:	4625119	00955972	2151	17°
R1:	4625118	00955970	2152	11°
R2:	4625120	00955968	2150	16°
R3:	4625122	00955971	2152	13°

The elevation was measured to be about 17m lower than two weeks ago. That difference is not explainable by the glacier ice melted away within the past two weeks. Some GPS-based inaccuracy is involved in this. However, since the differences were not major in general, it was assumed that they were neglectable. The measurements of N: and E: differ a little and are not worthy of more attention. The inclination however seems to have increased everywhere by at least 3°. A possible explanation for that could be that the end of the glacier tongue can be the steepest part of the tongue. And with much more of the glacier melting away, the site turned out to be closer to the end of the tongue. However, more information would be needed to explain this. This might have an influence on the *Icf* which is relevant for the *SWin*. However, since the difference is not immense and the calculation of the *Icf* is

based on numerous assumptions, attempting to implement changes over time on the inclination to generate a dynamic *Icf* would lead to further uncertainties.

Following is one of the most important basic results of this entire thesis, the measured cumulative melt of the three reference stakes on clean ice as well as the S stake for the ice-covered with two layers of non-woven geotextile (Geoproduct, 2021):
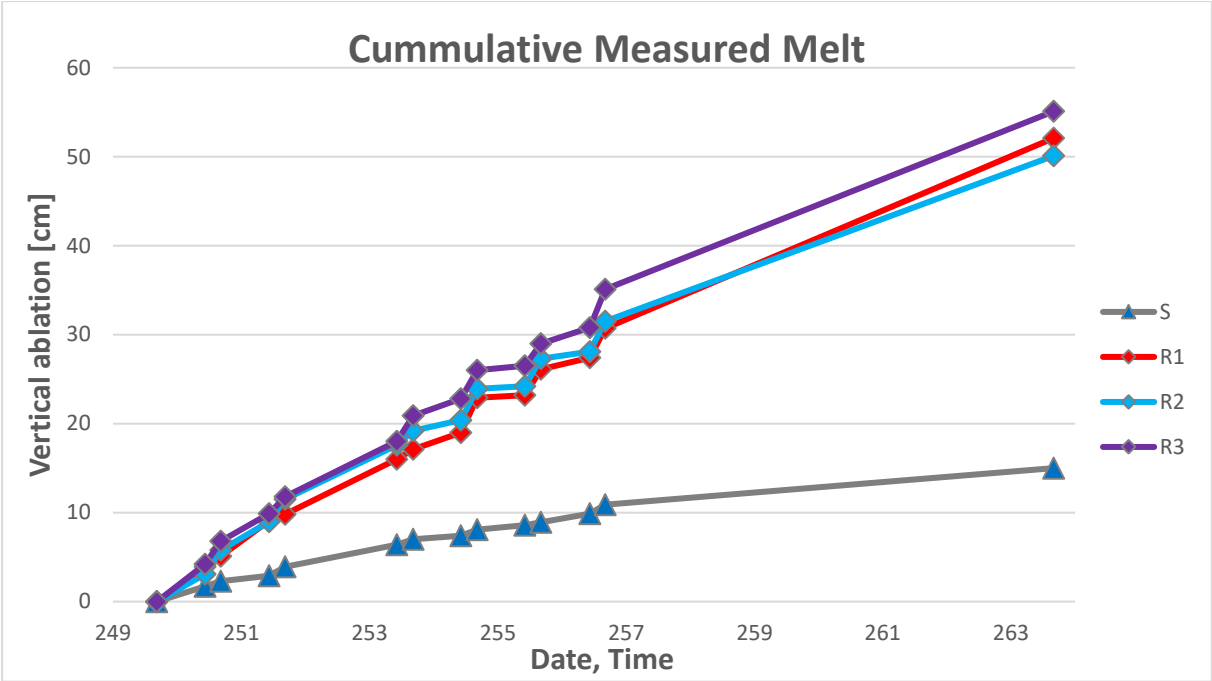
Figure 8: Cumulative measured melt for the 3 reference stakes on clean ice and the S stake on covered ice for the entire measurement period.

It is visible from Figure 8 that the cover had an immense effect on ice melt reduction. After two weeks of measuring, 15cm of glacier ice under the cover melted away. As for the clean ice, 50.1cm up to 55.1cm was measured. The mean of the three clean ice reference measurements equates to 52.43cm. Dividing the melt under the cover by the mean of the reference clean ice melt results in results in about 28.6 %. Subtracting that value from 100 % equates to the reduction in ice melt over those two weeks which is about **71.4 %**. With that, the first research question is answered. Regarding the initial hypothesis for the first research question, the hypothesis was almost right, but not quite. It was stated that the presumed reduction factor of two layers of geotextile cover on the ice would result in about 50 – 70 % melt reduction. The effect measured was even above that.

What was measured as well, was the albedo. The following figure displays all the albedo measurements as well as a calculated albedo from the WS measurements.
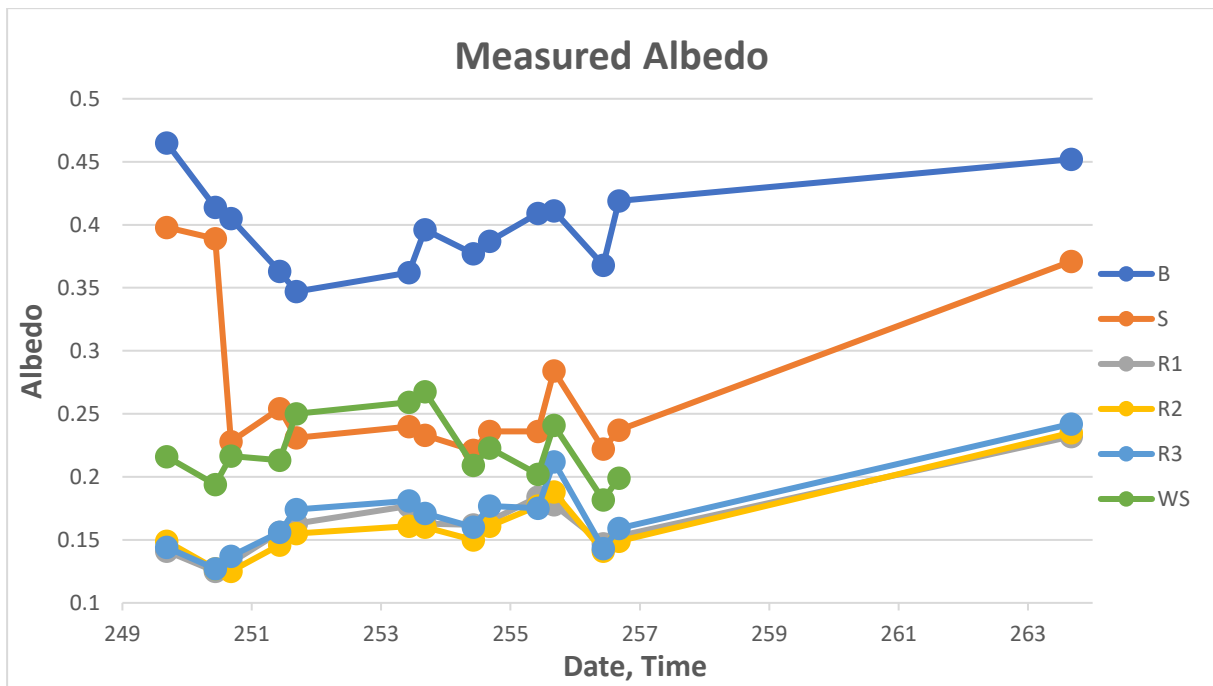
Figure 9: All albedo measurements and WS-based calculated albedo.

When it comes to albedo measurements, a few things need to be addressed. First, there is a clear difference in albedo between the clean ice and the covers. The albedo of the cover is much greater. However, there is still a huge difference in albedo between the two covers. Possible reasons for that will be addressed in chapter 5 of this thesis. The three clean ice albedo measurements seem mostly consistent with each other. Overall fluctuations for all albedos will also be addressed in Chapter 5.

What is noteworthy, is that the relation of the highest measured albedo average of any cover (in this case B) to the albedos of clean ice put together and averaged over the first week is about 252.5 %. That means that on average, the albedo of the cover was about 2.5 times higher than that of the clean ice. If compared to the melt relation, the melt was about 350 % for clean ice as compared to covered ice. The data found some differences in *SWin* when comparing the WS data to that of the clean ice measurements. Potential reasons for that will be discussed in chapter 5 as well.

Melt differences analyses between cover/clean ice and day/night were conducted as well. The result of that is visualized in the following two figures.
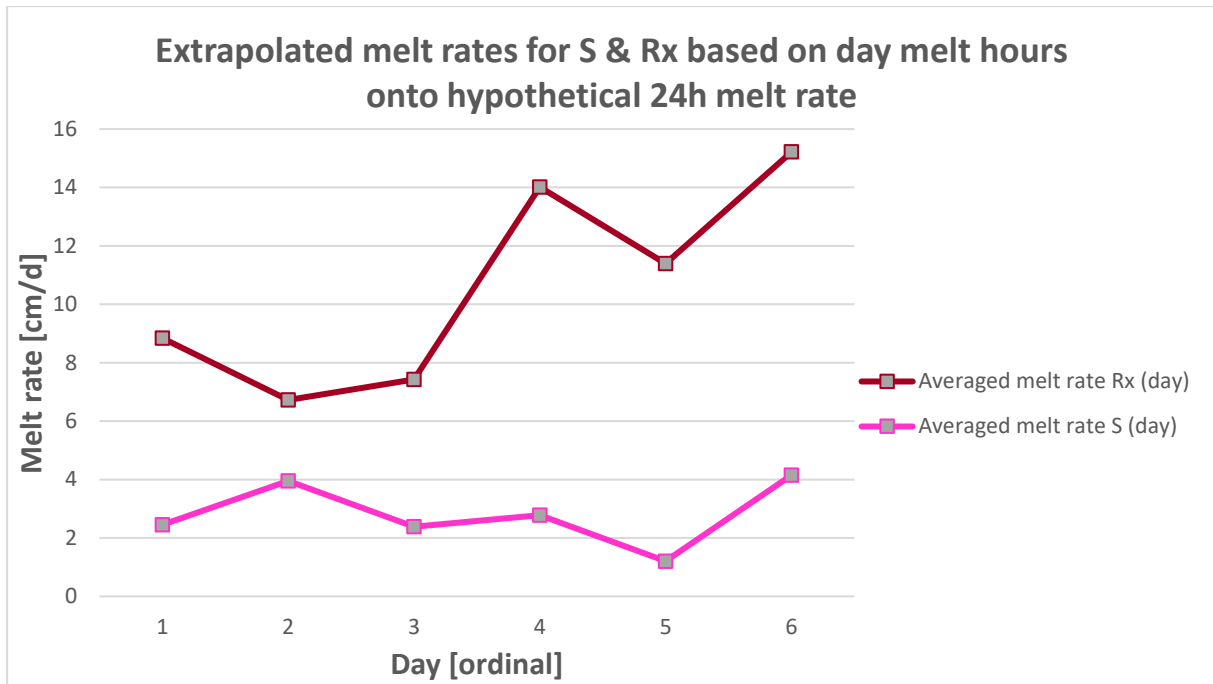
Figure 10: Extrapolated melt rate for each whole day based on averaged melt rates during day hours (10:00 – 16:00) for the first week.

Figure 10 shows a hypothetical melt comparison between covered ice (S) and clean ice (Rx). Based on the self-defined day melt hours (10:00 – 16:00), the respective mean melt rate per hour was calculated and then multiplied by 24 to get an idea of how much glacier ice would have melted if the given conditions during the respective day would have been kept constant for 24 hours. It is noteworthy that for five out of the six days (extrapolated), the melt of S and Rx respectively seem to behave similarly if compared to the respective previous and following day. Only day two shows differences. While for Rx, there was a lower melt rate the day before than day three, for S the day before had a higher melt than day three. If day two for S was lower than day one and day 3, the behaviour would have been the same as for Rx.
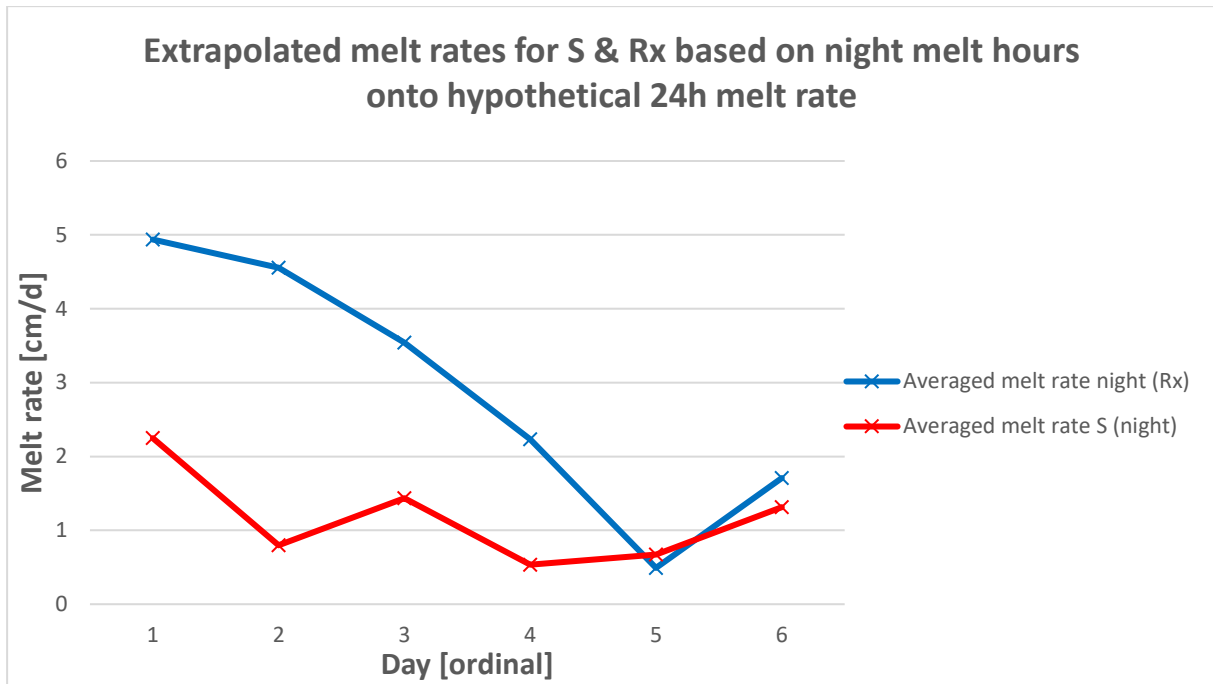
Figure 11: Extrapolated melt rate for each whole day based on averaged melt rates during night hours (16:00 – 10:00) for the first week.

Similar results can be seen for the extrapolated night hours based on the average melt rate for S and Rx respectively. In the case of the night, the extrapolated melt rate for S increased for the third night if compared to the second night while the opposite is the case for Rx. On the fifth night, the melt of clean ice was even smaller than that of the covered ice

Plotting day and night values in that sense of Rx or S respectively makes not much sense, since day and night data are directly independent from one another.

Aside from the most crucial measurements and extrapolations, various data were plotted against each other to get a better understanding of the physics at hand. Some highlights are presented below.
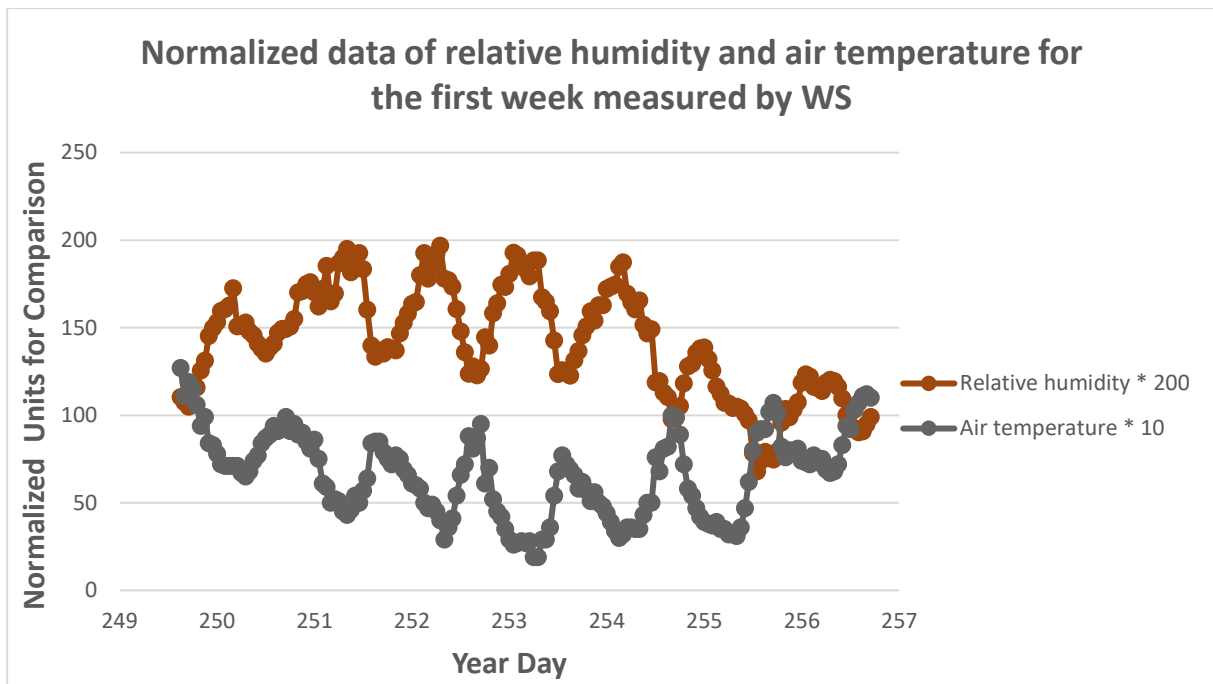
Figure 12: Plot of relative humidity (*200) and air temperature (*10). This was done to be able to compare the behaviour over time. No conclusions for absolute values can be derived from this.

What can be seen in Figure 12, is how air temperature and relative humidity behave in relation to one another. It has to be stressed that these are normalized and not absolute values. This plot simply attempts to show the behaviour of the data with respect to each other. It is to be expected that relative humidity decreases as air temperature increases. Warmer air has a greater capacity to carry water vapor. Thus, as soon as air temperature increases, the potential to carry more water vapor increases as well, and as such the actual workload of the air-carrying water vapor decreases.
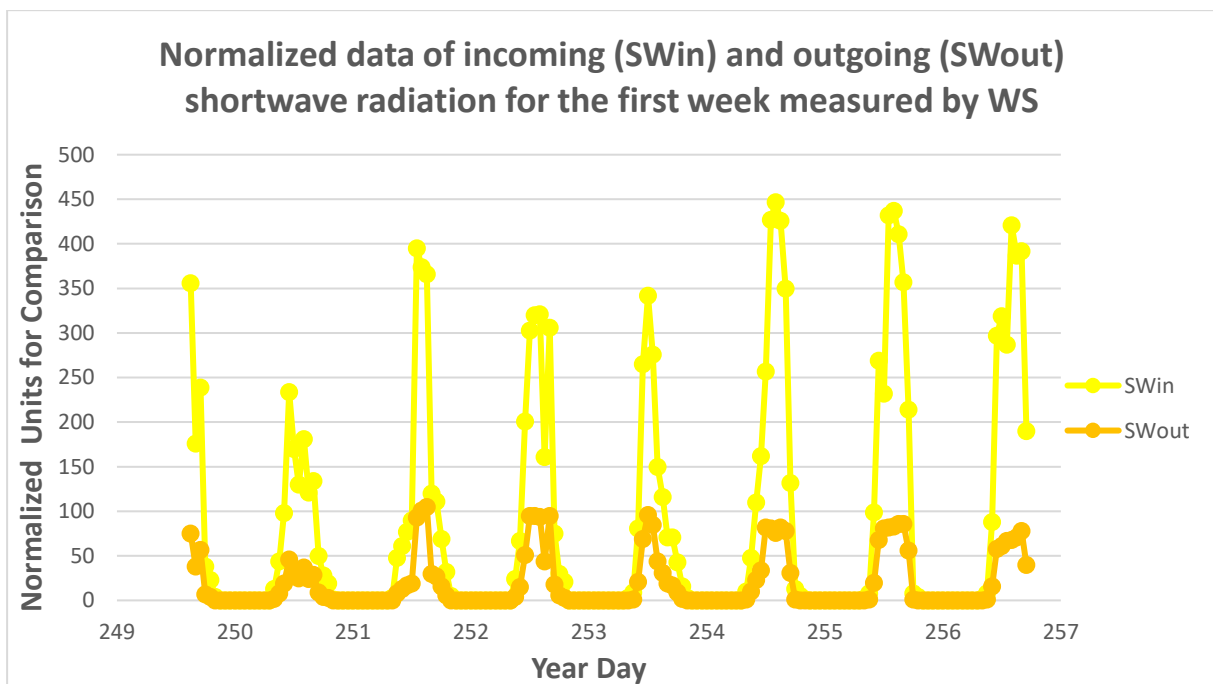
Figure 13: Plot of SWin and SWout. This was done to be able to compare the behaviour over time. No conclusions for absolute values can be derived from this.

As can be expected from *SW*, the *SWout* is visibly the dependent variable in this context, since as *SWin* increases, so does *SWout* (Hock, 2005). *SWout* is the part of *SWin* which was not absorbed by the glacier ice. One good example of that can be seen for the 252nd day, where through the day, there was a dent in the data, presumably due to cloud cover in the sky.

4.2 ePDH-Dependent Work

As introduced in the chapter on methodology, the next step in the process of this thesis was to generate the ePDH. This was done based on the acquired data and Equation 5 including the implementation of the *Icf* for the temperature-independent part of the model. However, to get a model output, the two empirical factors *TF* and *SRF*, also need to be defined. These were generated by the MC approach. MC used 100'000 iterations of pairs of random numbers for both empirical factors (range *TF*: 0.1 – 0.2, range *SRF*: 0.01 – 0.05) (Pellicciotti *et al.*, 2005). The best result was defined by the pair of numbers with the lowest *RMSD* (*Rx*) score as introduced in Equation 6. The result of the calibrated ePDH is depicted below.
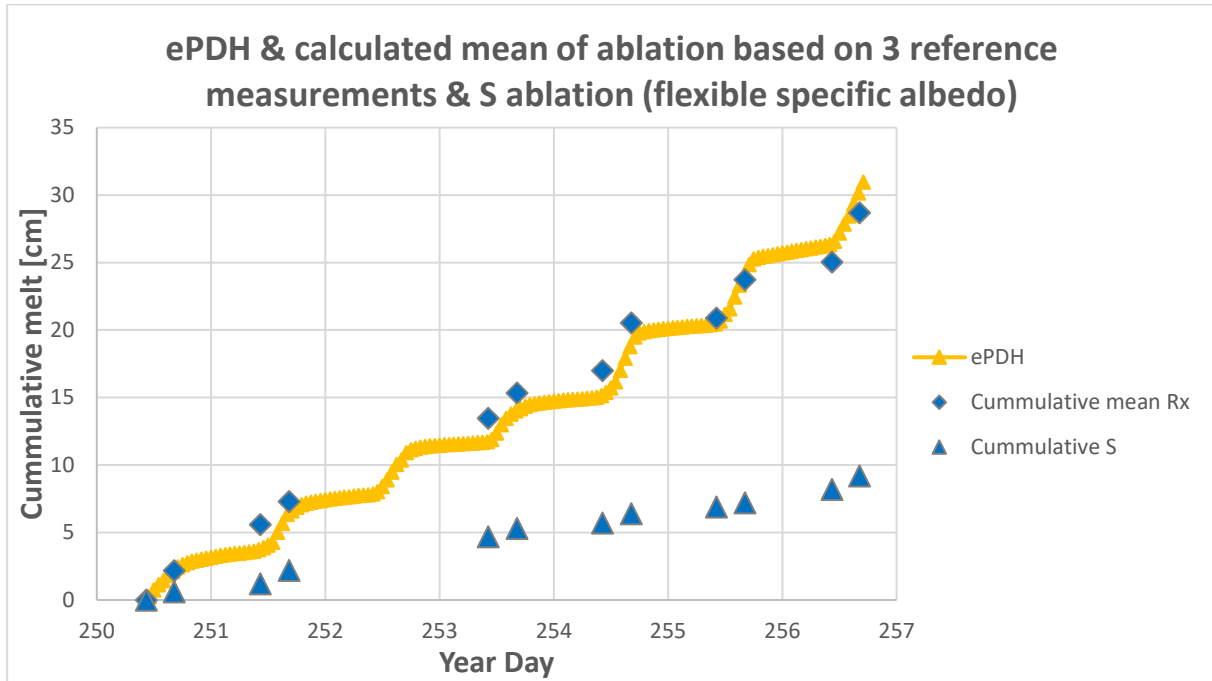
Figure 14: Calibrated ePDH with Rx and S melt measurements depicted in it as well for clean ice conditions.

It is noteworthy that the measurement of the first day (06.09.2022) is not included in the time range of the model. The reasons for that will be discussed in chapter 5. The respective empirical parameters as well as the *RMSD*s for *Rx* and *S* are shown in the table below.

Table 3: Display of the MC-based best-found model parameters for the ePDH as well as the RMSDs for Rx and S respectively. RMSD (S) does not play a role yet in this model but will be the main efficiency criterion for the eePDH.

TF	0.199974054
SWRF	0.039267731
RMSD (Rx)	1.311777338
RMSD (S)	12.214766429

Further, the sensitivity of the model parameters was researched and illustrated in two plots, one for each empirical model parameter (Pellicciotti *et al.*, 2005). Further sensitivity analyses were not conducted as was done in other research as checking the sensitivity of the slope gradient, the time of the year, or anything related to the *Icf*, as these are more or less fixed in the context of this research. Further research on this is advised. However, that is not within the scope of this thesis.
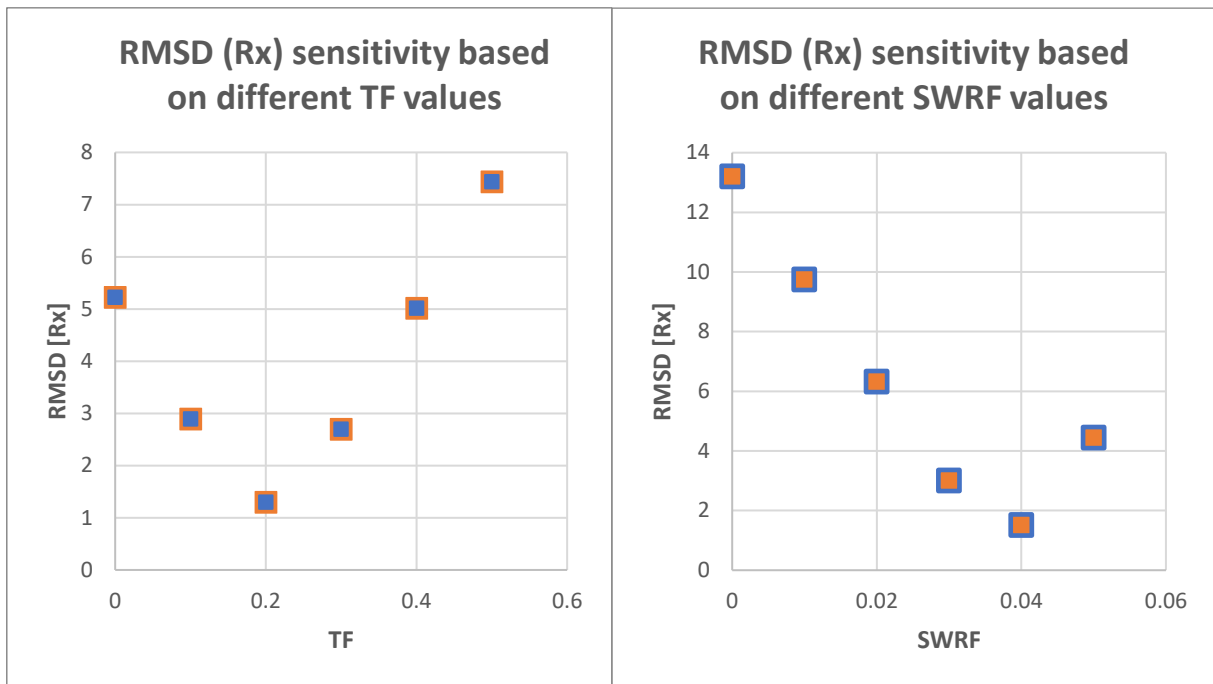
Figure 15: ePDH sensitivity based on variation of the empirical model parameters for RMSD (Rx).

Figure 15 shows the sensitivity of the two empirical model factors. *SWRF* is immensely more sensitive as only reducing it by 0.04 results in an *RMSD* (*Rx*) of more than 12, while for the PDD_MF reducing that for the same amount would probably result in an *RMSD* (*Rx*) of about 2. Implications of this will be addressed in the discussion chapter.

4.3 EBM-Dependent Work

As it was done for the ePDH, the generation of the EBM similarly took place. First, the model structure was formulated, and then the *RMSD* criterion for *Rx* and *S* was defined. On the base of those two things, with MC, the ideal model parameter values were generated, namely for C_{trans} and ε. Based on that, the EBM for clean ice was generated.
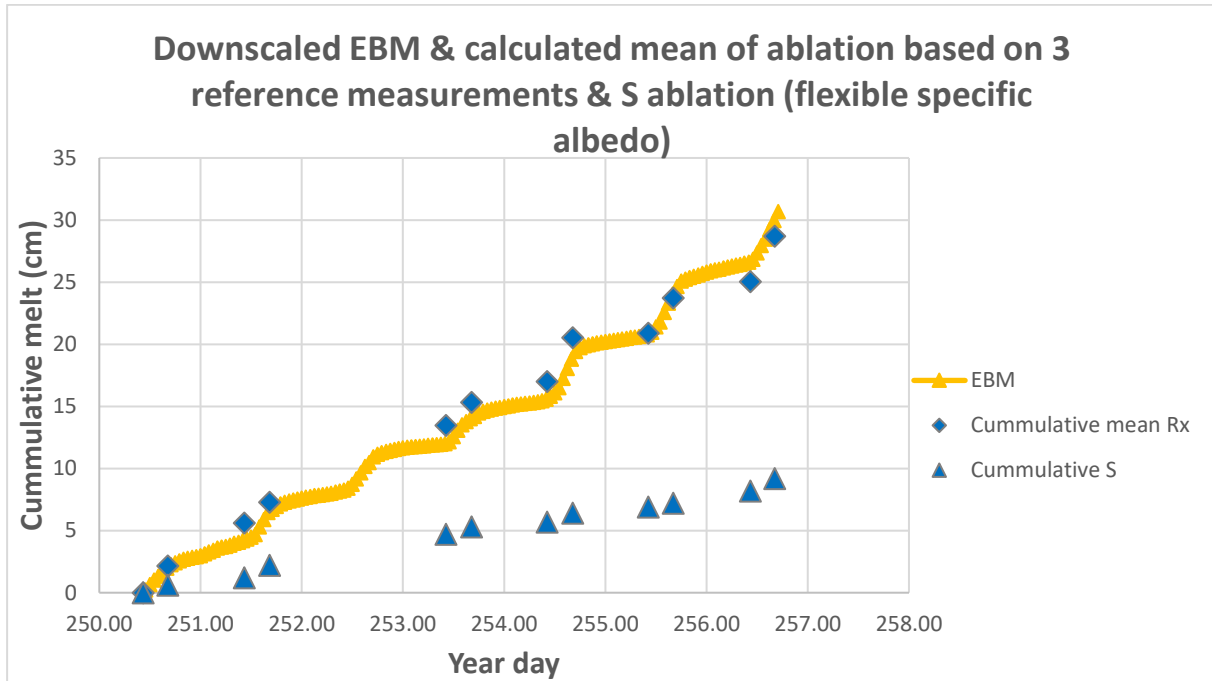
Figure 16: Calibrated EBM with Rx and S melt measurements depicted in it as well for the first week for clean ice conditions.

Same as for the ePDH, the fit is quite all right. The *RMSD* (*Rx*) for the EBM indicates an even better fit than for the ePDH. The respective *RMSD*s and the empirical parameters are displayed below.

Table 4: Display of the MC-based best-found model parameters for the EBM as well as the RMSDs for Rx and S respectively. RMSD (S) does not play a role yet in this model but will be the main efficiency to scale down the EBM in the following steps.

C_trans	0.0012000262320042
emiss	0.9697920703887940
RMSD (Rx)	1.180798771
RMSD (S)	12.300090028

With this calibration, the EBM manages to have an average deviation from the observed melt in the field of less than 1.2cm per measurement. The sensitivity of the two empirical parameters is also plotted for the EBM.

It is visible that C_{trans} is the more sensitive out of the two model parameters. Possible explanations on why that could be followed in chapter 5 as well.
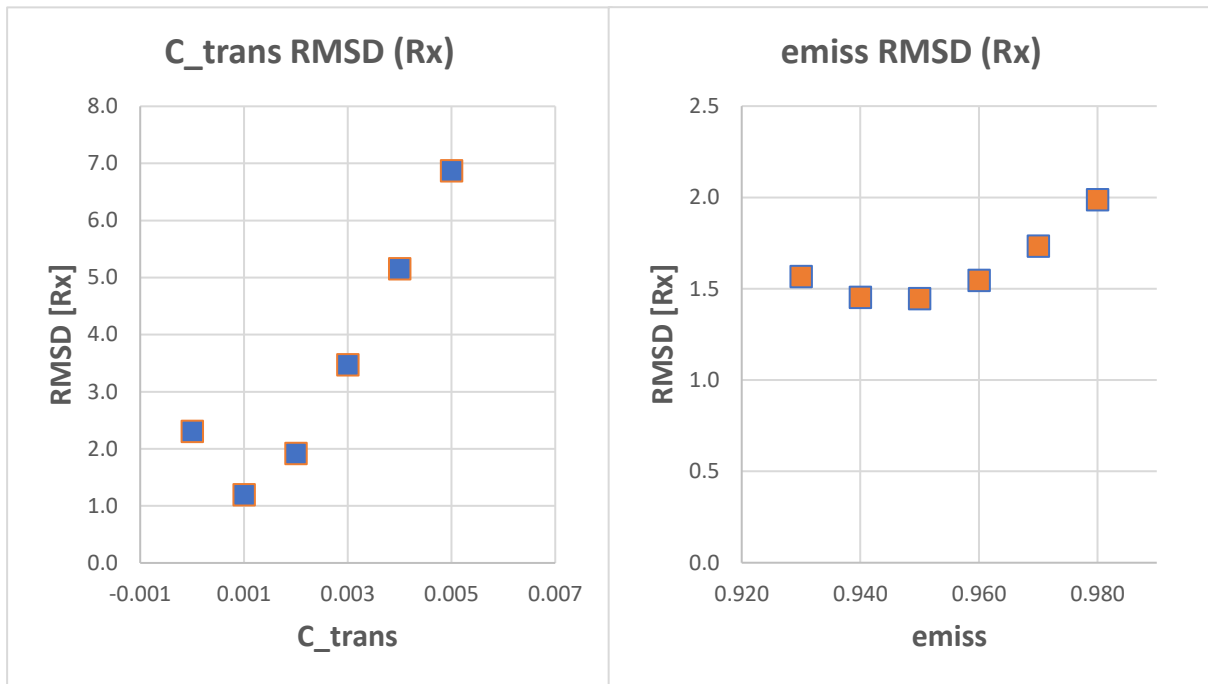
Figure 17: EBM sensitivity based on variation of the empirical model parameters for RMSD (Rx).
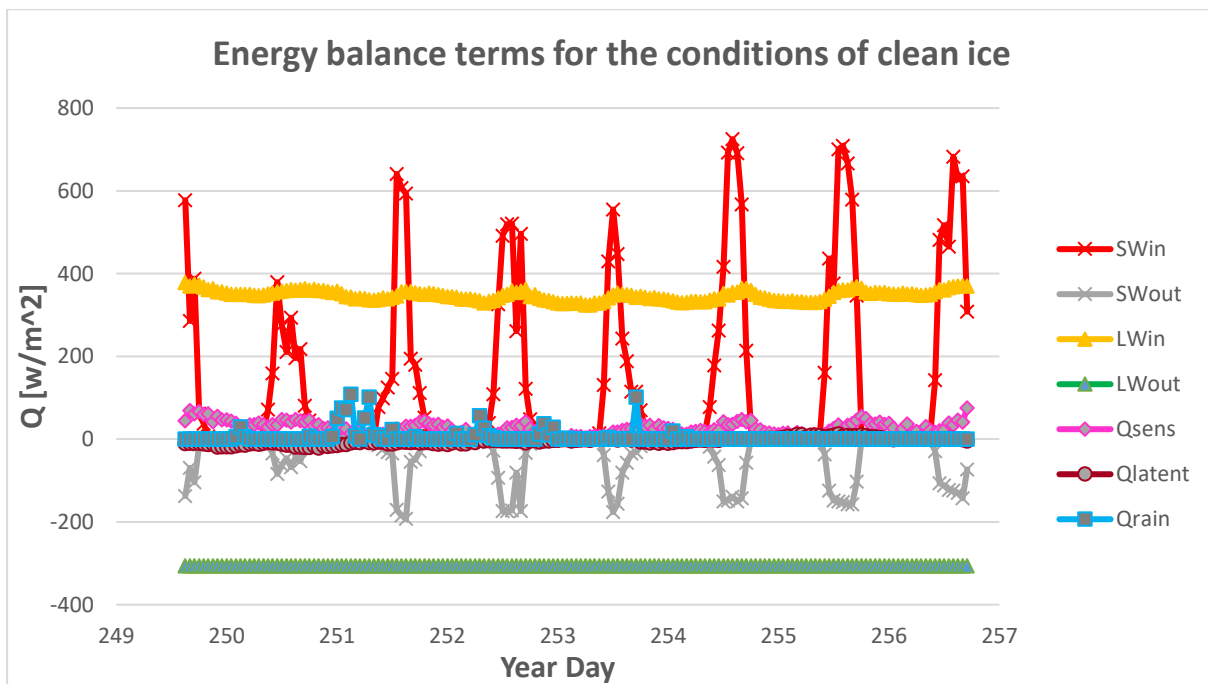
Figure 18: Display of all the included energy sources for the EBM for the conditions of clean ice on the glacier for the first week.

Figure 18 displays the behaviour of the different energy sources available for the melting of glacier ice for clean ice conditions. The available energy is the sum of the underneath area of the respective curves. Of course, there are two curves going clearly below 0 w m^{-2}. Those are the outgoing short- and longwave radiations. Those have to be added to their respective incoming counterparts to result in a

new, for this plot, hypothetical curve. And the sum of the area, which is the integral of the respective function, equates to the respective energy available for melt. It is well visible that the *SW* plays a major role in the EBM. Q_{sens}, while continuously available, plays a smaller role in the EBM. *LW* is similar to Q_{sens}. Q_{rain} is way smaller and Q_{lat} even takes a total negative amount of energy in the EBM. The proportions of total energy available for the first week for clean ice conditions or as follows:

SW ≈ 59 %, *LW* ≈ 24 %, Q_{sens} ≈ 16 %, Q_{lat} ≈ -2 %, Q_{rain} ≈ 3 %

After having calibrated the EBM, the next step is to scale down each of the energy balance terms above to fit the cumulative melt measured under the cover S. This was done by assigning a factor to each of the terms on the right side of Equation 19 with a respective factor. This was done by using MC and GAP. Each of the simulations were done $10*10^5$ times. The reason for the use of both approaches was described in chapter 3.3.3. The best result was achieved with MC, scoring 0.318853160538206 for *RMSD* (*S*). The best result from GAP was 0.321623221414 for *RMSD* (*S*). Thus, the following factors resulting from lowest RMSD-score based on MC were used to scale the energy terms from the EBM down to fit the cumulative *S* melt:

SW: **0.136102617**

LW: **0.766905189**

Q_{sens}: **0.053635657**

Q_{lat}: **0.093529701**

Q_{rain}: **0.96109122**

The top 40 results of MC and GAP can be seen in Appendixes E and F.

With the calibration of the EBM to be scaled down to the melt under geotextile, the new EBM looks as follows:
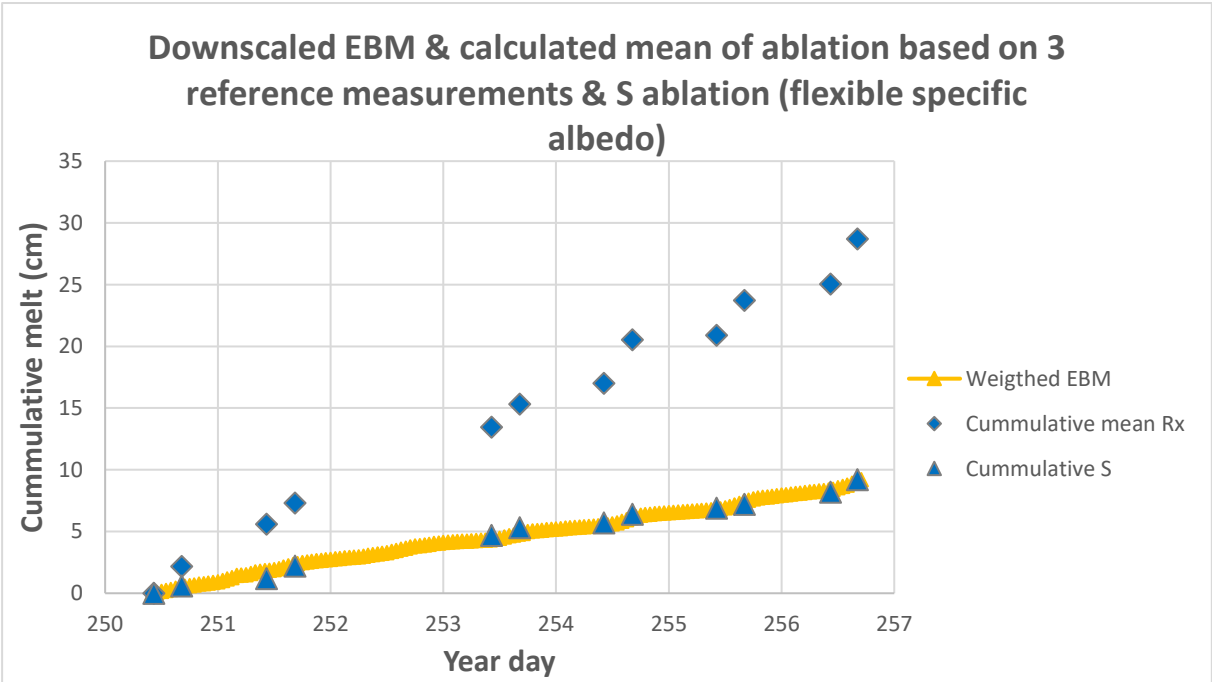
Figure 19: Calibrated EBM with Rx and S melt measurements depicted in it as well for the first week for covered ice conditions.

The respective calibration parameters are again displayed in the table on the next page:

Table 5: Display of the MC-based best-found model parameters for the EBM as well as the RMSDs for Rx and S respectively. RMSD (Rx) does not play a role a role for this model anymore since that is the reference score for clean ice conditions.

SWin	0.136102616787
SWout	0.136102616787
LWin	0.766905188560
LWout	0.766905188560
Qsens	0.053635656834
Qlatent	0.093529701233
Qrain	0.961091220379
RMSD (RX)	**12.3367066630**
RMSD (S)	**0.318853161**

The *RMSD* (*S*) for conditions when ice is covered with geotextile, is in absolute terms way lower than the *RMSD* (*Rx*) for clean ice conditions as shown in Table 4. However, this does not necessarily mean that the calibration was more successful for clean ice conditions. One has to put this into relation. One approach to that is to compare the final and thus maximum melt measured for clean ice and covered ice concerning their *RMSD*s as depicted in the following formula:

$$\frac{Rx(f)}{RMSD(Rx)c} \approx 24.31 < \frac{S(f)}{RMSD(S)g} \approx 28.85 \tag{27},$$

where *Rx(f)* is the mean final cumulative melt measurement of the first week for the reference stakes, *RMSD*(*Rx*)$_C$ is the *RMSD* of *Rx* for clean ice, *S(f)* is the final cumulative melt measurement of the first week for covered ice (geotextile) and *RMSD*(*S*) is the *RMSD* for S for covered ice. With that, it becomes evident that the calibration for clean ice was more successful since the respective ratio is smaller.

4.4 eePDH-Dependent Work

As the reduction factor within the EBM for *SW* is defined, it can be translated directly into the eePDH in accordance with Equation 21 for the temperature-independent term in the model. And also, based on MC, *ft* was calibrated with the base of *f1*. Thus, *f1* and *ft* in this case are:

$$f1 = \mathbf{0.136102617} \tag{28}$$

$$ft = \mathbf{0.822569907} \tag{29}$$

With those two factors, the novel eePDH can be calibrated as displayed below.
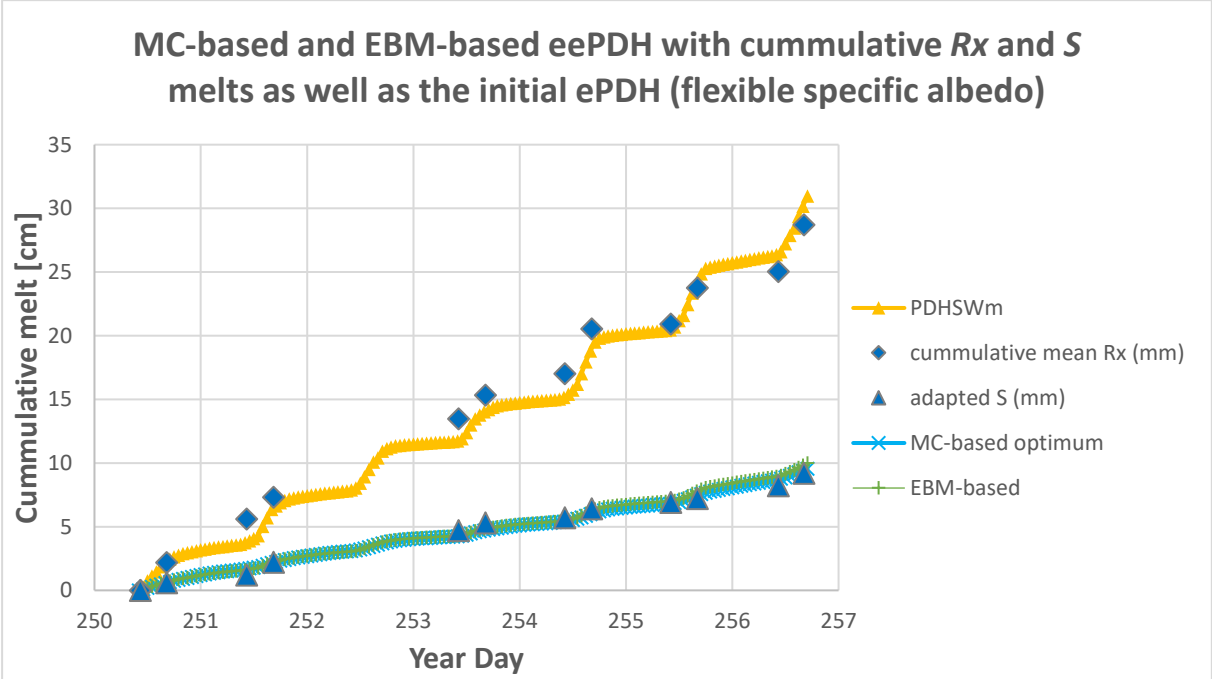
Figure 20: EBM-based calibration and MC-based calibration of the novel eePDH for covered ice conditions with Rx and S melt measurements depicted as well as the initial ePDH.

This is the novel eePDH, with two approaches to calibrate it appropriately. The EBM-based approach has been explained thoroughly so far. However, an additional approach to calibrate the eePDH, just for comparison reasons, was defined based solely on MC. One can see that the two calibration methods are pretty similar. The MC-based one has a slightly lower *RMSD score* as shown in Table 6.

PDDMF_SW	0.199974054
SWRF	0.039267731
ASWRF_MC	0.071247518
AT_MC	0.995161891
ASWRF_EBM	0.136102617
AT_EBM	0.863897383
RMSD **(Rx) (MC-based)**	12.295901411
RMSD **(S) (MC-based)**	0.360438058
RMSD **(Rx) (EBM-based)**	12.099443185
RMSD **(S) (EBM-based)**	0.435782563

The adaptation factors based on the two approaches vary to some degree. The reason for the implications this has for the overall novel model, will be addressed in the following chapter.

Now, the time extension of the novel model into the second week is the next necessary step to being able to validate the model. However, before that, the aforementioned data issue needs to be addressed here as well. As the WS did not last through the entirety of the two weeks, specific *SWin* as well as air temperature data was required to be able to extend eePDH into the second week. The extrapolation with temperature was well manageable. However, the announced difference in *SWin* needs some further focus here.
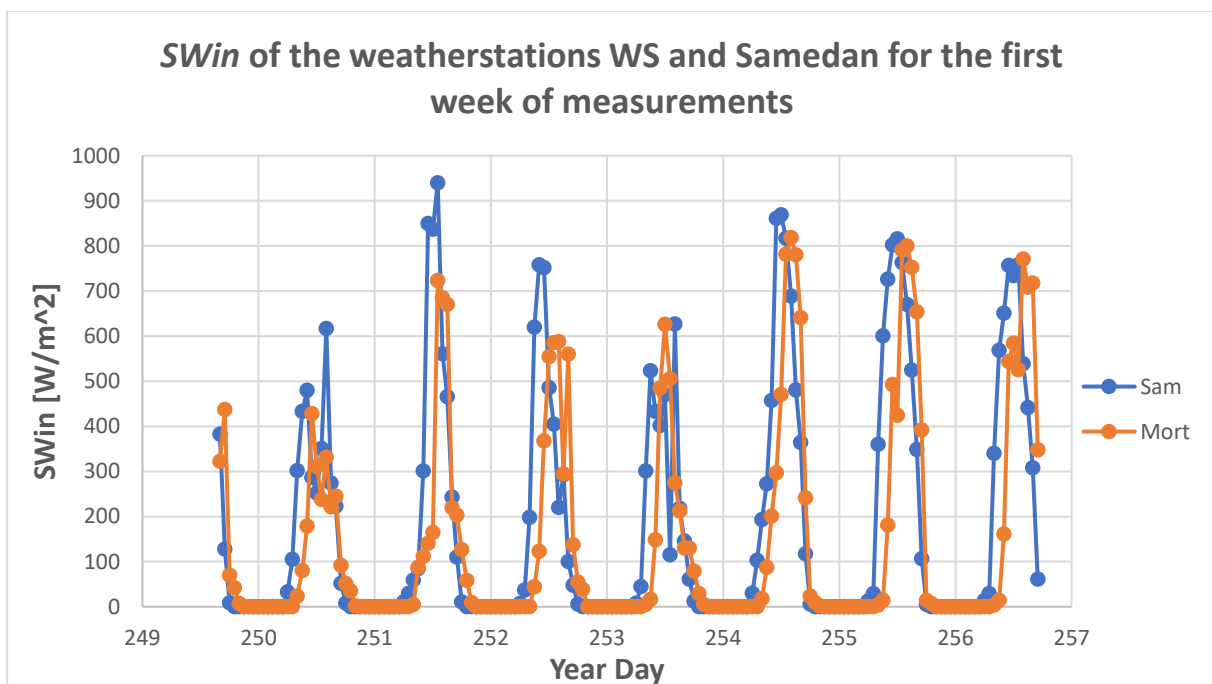
Figure 21: Display of SWin for the WS and Samedan for the first week of measurements (MeteoSchweiz, 2022).

What becomes visible, is that Samedan has an earlier start with *SWin* every day, the maximums tend to be higher than on the Morteratsch glacier, and that it ends a little earlier every day in the evening. According to the data, Samedan has close to 25 % more *SWin* through this week (MeteoSchweiz, 2022). This needs to be remembered for the Interpretation of the extension of the eePDH to the second week, as this surplus of *SWin* is capable of affecting the model immensely (MeteoSchweiz, 2022).
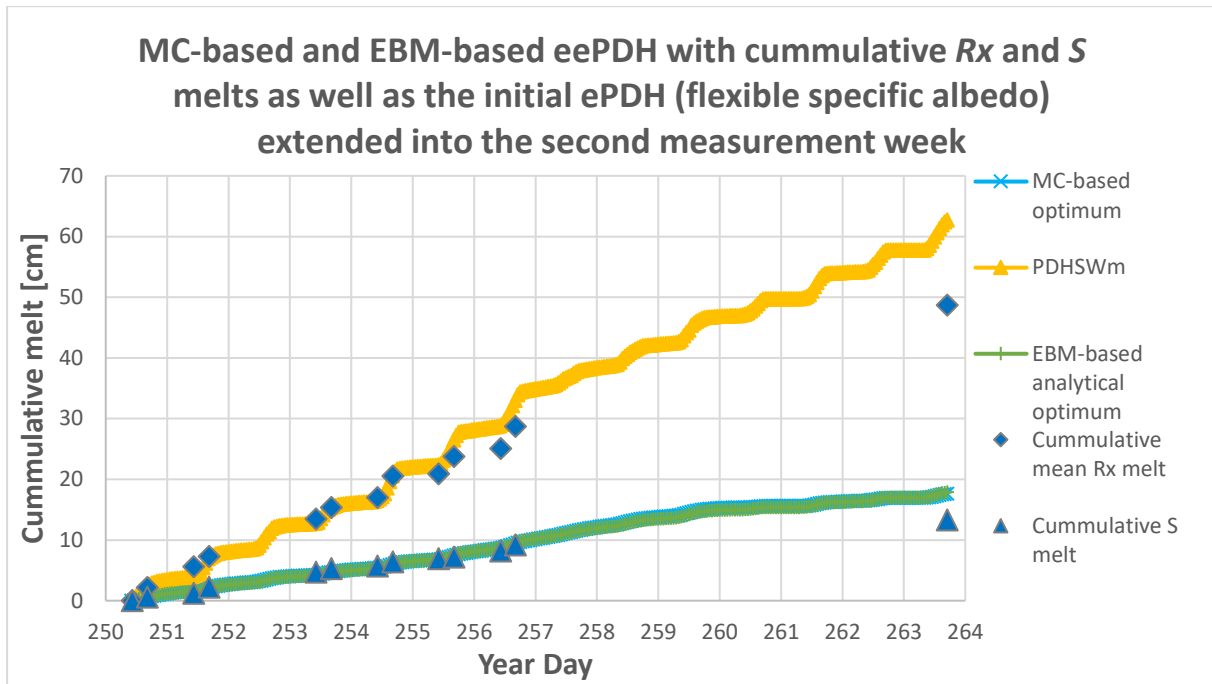
Figure 22: EBM-based calibration and MC-based calibration of the novel eePDH for covered ice conditions with Rx and S melt measurements depicted as well as the initial ePDH, extended for both weeks of measurements.

For validation purposes, the eePDH has to be extended to the second week to be able to test the efficiency based on data independent for calibration of the model. Basically, the data for the second week of measurements from the weather station in Samedan was added to the already-existent data from the WS on the glacier to construct the model for the entire period of measurements. The result looks promising. While the initial ePDH for clean ice shoots severely over the final field measurement, the two approaches to scale down the model (eePDH) to account for geotextile cover on the glacier ice look quite all right visually. They also overestimate the melt in the long run.

Table 7: Display of the MC-based best-found model parameters as well as the analytical EBM-based best-found model parameters for the eePDH as well as the RMSDs for Rx and S respectively, extended for the second week of measurements. RMSD (Rx) does not play a role anymore for this model.

PDDMF_SW	0.199974054
SWRF	0.039267731
ASWRF_opt	0.071247518
AT_opt	0.995161891
ASWRF_EBM	0.136102617
AT_EBM	0.822569907
RMSD **(Rx) (MC-based)**	12.42030995
RMSD **(S) (MC-based)**	1.283442741
RMSD **(Rx) EBM-based)**	14.762933
RMSD **(S) (EBM-based)**	1.370837052

The *RMSD* (*S*) for both approaches shows a result of the estimate deviating from the observations by about 1.2cm – 1.5cm on average. Interpretations of the reasons for those values follow in chapter 5. With that, the research question 2 has an answer. For that, an EBM-based answer will be used. It can be stated that the results of Equations 28 and 29 are the answer to research question 2. The shortwave term in the eePDH has to be reduced by a factor of **0.136102617** and the temperature-dependent tern has to be reduced by a factor of **0.822569907**. Concerning the working hypothesis, based on the initial

thought, it was correct to assume that the temperature-independent term needs to be scaled down way more than the temperature-dependent one.

Finally, the additional model efficiency criterion scores are displayed in the following table. Those involve the Nash-Sutcliffe efficiency criterion (*NSE*) as well as the Kling-Gupta efficiency criterion (*KGE*). For both efficiencies, the specific scores have been calculated for the two different calibration approaches for the eePDH, for the first and second week as well as for both weeks together. The results are displayed in the following table.

Table 8: Model efficiencies, based on efficiency criterion (NSE/KGE), calibration approach (MC/EBM), and time frame (both weeks/second week/first week).

Total MC-based NSE	-0.517337232	**Total MC-based KGE**	0.289130988
Total EBM-based NSE	-0.739905673	**Total EBM-based KGE**	0.273136272
2nd week MC-based NSE	-5.183898474	**2nd-week MC-based KGE**	-6.51695E+14
2nd week EBM-based NSE	-5.943264061	**2nd week EBM-based KGE**	-6.99905E+14
1st week MC-based NSE	0.302172135	**1st-week MC-based KGE**	0.448130121
1st week EBM-based NSE	0.173872315	**1st week EBM-based KGE**	0.523976733

It is visible that for NSE, the MC-based approach batters the EBM-based approach since the perfect score for the NSE criterion would be 1, and anything short of that is a smaller number than 1, going to - ∞ (Cooper, 2010; Knoben, Freer and Woods, 2019). Frequently, scores above 0 are considered viable when it comes to *NSE*. This applies only to the first week though, which can also be regarded as the respective score for calibration. However, validation usually is based on feeding the model completely independent data, which in this context would mean that the proper validation is the second week. Now, for the data from the second week, both scores do not look promising. What the reasons could be for that, will also be discussed in the fifth chapter of this thesis. Going over to the *KGE*, a similar result is depicted. While the overall scores for both weeks as well as for the first week look viable, it is especially the second week which suffers from bad scores, as it is argued that about -0.42 is the benchmark for KGE viability. Again, the first week can be considered in this case as a calibration score as well (Knoben, Freer and Woods, 2019).

5. Discussion

5.1 Interpretation of the Model Independent Work

5.1.1 Deployment and Instruments

Starting off with the deployment, the two covers placed did reduce the ablation significantly as is visible in Figures 5, 8 and 23. The fixation of the covers with rocks was a suitable approach since it did not require either further synthetic materials which could pollute the glacier or the water resulting from ice melt, nor did it require further material to be transported onto the glacier. Rocks and debris can be found on the glacier. Using what is already there does not change the circumstances significantly when measuring. The only problem was that the rocks holding the geotextile down would heat up during the day and then radiate thermal energy which would then increase the melt of the ice at the corners of the cover. A suitable approach to reduce that effect and thus the influence of the rocks onto the covers and their connected measurement would be to drop the rocks into bags made of the same geotextile (Senese *et al.*, 2020). This realisation came after the fieldwork was already completed. Considering the layering, it can be assumed that using two layers of cover surely made sense as was suggested previously (Olefs and Fischer, 2008). No quantified comparisons of the number of layers were measured since that is outside the scope of this thesis. However, it would certainly make sense to analyse the differences in melt reduction effect based on the number of cover layers further in the future.

When it comes to the ablation stakes, the approach to measure ablation with them was viable. Having stakes measuring the clean ice ablation as well as the covered ice ablation is not a novel approach when researching glacier ablation under covers (Olefs and Fischer, 2008; Senese *et al.*, 2020; Liu *et al.*, 2022). In the case of this thesis, it can be argued that the number of stakes was suitable for the size of the deployment at hand. However, more stakes and measurements could increase accuracy and reduce uncertainty. The holes dug to insert the ablation stakes were not found to have a notable effect on the overall ice melt around them.

The next part of the deployment are the iButtons, which were spread across the deployment to measure temperatures. Regarding the measurement precision, it was quite on point as is to be expected from such instruments. They had a slight deviation which was corrected after the entirety of measurements by putting all used iButtons into an ice bath for about five hours (30.09.2022, 10:49). Even though the height of the iButtons above or within the ice was measured approximately, if that data was used for instance to model vertical temperature flux above the ice or the temperature gradient within the upper ice layers, more exact measurements of the distance of iButtons to ice surface would be required. That data could be potentially used for the EBM to increase its complexity, but also its accuracy.
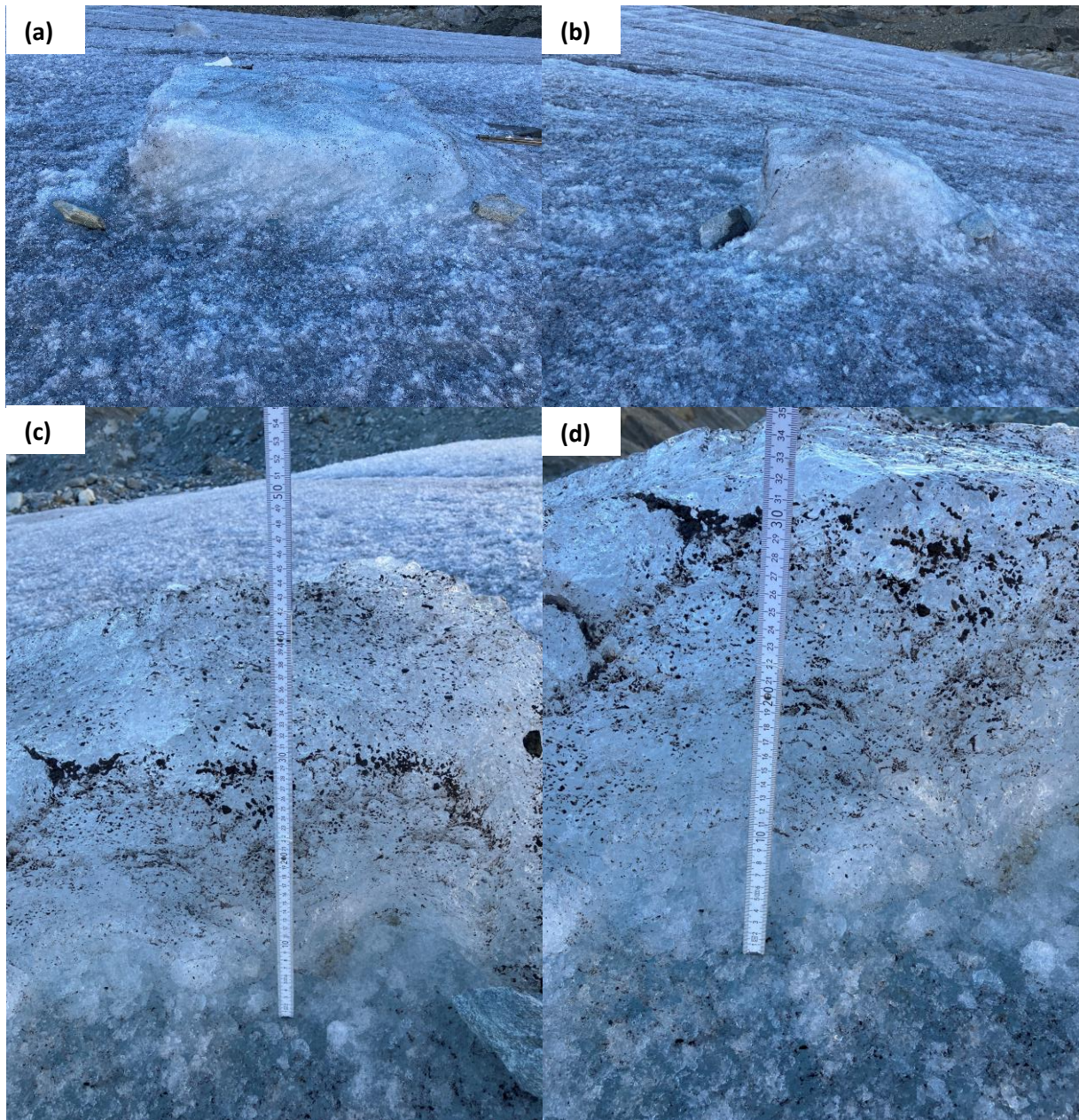
Figure 23: (a) B after measurement period and removal of the cover, (b) Analogue for S, (c) relation of size of B with a ruler from the upper side, (d) analogue for S (20.09.2022, 16:41).

The WS was crucial to the experiment since it provided essential data (Pellicciotti *et al.*, 2005; Olefs and Fischer, 2008; Carenzo *et al.*, 2009; MacDougall, Wheler and Flowers, 2011; Oerlemans, Haag and Keller, 2017; Senese *et al.*, 2020; Liu *et al.*, 2022). The instruments themselves seemed to be accurate with their measurements after having consulted the data, with the exceptions of the blunders as discussed in chapter 3.1.2 (precipitation measurement and Davis Cup), which were corrected afterwards. The conditions of their measurements changed nonetheless as the metal bar of the WS holding all the devices tilted. The interpolations of the faulty precipitation measurement and the interpolation of the missing wind data add some uncertainty to the experiment. However, that uncertainty is assumed to be rather low, since the corrected precipitation is assumed to be right after correction and the wind data is mostly similar throughout the day. As for the WS overall, therein lies a likely shift of the measured data. One has to be aware that the WS tilting brings another source of uncertainty into the modelling aspect. For future fieldwork, it can be recommended to either use a

tripod as a base for the WS, fix the WS with strings into the ice, or at best a combination of both. The possibility of the WS tilting was overlooked during the planning. The degree of tilt is shown in Figures 24 and 25.
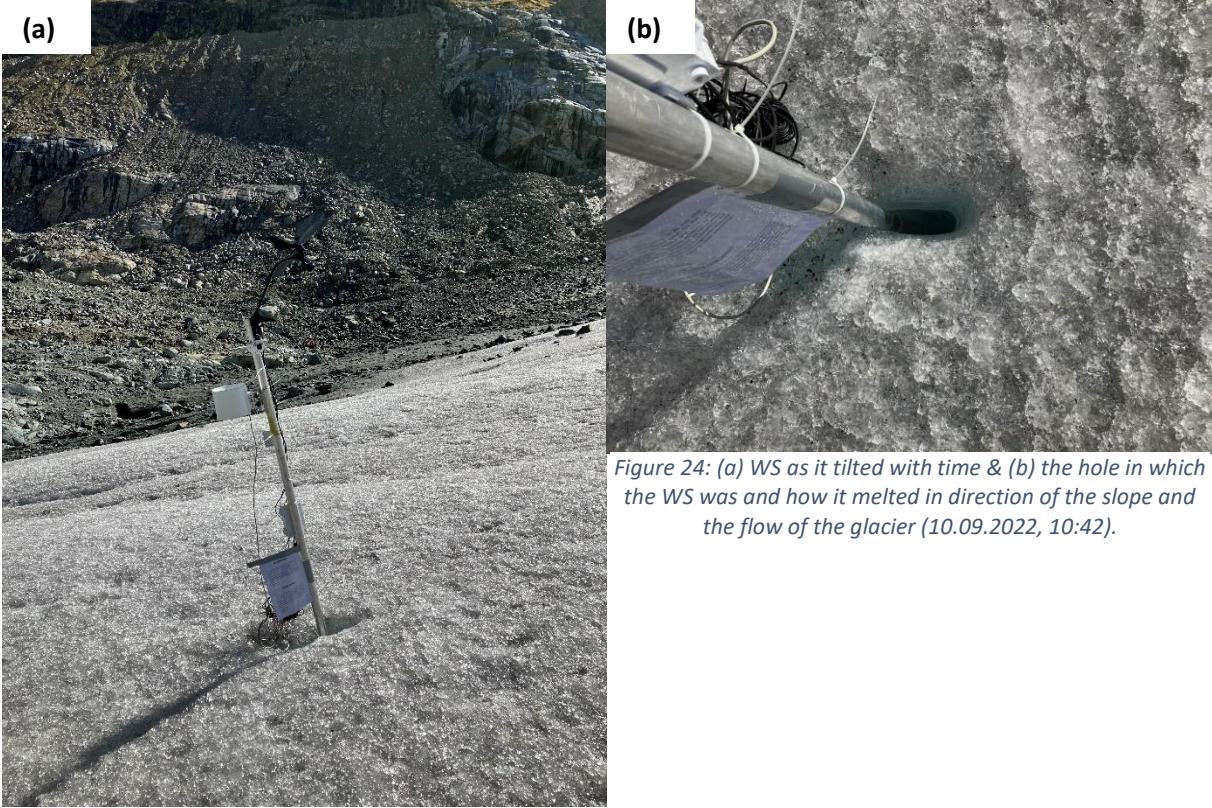
Figure 24: (a) WS as it tilted with time & (b) the hole in which the WS was and how it melted in direction of the slope and the flow of the glacier (10.09.2022, 10:42).

Figure 25: The WS after returning to the glacier for the final measurements with a week of absence (20.09.2022, 15:55).

5.1.2 Manual Data Acquisition Through Field Work

The first as well as the final part of the data acquisition is the exact description of the measurement locations, involving latitude, longitude, altitude, slope aspect, and exposition angle (Pellicciotti *et al.*, 2005; Olefs and Fischer, 2008; Carenzo *et al.*, 2009; Senese *et al.*, 2020). As introduced in the methodology, measurements were taken multiple times and the median of the results was taken to keep human measurement blunders as low as possible. Potential deviations would result in a slight *Icf* deviation which would barely affect the model since the *Icf* is based on some assumptions and simplifications as is explained in Appendix D. However, the data deviation based on the tilted WS in combination with deviations in the location measurements could multiply uncertainty. This could be regarded as a propagation of uncertainty.

One potentially major source of uncertainty is the manual measurement of ablation based on ablation stakes. Even though the measurements were taken always in the same way paying close attention to the setting of the ablation disk, the stake, and the ruler, and with multiple measurements being done and the median taken, measurement blunders are probably still existent. Automated approaches to measure ice melt on such as scale could be useful since they would increase measurement consistency. However, there are not too many options for that. Further instruments are necessary. And what the deployment would look like with such instruments, would need to be elaborated thoroughly to minimize the impact of the presence of such instruments on glacier melt by throwing shadows (MacDougall and Flowers, 2011; Senese *et al.*, 2020). In the case of rather narrow ablation stakes, that effect can be neglected. That argument is made based on the realization that none of the consulted literature addressed this issue which led to believe that it is neglectable.

Almost analogue to the measurement of the glacier ablation based on the stakes, the same blunders and possible uncertainties apply to the measurement of the albedo with the hand-held device (Apogee Albedometer). And while paying close attention to the device (altitude above the ice, horizontal angle concerning the holding bar), making multiple measurements from four different sides, and taking the median of the respective measurements, some slight deviation and thus uncertainty can also be expected for the albedo measurements. Again, this source of uncertainty has also to be regarded in the context of uncertainty propagation.

5.1.3 First Data Analysis

Aside from the aforementioned uncertainty sources, which were corrected as well as possible, no direct source of uncertainty for the analysed data could be found for this chapter.

The measured ablation gives a viable picture (see Figure 8). As *SW* is the main driver for glacier ice melt in the Alps, the daily variation in melt is well visible for the clean ice and even for the covered ice (Hock, 2005). Interestingly, R1 was the reference ablation stake with the smallest ice melt measured out of the three in the first week. However, for the final measurement in the second week, it overtook R2 with the measured melt. That could be due to chance. The microtopography on the glacier changes steadily as it melts. And since meltwater on the glacier can reduce the albedo, more melt could occur on that specific spot (Hock, 2005).

Part of that can actually be explained by albedo as for R1 the albedo was constantly higher during the first week, while for the final measurement in the second week, it was lower. The overall consistency of the three reference measurements, however, indicates that the approach to the measurements was accurate to some degree. The difference in the references to the WS-based albedo measurement turns out to be difficult to explain. One possibility is that the sensors from the WS either had a different sensibility to *SW* than the sensors from the Apogee Albedometer. Another possible interpretation could be that the metal bar of the WS as well as some of the instruments from the WS, which are

mostly white, were located in the viewshed of the sensor measuring *SWout* thus increasing the amount of measured reflected light which leads to an increase in albedo.

The higher albedo has however significant implications for the entire modelling process, as for the first week of measurements, both the ePDH as well as the EBM used the data from the WS as sources for the temperature-independent model terms. This increases the uncertainty to a high degree. The reason for taking that data is that albedo fluctuates throughout the day, as is visible from Figure 9 since that is dependent on the amount of water on the glacier (Hock, 2005). For further approaches in the research of melt reduction strategies and the use of AWSs, it is advised to use multiple AWSs and one should be kept separate solely for measuring *SW* and nothing else due to the high sensitivity of the *SWout* measurements. As for the covered areas, their albedos differ immensely as well. There is a simple and rather probable explanation for that. S has only a 1m^2 surface area while B has a 4m^2 surface area. The albedometer was held about 1m above the surface. The sensors of the albedometer have probably a vision angle of at least 45° in all directions. With that, the lower sensor probably measured clean ice surrounding the cover as well for S. Thus, the albedo data for S is falsified. B has a higher albedo since presumably surrounding ice was not caught by the lower sensor while measuring.

Regarding the fluctuations over time for all albedo measurements, these can be partly explained again by the amount of water on the glacier. There might also be the effect of dust being blown onto the glacier ice as well as onto the covers. However, by the end of the measurement period, albedo increased for all locations as compared to the final measurement of the previous week. This is contrary to what was found in literature, namely that the albedo of covers tends to decrease with time due to dust and similar being blown onto the cover and settling there (Olefs and Fischer, 2008; Senese *et al.*, 2020). The divergence of findings between consulted literature and self-measured results can be explained though. Two reasons can be named. First, the time horizons between the experiments in the literature and this one differs immensely. While other experiments kept the covers over multiple years, this experiment only lasted two weeks. It was too short to experience dust deposition to such a high degree so that the albedo would be changed permanently. The second reason is that none of the consulted literature addressed the possibility of the albedo of the covers increasing after precipitation events in the form of rain. After rain events, when the deployment was approached for the daily measurements, it was visible from afar that the albedo of the covers increased. Rain was probably capable of washing away the dust from the geotextile which increased its reflectance. The data suggests that rain affects the albedo of not only the covers but also the ice itself. A comparative normalized plot of the WS-based albedo and the precipitation measurements is displayed in Figure 26.

Concerning the temperature measurements of the iButtons on B, ANOVAs were calculated for all aforementioned combinations. The null hypothesis is that there is no significant difference in variance between the considered iButtons. In none of the cases was there a significant difference in variance between the iButtons. Thus, none of the null-hypotheses can be rejected.
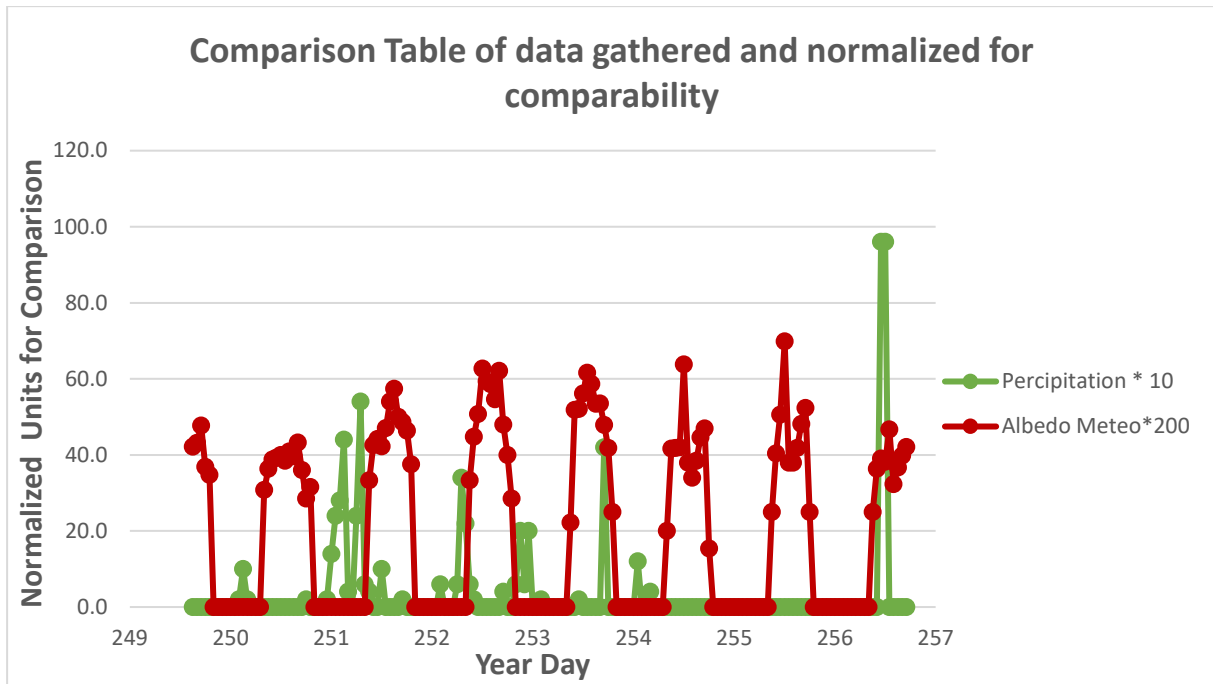
Figure 26: Comparative normalized data of precipitation and WS-based albedo. Albedo tends to increase after precipitation events.

The extrapolated melt rate comparisons between clean ice and cover, respectively for day and night, leave room for speculation as to why occasionally the change of melt rate under the cover does not behave similarly to that of the clean ice. An assumption is that underneath the cover, physical processes on a micro-scale take place, which could perhaps be modelled by a more sophisticated EBM. Further research is advised, perhaps even in laboratory conditions to be able to fully understand those microprocesses. As the EBM already suggests, linearity in those physical processes cannot be assumed (Munro, 1989; Brock and Arnold, 2000; Hock, 2005; MacDougall and Flowers, 2011; MacDougall, Wheler and Flowers, 2011).

Overall, in the fieldwork as well as in the primary data analysis, various sources of uncertainty were present. It is important to keep track of those and keep them in mind as the research progresses since those can affect all models that were used.

5.2 Interpretation of ePDH-Dependent Work

5.2.1 Generation of the ePDH

Concerning the generation of the ePDH, it is safe to say that the additive model version D (initial journal article) is suitable since the measurement period is short enough that daily variations in temperature, as well as *SWin*, could have a significant impact on the model output. Further, to simplify the approach, the assumption about the missing time delay between energy input and surface lowering due to melt makes this study possible (Pellicciotti *et al.*, 2005). While the TIM can be of some use, it disregards *SW* as one of the major energy sources for melt (Hock, 2005; Matthews *et al.*, 2015). That is why later research tends to use the PTIM (MacDougall, Wheler and Flowers, 2011; Fuchs, Asoaka and Kamaza, 2013; Carenzo *et al.*, 2016). Perhaps, one of the major differences between the initial PTIM and ePDH as used in this thesis, is that the PTIM tends to use α to determine the net *SW* balance, which can be based on measurements of *SWin* and *SWout*, or on an empirical and fix α, while the ePDH explicitly makes use of direct measurements of *SW* (Carenzo *et al.*, 2016). The problem with the approach of a fixed α in time is that it does not represent reality well as α does vary in time, as was suggested by literature and also proven to be the case on the Morteratsch glacier (Hock, 2005). Multiplying temperature with radiation makes physically not much sense as already mentioned. Multiplication of those two terms while having a limit for both terms as to from which point on they cause melt means mathematically that both are considered a mandatory condition for melt (MacDougall, Wheler and Flowers, 2011). In other words, that model structure claims that there cannot be any melt if there is either no *SW* or no temperature above, in this case, 0°C. That might be unrealistic as well as melt can take place as long as there is enough energy affecting the system at hand. The source is irrelevant as suggested by the EBM (Brock and Arnold, 2000; Hock, 2005; MacDougall and Flowers, 2011; MacDougall, Wheler and Flowers, 2011)). That is the reason why no multiplicative model was chosen for this thesis. As for the PTIM, it has been shown that it works very well at a point scale for alpine glaciers, which is what this thesis researches (Silwal *et al.*, 2023).

Another addition, which diverges from the former PTIM (model D), is that the ePDH in this thesis has an additional factor built in, namely the *Icf* (Pellicciotti *et al.*, 2005). Assuming that the entirety of the *SWin* can be used to melt glacier ice, is somewhat naïve. This can be explained well by a hypothetical example. Let there be a measurement device somewhere in the far north, let us say in Greenland in spring when there is more daylight in 24h than there is not. The device is positioned to being able to measure the maximum possible amount of *SWin*. If the angle of the device is set right, it will measure a lot of *SWin*. Yet only a fraction of that *SWin* will be utilized for melt since due to the flat angle of the *SWin*, the radiation cannot enter the ice effectively (Hock, 2005). The same applies to the Morteratsch Glacier but to a lower degree. According to the calculation (Appendix D), the *SWin* only gets reduced by about 12 %. This factor, while still somewhat simplified and generalized, makes sure that *SW* and its impact on glacier surface melt does not get overestimated. Therefore, this approach gets the ePDH closer to physical reality than the PTIM while still maintaining the same data requirements.

When it comes to uncertainties though, every model which is calibrated encapsulates uncertainty with each model parameter. While the inclusion of the *Icf* moves the model arguably closer to reality and thus reduces uncertainty, the definition of the *Icf* for this thesis itself is based on assumptions and generalizations which again involve uncertainty of the model parameters.

5.2.2 Calibration of the ePDH

First of all, what differs in this approach to calibrate the TIM at hand, namely the ePDH, is that the ePDH was not calibrated against the values of an EBM as it is the case otherwise. Usually, only the EBM is calibrated against field measurements directly (Pellicciotti *et al.*, 2005; MacDougall, Wheler and

Flowers, 2011; Carenzo *et al.*, 2016). A combination of three reasons justifies why the approach in this thesis can be viable. First, the overall measurement period was rather short with a high frequency of field measurements. The amount of data per given time allows for a distinct picture of the diurinal behaviour of the glacier surface melt. Secondly, the approach is based on a point scale. All the measurements were taken so close from one another spatially that assumed differences can be regarded as neglectable. Finally, the defined EBM for this thesis is simplified in some points making it perhaps a slightly less physical model and thus involving more uncertainty than it should have to compare other model results to it. If one compares other model results to the EBM, it is based on the assumption that the EBM at hand is very accurate and thus representative of reality. With the simplifications and assumptions involved in this less complex EBM at hand, making the assumption that it is a good representation of reality is slightly off. Due to this, comparing other models to it would increase uncertainty again, which is tried to be kept as low as possible under the given circumstances.

Next, the interpolation approach of the data at hand needs to scrutinised. As it was described in the methodology chapter, the measurements for the ablation stakes were not conducted exactly during a full hour, while the models predict melt exactly to the full hour. The choice of interpolation method is a linear interpolation. While it could be argued that other methods might be more accurate and closer to reality, the differences were so minor that the choice of interpolation is neglectable as the results would vary very little. The same applies to uncertainty in this context, as diverging values based on different interpolation methods are about as uncertain as ablation measurements. Linear interpolation is transparent and well understood. Therefore, it is used here.

Next, while calibrating a model, the model should be put into a context to being able to evaluate the accuracy of the model (Cooper, 2010). There is a great variety of contexts, or rather criterions such as the *NSE* (Gupta *et al.*, 2009; Cooper, 2010; MacDougall, Wheler and Flowers, 2011; Knoben, Freer and Woods, 2019), the *KGE* (Gupta *et al.*, 2009; Knoben, Freer and Woods, 2019; Pool, Vis and Seibert, 2021), the weighted coefficient of determination (ωR^2) (MacDougall, Wheler and Flowers, 2011), the mean absolute error (*MAE*) (MacDougall, Wheler and Flowers, 2011), or the mean percentage error (*MPE*). One of the simpler and perhaps more transparent ones is the *RMSE*, or as it was defined in this thesis in Equation 7, the *RMSD*. While some of the others are capable of describing a model more distinctly, it is argued that for such a novel approach to an inexistent model, it makes sense to keep the approach simpler in a first attempt. This is even more so the case, when the novel model is compared to direct field measurements which are associated with uncertainty as compared to the usual method to calibrate the model to an EBM. The usual approach, as mentioned afore, would not make sense here due to limited resources and with-it associated simplification and increased uncertainties. While the *RMSD* cannot answer questions about the origin of the deviation of model performance as for instance a *KGE* could, it enables an easier understanding of the approach, and the basic results and therefore also swifter potential for improvement as well as clear sources of uncertainty.

With only two empirical factors to be calibrated, the calibration approach can be automated. One of the simpler and more prominent automated calibration approaches is the Monte Carlo simulation, which can be used to run a large number of simulations for any number of parameters while also defining the parameter boundaries (Seibert and Vis, 2012). A large enough number in this thesis is considered to be 100'000. This applies to all Monte Carlo simulations done in this thesis. It is argued that especially for two empirical parameters to be calibrated a MC with the given number of iterations is suitable to calibrate the model accurately. Proof of that can be found in Appendix E, where even for the case of calibrating five parameters (part of the EBM downscaling results), the *RMSD*s vary only very little within the best-achieved results.

The programming of the simulations was done, as all modelling was done, in MS Excel. As it was shown for EBM, this software allows to program MC as well as GAP which proves to be a viable tool to use when dealing with TIMs, EBMs, and perhaps even other models (Brock and Arnold, 2000).

Considering the results of the calibration, the model appears to have been calibrated quite all right. The *RMSD* indicates the same as shown in Table 3. The best-found pair of empirical factors to calibrate the model is higher when compared to scientific literature using the PTIM (Pellicciotti *et al.*, 2005; Fuchs, Asoaka and Kamaza, 2013). The presumed reason as to why that is the case is, again that the measurement period within the context of this thesis was two weeks while the others were at least a year long. Considering seasons and thus differences in *SW* and temperature, the variation is strong. Further, even if all conditions were the same, there is no guarantee that the empirical factors would turn out to be very similar due to different geographic conditions. While it can be assumed that closer glaciers might have a greater opportunity to have similar conditions, it is still no guarantee. Thus, due to an immense difference in circumstances, the parameters are not directly comparable. Consequently, no uncertainty estimation can be derived from such comparisons.

Concerning the sensibility of the parameters, it was found that the *SWRF* is immensely more sensitive than the *TF* which is in line with the findings of the journal article defining the PTIM (Pellicciotti *et al.*, 2005). A direct comparison, however, is not possible due to two reasons. First, the circumstances are again so different from the two studies (different measurement periods, different geography, slightly different model). Secondly, the model in the previously cited journal article uses *NSE* as its efficiency criterion for modelling, calibrating, and validating, while in this thesis the *RMSD* is used.

What is crucial to address, is the fact that all the models have their starting date on 07.09.2022 at 10:00. The measurement period, as mentioned in the previous chapter already started on 06.09.2022. The reason for the exclusion of the first day came to be after initially having modelled everything with the first day included. As can be seen for the ePDH in Figure 14 as well as in all the other models later, there seems to be an underestimate of the melt in the beginning of the period and later an overestimate. That was even more so the case for all the models while having included the first day of measurement as well. One potential and arguably rather probable interpretation of that is that there were some adaptation effects taking place. The entire deployment was built within 24 hours. After completion, the measurements started immediately. The reason for the rush was a potential time crunch. The measurements took place in September. During that time of the year, it is possible for such a place to have snowfall. If that were to happen, the measurements would have been disturbed to a point where lots of acquired data would not be useful anymore. Thus, there was a great interest in acquiring the data as soon as possible to have useful data. After the realization that such adaptation effects could be at least part of the reason, why the models overestimate melt in the beginning and later underestimate it, the decision was made to adapt all models to a new starting point, namely the current set starting date stated above. As all models were recalibrated to the new starting point, the model efficiencies all improved slightly which seems to indicate that such adaptation effects really are at least part of the reason for this over-/underestimation of modelled glacier ice surface melt. Thus, those adaptation effects also make up some part of uncertainty. These adaptation effects and all their implications apply analogue to all other models and parts of the modelling process.

5.3 Interpretation of EBM-Dependent Work

5.3.1 Generation of the EBM

Again, the assumption is given that there is no time delay between energy input and surface melt for the EBM either (Pellicciotti *et al.*, 2005). The formulated base model as depicted in Equation 19 seems to be viable. While there is a broad consensus on the terms *SW*, *LW*, Q_{sens}, and Q_{lat} (Brock and Arnold, 2000; Zekollari, Fürst and Huybrechts, 2014; Senese *et al.*, 2020), the presence or absence of other terms is up for discussion (Hock, 2005; MacDougall and Flowers, 2011; MacDougall, Wheler and Flowers, 2011). In the case of this thesis, it can be argued that the inclusion of Q_{rain}, while in literature being described as having a neglectably small influence on the energy balance, still had an overall effect of about 3 % on the point scale energy balance on the Morteratsch glacier. While it can be argued that 3 % is still very small, it has to be stressed that the intention of the EBM is to be as close to reality as possible. Thus, it was a good decision to include it. The exclusion of *Qg*, as described by MacDougall et al. (2011) makes sense, as that describes "… the energy released or absorbed by the subsurface when the snow or ice changes temperature.". While it cannot be denied that such processes take place, it is argued that in a period of two weeks, not much of the *Qg* occurred so that it makes it neglectable.

The translation of the energy balance to the equivalent of ice melted is straightforward and does not require much commenting except for the constants which are used as shown in Equation 19. Those constants are not necessarily as rigid as they seem to be. Ice density varies with temperature for instance. However, it is assumed that the fluctuations are so small that it makes the differences neglectable. Thus, *ρw* and *Lf* can be regarded as constants for the sake of this approach.

Next, all the terms involved in this EBM will be discussed. It starts with the temperature-independent term, the *SW*. *SW* is straightforward. Since the used WS measured both *SWin* and *SWout*, that data can be taken and fed into Equation 12. Aside from that, there is the *Icf* as well in the temperature-independent part of the EBM as it is in the ePDH. *SW* is simple to model and calculate. Yet, three sources of uncertainty can be named which were already addressed previously to some degree in other contexts. First, the *Icf* is simplified and generalized. Next, the occasional tilt of the WS during the first week could have an influence on the measurement devices. Last, but not least, as shown in Figure 9, there is a potential that the WS measured more reflectance from below due to the other white-coloured instruments on the WS being in the viewshed of the sensor. All this is important to keep in mind while interpreting the results. It could be that less ice melt was attributed to *SW* due to the higher albedo/higher *SWout* measured. It is difficult to quantify these deviations, especially in combination. It is advised that in further research in this field, these uncertainties are attempted to be minimized. Two out of the three could be removed by designing the WS differently as already suggested (2 WS, fixed with stings and standing on a tripod). The other uncertainty involves perhaps a dynamic and more accurate model of the *Icf*, dependent on the exact day.

Following are the temperature-independent terms. Starting off with *LW*, it had to be described in a simplified way. In a simplified way, *LW* can be described as being dependent on three different things: the Stefan-Boltzmann constant σ, temperature *t* (air and ice), and the emissivity ε (Brock and Arnold, 2000; Hock, 2005; MacDougall and Flowers, 2011). And while the first two are given, the ε is not. Defining it is rather complex and based on measurements and observations which were not done within the scope of this thesis. While the deployment was in place and measuring, there was no awareness that such measurements would be required from the beginning of this thesis. Thus, the approach to assume that there is simply a ratio between the ε of the sky and that of the glacier, which then could be calibrated, can be considered a viable approach under the given circumstances. For further research, measurement devices are suggested to be put on an AWS (Senese *et al.*, 2020). Otherwise, *LW* can also be modelled instead of measured directly if appropriate measurements are

prepared and done accordingly (Brock and Arnold, 2000; Hock, 2005; MacDougall and Flowers, 2011). The relation between the ε of air and glacier surface was assumed to be slightly above 1 (not more than 1.1). Admittedly, this assumption is based on insights from a course taken before dealing with EBMs. However, even without that assumption, the ratio turned out to be in the expected region based on MC as was shown in Table 4. ε was thus calibrated for purpose. First of all, ε varies with weather conditions, consequently with time, and is thus not constant. Second, this derived ε cannot be used in any other context than this thesis, since it is dependent on this specific data. It is important to keep this uncertainty in mind.

Next, the turbulent heat fluxes were also defined. While the complexity of them has been already addressed in the methodology, the point worth discussing is the C_{trans}. Such a coefficient is viable when surface roughness information is missing. It can be calculated or in this case empirically modelled (Braithwaite, 2009). Aside from ε, C_{trans} is the only other coefficient used to calibrate the EBM for this thesis. And while the entire heat fluxes are dependent on wind speed, vapor pressure, and air temperature and thus dependent on time, C_{trans} is arguably still slightly rigid since glacier surface conditions may change daily (Hock, 2005). Therefore, C_{trans} is a source of uncertainty per definition. Further uncertainties in the context of turbulent heat fluxes involve that the WS data, most likely wind speed though, was affected by the tilt of the WS to some degree. Temperature and vapor pressure are most likely unaffected since they, in the context of the EBM, do not have a direct and specific vector of flow. The uncertainty deriving from C_{trans} is arguably greater than that of the slightly deviated wind data.

Finally, the energy by rain being added to the system will be discussed. It being straightforward, not much uncertainty is involved in it except for one aspect. As Q_{rain} depends on the temperature of the rain, which was not acquired during the two weeks of measurement, a basic assumption was stated that the temperature of rain is equal to that of the surrounding air. Measuring rain temperature would have been one option. However, the implications of rain bringing energy into the system of the glacier surface could be defined in a more complex way as well. Aside from the temperature of the rain, the impact upon falling onto the glacier surface also releases some energy. It is assumed though that the portion of energy added by those means is neglectable.

5.3.2 Calibration of the EBM

Analogue to the ePDH, the calibration of the EBM involves also two parameters which were both calibrated with MC. And analogue to the ePDH, the calibration was successful as well as can be seen in Table 4. What becomes evident when looking at Figure 16, is that, again analogue to the ePDH, the model does underestimate the melt in the beginning and overestimates it in the end. The same reasoning as to why that is the case here can be derived from the argument for the ePDH.

The sensitivity analysis of the two model parameters is given in Figure 17. It seems as though that C_{trans} is way more sensitive than ε. However, if one accounts for the absolute values and the relative deviations of those for the respective parameters, it becomes evident that the first sight might be misleading. While in the sensitivity analysis, C_{trans} is increased by a factor of close to 5, ε varies only on a small percentage. However, it is inappropriate to also put the parameters into such a relation since depending on the parameter, its range of deviation might vary. So, one would have to contextualize the maximum range to be able to adequately and relationally represent the real sensitivity of each parameter. However, since it is not clear how large the ranges of deviation of both parameters are, since both parameters have been constructed to fit the purpose of this thesis, there is no adequate comparison existent to arrange a correct sensitivity analysis.

5.3.3 Downscaling of the EBM

The approach to downscale the EBM to fit the melt for the covered glacier area worked out well (Olefs and Fischer, 2008; Senese *et al.*, 2020; Geoproduct, 2021; Xie *et al.*, 2023). It is important to note that different automated approaches for calibration were used. There are multiple reasons for this. First, it is important, while doing something novel in a sense, which depends on automated calibration and not completely on a physical basis, that it can be double-checked if the result is a matter of mere chance. If both approaches achieve a similar result, it indicates a smaller probability of the fitting results just being achieved by chance. The second reason is to see if there is a great variability of possible solutions as compared to a very good one. The very good one can be expected from the GAP, since its iterative approach will narrow down the best result in a sophisticated procedure, while the MC could, with five parameters at hand, perhaps achieve good fits through various combinations of possible factors (Seibert and Vis, 2012). Comparing the results of the two approaches can be insightful as to how big the differences in factors are. If there is some level of accordance for all factors, one can perhaps also derive to some degree the physics behind it, or at least get an idea or inspiration on what experiments to design for future research (Appendix E & F).

In the case of this thesis, *SW* seems to be reduced to only about 10-15 %. Q_{lat} is frequently below 10 % weighting for the top 40 MC results. Q_{sens} shows a great variability in the top 40 MC results, but always in the lower 50 %. It is similar to *LW*, except that it shows a high variability in the upper 50 %. Q_{rain} seems to still have a major effect, even with the cover, since its weighting goes rarely below 60 %. This is in accordance with other findings (Huss *et al.*, 2021). And if compared to the GAP results, even if the numbers vary to some degree, in relative statements it can be said that *SW* and Q_{lat} experience a very strong reduction under such covered surfaces and Q_{sens} decreases strongly while *LW* and Q_{rain} seem to require only a slight reduction.

Figure 19 and Table 5 show that the results are all accurate. However, a few things have to be kept in mind while looking at those results. First, even while the new *RMSD* for the covered area is much smaller than the initial one for clean ice, relatively speaking the score is still worse if compared to the clean ice counterpart as was shown in Equation 26. Secondly, and even more importantly, this is a recalibrated model of an already beforehand calibrated model. Every calibration involves some uncertainties. And if a model is calibrated twice, once for the first purpose and then afterwards for a second different purpose based on the first calibration, the uncertainty is likely to propagate. And considering that even the base of the initial model, before even calibrating, is associated with numerous uncertainties deriving from fieldwork, data acquisition, and similar, then one has to be rather careful when looking at these results. Consequently, the results presented in this thesis constitute a first possible attempt at what the results may look like. Those results cannot be claimed to have an overall validity in every aspect.

5.4 Interpretation of eePDH-Dependent Work

5.4.1 Translation of Reduction Factors from EBM to eePDH

The approach to translate the factor for the temperature-independent terms of the EBM to the temperature-independent terms of the eePDH, as it was displayed in Equations 18 – 22, works under the assumption that both model terms model exactly only the temperature-independent fraction of the energy in the system of the glacier surface which causes melt. For the EBM part, that is definitely the case, since the core of the EBM is that it is a physical model. The model equations make it per definition impossible that there is a temperature-dependent component in temperature-independent term (Brock and Arnold, 2000; Hock, 2005; MacDougall and Flowers, 2011; MacDougall, Wheler and Flowers, 2011; Zekollari, Fürst and Huybrechts, 2014; Senese *et al.*, 2020). This might seem also to be the case for the PTIM and analogue for the ePDH, as temperature and *SW* are clearly separated (Pellicciotti *et al.*, 2005; MacDougall, Wheler and Flowers, 2011; Fuchs, Asoaka and Kamaza, 2013). However, it has to be argued that these are empirical models meaning that their empirical factors have to be estimated. For this study, this was done via automated calibration process, specifically via MC (Seibert and Vis, 2012). And even while 100'000 iterations were used to make sure to get a very exact result, the possibility, even while narrow, can still not be completely excluded that some part of the *SWRF* is based on temperature due to chance and the other way around. Yet, even if, that proportion is assumed to be very small.

Having said that, it is possible to translate the *f1* from the EBM to the eePDH directly. This does not apply to the *ft* for the temperature-dependent as explained in chapter 3.4.1. And since, with the previous assumption of *f1* being correct due to the aforementioned reasons, *ft* can be calibrated easily by the means of automated calibration. It is noteworthy that for this calibration, there is only one factor that needs to be calibrated. Thus, it can be argued that *it* could also be calibrated by the means of a regression model. However, MC was used here again for consistency reasons. Future work on this topic could focus on various approaches to calibrate the model.

5.4.2 Generation of the eePDH

It is important to stress that there is no known approach to extend a TIM for a specific synthetic cover. The only approach close to this is the extension of a TIM for existent debris cover on a glacier, also by including additional factors putting the glacier surface melt into perspective (Carenzo *et al.*, 2016).

With the two factors given to reduce the two terms of the ePDH respectively, as they are shown in Equations 27 and 28, the eePDH could be defined as in Equation 23 (Pellicciotti *et al.*, 2005). With the two factors and the formulation of the eePDH, research question 2 is answered. However, that answer is not definitive. It is to be understood as a first result within the context of a study with its uncertainties and limitations. More research has to be conducted to be able to give a very accurate answer to the second research question.

And starting to put this first answer to research question 2 into context is done by, instead of using the analytical, EBM-based approach to determine factor *f1* and afterwards *ft* with MC, both factors were determined by MC as a second version of the model to be able to compare it to one another. The results of both approaches are displayed in Figure 20 and Table 6. What becomes evident, is that the MC-based approach manages to deliver a better result according to the *RMSD*. The reason for this could be the afore-discussed sources of uncertainties within the EBM itself, be it data uncertainty or model uncertainty due to model structure. It is assumed that the integration of two empirical parameters (C_{trans} & ε) while not solely being empirical, but also simplifications due to a lack of data, measurements, and insights, is the core reason for the notable difference in calibration approach-

based model performance. It is unclear though as to what extent that is the case. As described before, a better EBM is required for future research on this topic.

5.4.3 Extension of the Calibrated eePDH to the Second Week

As it was described in Chapter 3.4.3, the extension of the model into the second week of measurements is based on data from a weather station in Samedan. The reasons for not using part of the WS data that is available for the second week was also explained and will not be discussed here anymore. The used data is solely *SWin* and temperature data as that is the required data for the eePDH. When it comes to the Morteratsch glacier, data from that specific weather station has been used in previous research (Zekollari, Fürst and Huybrechts, 2014; Zekollari and Huybrechts, 2018). And while it was claimed that data from that weather station is viable to use when modelling surface melt modelling, it is argued that in the case of this research, the viability must be questioned.

First of all, the aforementioned sources depended on precipitation and temperature data (MeteoSchweiz, 2022). And while temperature is a common data source in both cases (other studies and this thesis), temperature is the one that leads to little uncertainty since it can be extrapolated from the weather station in Samedan to the Morteratsch glacier. This process of temperature interpolation was explained in chapter 3.4.3. Precipitation can also be interpolated more or less well over space as it was done in the mentioned studies (Zekollari, Fürst and Huybrechts, 2014; Zekollari and Huybrechts, 2018). For the case of this study, *SWin* was required as data for the eePDH. And *SWin* is dependent on various local geographic predispositions. That involves especially the horizon surrounding the location. Proof of that is given by Figure 21. It is arguably evident to some degree already by that figure that the net *SWin* amount in Samedan is way higher than that on the Morteratsch glacier (comparison of the first week of measurements). The data proves that point and shows that there is about 25 % more *SWin* in Samedan during the first week of measurements than there is for the deployment location on the glacier. This is important to keep in mind for the following chapter of the validation of the eePDH.

Next, the two studies having used data from the weather station in Samedan researched long-term processes for over a multitude of years. In comparison, this study has a time horizon of two weeks, and even more accurately, the validation and thus the use of data from the weather station in Samedan is only one week. For such short time horizons, it is even more so important to have as accurate data. Interpolated data from close-by is suitable for longer time horizons as small fluctuations do not weigh too much in the grand scheme of the research. In that sense, the data used here leads to a lot of uncertainty. The following validation of the model has to be regarded with care.

The data from the other weather station was used for one reason. There was a lack of data due to the unforeseen situation within the deployment. The model had to be validated in some way since, otherwise, it would not possess much meaningfulness (MacDougall and Flowers, 2011; Seibert and Vis, 2012). Thus, the second week of the model was constructed by the means of available data to at least present a framework on how the model could potentially be validated if the experiment was to be reproduced. So, the data from the weather station in Samedan as a time series of was added to the data of the WS.

5.4.4 Comments on Further Approaches to Validate the Model at Hand

The main score to calibrate and validate the efficiency of the models used in this thesis is the *RMSD* (Brock and Arnold, 2000; MacDougall and Flowers, 2011; MacDougall, Wheler and Flowers, 2011; Carenzo *et al.*, 2016; Pool, Vis and Seibert, 2021). The *RMSD* is a very basic and thus not very robust score to evaluate model performance (Cooper, 2010; Pool, Vis and Seibert, 2021). Yet, due to its simplicity, it is argued that it is more transparent than other scores and therefore more transparent.

To obtain a better idea of the performance of the model, more scores can be used (MacDougall and Flowers, 2011; MacDougall, Wheler and Flowers, 2011). For this thesis, the following two scores are suggested to be added as efficiency criterions, namely the *NSE* and the *KGE*. The *NSE* alone measures efficiency based on the model's average compared to the specific model output at each time step. Therefore, it alone is incapable of determining the source of deviation (Gupta *et al.*, 2009; Cooper, 2010). The even more sophisticated score is the *KGE*. It accounts for correlation, averages, and standard deviations between the modelled and the observed values (Gupta *et al.*, 2009; Knoben, Freer and Woods, 2019).

Now, the approach to validate the model in this thesis is rather different in the core if compared to the validations of other TIMs. The basic concept is that modelled values are compared to observed values. In the case of this thesis, the modelled values are evident. The observed values however differ from other studies. Other studies tend to use an EBM to compare it to the respective TIM (Pellicciotti *et al.*, 2005; Matthews *et al.*, 2015; Carenzo *et al.*, 2016). This thesis however uses mean interpolated values of the ablation stake measurements, since the EBM was not fully physical. Further, if the EBM was extended to the second week as well, it had to be done so with the weather data from Samedan, which would result in even higher inaccuracy of the EBM and thus further deviation from physical reality. The used approach here with the mean interpolated ablation stake measurements is not accurate either. However, due to its simplicity and thus arguably higher transparency of the approach, it was decided to be the better choice. Occasionally, at the exact moment of measurement of the ablation stakes, there is a certainty that the observed value is rather accurate. An automated approach measuring ablation which perhaps could be installed onto the ablation stakes might be of good use for this approach (MacDougall and Flowers, 2011; Senese *et al.*, 2020).

After extending the model into the second week of measurements with the above-stated distinction between modelled and observed values, the outcome is visualized in Figure 22 and the scores in Table 7. Looking at Figure 22, it becomes evident that the deviation from the final measurement in the second week is even greater than from the last one in the first week. It is argued that there are two specific reasons for that. First, as discussed earlier, the adaptation effects from the first week, which led to an underestimation of the melt in the beginning and an overestimation of the melt by the end of the first week, propagates into the second week. Second, the net *SW* flux for the second week is greater due to the higher *SWin* from the weather station data in Samedan. The combination of those two circumstances lead to the big gap between observed and modelled melt.

Table 7 does not do that deviation justice. The *RMSD*s for, both the MC-based as well as the analytical EBM approach, are below 1.5cm. The deviation of the second week is not represented equally as the one in the first week since there is only a starting and an ending measurement of ablation for the second week. The first week has a total of twelve ablation measurements to compare to two in the second week. Paired with the fact that the deviation is especially higher in the second week due to the two circumstances explained in the previous paragraph, the scores make the model look better than it actually is.

Comparing the two weeks is even more suitable with the two additional efficiency criterions. Those are displayed in Table 8 for both model approaches, both criterions, and for all time horizons (1st week, 2nd week, both weeks). For both criterions, the best possible score is 1. Anything lower means a certain amount of deviation between model and reality. While the *NSE* has about a limit of 0 distinguishing usable from bad models (*NSE* > 0 → usable), the benchmark for the *KGE* is at about t -0.44 $(1 - \sqrt{2})$ (Knoben, Freer and Woods, 2019). Table 8 shows values for both criterions far below the respective benchmarks for the second week and for both weeks. The reason for that is the same as for the *RMSD*s

for the same time horizons, namely the number of observations between the two weeks, adaptation effects, and too much *SWin* for the second week.

Only the first week seems to be adequate according to the scores for both approaches to the model and for both criterions which can also be regarded as calibration efficiency. That is to be expected because of three reasons. First, there was enough useful data around for the first week (WS). Secondly, the number of observed values is far greater (twelve ablation stakes measurements during the first week). Thirdly, the model was calibrated in the first week against the adaptation effects, thus working itself around them. Or to rephrase it, even though adaptation effects are assumed, the calibration was conducted in a way to minimize the deviation between observed and modelled values independent of the adaptation effects.

Further, validation is done with data directly independent of the data used for the calibration of the model (MacDougall and Flowers, 2011). Consequently, the deciding scores for validation are the ones for the second week. Concludingly, it has to be said that the model validation scores are expectedly low. That however is so if it is ignored that the data needed for a correct validation is not available. Thus, no definitive statement can be made as to how efficient the eePDH is. It is argued that the approach to being able to define the model conceptually is based on a viable methodology. Shortcomings hindered an appropriate execution of all the work required to adequately validate the attempted model.

5.5 Shortcomings of This Thesis

While it can be said that this thesis had novel findings, there are various shortcomings, not solely to the initial plan, but also realizations as to what needed to be done differently from the start.

Starting off, the numerously mentioned adaptation effect seems to be a major source of uncertainty. For future work, it is recommended to plan more time for the entire experiment. It is important to let the deployment rest for a while after finishing building it. Changing conditions lead to the Morteratsch glacier needing some time to adapt to it. Thus, an adapted time management and a greater time horizon for the experiment are recommended for future work. It is crucial to plan enough start-up time before the actual experiment and the measurements begin.

Next, the sampling strategy should be adapted. While for the calibration of the model, numerous measurements took place, only a total of two were taken for the validation period. Preferably, both periods should be equally long in a time horizon and have the same number of measurements. Also, included in the sampling strategy, the WS should be changed. This applies to three aspects. First, the WS should be stabilized with ropes and put on top of a tripod as was done in other research (Oerlemans, 2000; Senese *et al.*, 2020; Liu *et al.*, 2022). Further, it would even make sense to distribute the automated measurement devices from the WS onto two different WSs, thus decreasing the number of instruments per WS and consequently the influence of some instruments onto others. That shortcoming was exemplified by the measurements of the *SW* on the WS as compared to the measurements of the albedo as displayed in Figure 9. Also included in the sampling strategy is more caution towards the instruments and their functioning. As was stated multiple times in this thesis, the fact that the WS did not last until the very end of the measurement period, was a major incision in the quality of this thesis. Plus, loose contacts on the instruments, as it was the case for the Davis Cup for a few days. If it was not for the shortcomings of the WS data, the setbacks due to the weather station data in Samedan would not have been an issue at all to begin with, since that data would not have been required in that case in the first place.

One of the major setbacks for this thesis was the definition of the EBM. Since the EBM, as it was defined for this thesis, was not fully physical, it had to be simplified with empirical approaches. Those made the EBM, so it has been argued in this thesis, too inaccurate and therefore inappropriate to use to calibrate and validate the TIMs at hand, namely the ePDH and the eePDH, against the EBM itself (Pelicciotti *et al.*, 2005; Matthews *et al.*, 2015; Carenzo *et al.*, 2016). TIMs have to be calibrated against something else which can be considered an observation. And while with the measurements of surface ice melt with the help of ablation stakes that was the case, those measurements have a lower frequency than the models themselves. An hourly frequency to compare the model to would be more beneficial. In that sense, the EBM needs to be improved to be fully physical. And while at that, if somehow possible, the surface ice melt could also be measured with automated devices, one could compare the results of the TIMs, the EBM as well as the automated field measurements on the same frequency which would help with data security and uncertainty reduction immensely. However, as it stands now, it is not known if automated ablation measurements are viable and dependable.

Most of these shortcomings can be attributed to a lack of experience and a lack of routine in this field. It is very likely that with the insights of shortcomings from this thesis, experienced researchers can rid or minimize those shortcomings to a neglectable level when trying to replicate this approach.

5.6 Viability of Covering Glaciers

While the entire approach of this thesis is at point scale, it should also be contextualized further. Using covers to reduce ablation is usually done on bigger scales which requires a lot of material and humanpower. Expenses for these two alone are estimated to be a few 100'000€ depending on the glacier surface area to be covered. And the cover has to be taken away every year before snowfall season, just to be put back in place after the snowfall season (Senese *et al.*, 2020; Xie *et al.*, 2023). Costs increase further due to freezing and stretching of the material which breaks it (Liu *et al.*, 2022; Xie *et al.*, 2023).

Next, as stated above, the core idea is to cover the glacier for the season when there is no snowfall. However, determining that is difficult. Plus, depending on the glacier, its altitude, and typical local weather conditions, occasional snowfall can occur even throughout summer which would hinder the accumulated snow to settle on the glacier ice and be transformed into ice with time (Liu *et al.*, 2022).

The impact of the synthetic material is also questionable in that aspect. Material can rip apart and find its way into ecosystems while being washed away. This issue also needs to be addressed when analysing the viability of such glacier synthetic cover projects (Liu *et al.*, 2022).

Further, geotextile tends to reduce its albedo over time due to dust and similar accumulating on the material without a possibility of vanishing from the material again (Senese *et al.*, 2020; Xie *et al.*, 2023).

Finally, accessibility is an issue which needs to be addressed. Since lots of material has to be used, which in a total is very heavy, transportation can become very difficult. Aside from the transportation, accessibility for workers to set the cover-up or to take it away before snowfall season might lead to the only viable means of transport being helicopters, both for material and workers. Putting that into the calculation, including the transportation costs as well as the emitted CO_2, which is the main source of human-made global climate change, raises questions about the viability of such projects in the first place (Senese *et al.*, 2020; Xie *et al.*, 2023).

While there are lots of limitations to projects of covering glaciers with geotextile to reduce surface ablation, it can be argued that the potential of surface ablation reduction through such materials is real. It is therefore important to create models for surface melt under such covered conditions and to research them to be able to better estimate and evaluate the viability of such projects.

6. Conclusion

In this thesis, an attempt was made to extend an existent TIM, namely the PTIM, with a few adaptations such as a correction factor *Icf* and an hourly base of modelling, to being able to model glacier surface ice melt when the ice is covered by two layers of non-woven geotextile (Pellicciotti *et al.*, 2005; Olefs and Fischer, 2008). The modelling was conducted fully with MS Excel. The spreadsheet-based approach allows for easy handling as well as a widespread use among many computer users (Brock and Arnold, 2000).

First, a measurement deployment was installed on the Morteratsch glacier in September 2022. For two weeks, the deployment measured various data automatically such as surface temperatures, temperatures in the ice, air temperature, vapor pressure, relative humidity, wind speed, wind direction, wind gusts, precipitation as well as incoming and outgoing shortwave radiation. Aside from the automated measurements, in the first week, manual measurements were taken twice a day Those measurements involved surface melt with the help of ablation stakes (three reference clean ice stakes and one cover stake) and albedo measurements with the help of an albedometer. After the first measurement week, the deployment was left as it was to continue with its automated measurements for another week. After the second week, manual measurements were taken one last time before dismantling the deployment and the saving of all the acquired data. After preparing the acquired data, the first analysis was done.

The next step was the construction of the PTIM for the first week, on an hourly basis with the *Icf* adaptation based on the acquired data. The model being an empirical model by definition, required a calibration of the factors which was done by Monte-Carlo simulations. The calibrated model was defined as the ePDH.

Following was the construction of the EBM for the first week, a physical surface melt model as a counterpart to the general index model which is to be understood as a summarised version of an EBM (Pellicciotti *et al.*, 2005). The EBM was not fully physical, but partly also empirical. However, the distinction of the energy sources in the system of the glacier surface was clearly given. The empirical factors of the EBM were calibrated again with the same amount of MC iterations as the ePDH.

Now, with an existent EBM, the next step was to scale down each of the energy terms in the EBM to fit the measured melt under the geotextile cover for the first week. This was done with MC and GAP. (Seibert and Vis, 2012). The best-found result of both approaches was used to scale down the EBM to meet the conditions of surface melt under the covered area on the glacier. It was found that both calibration approaches deliver similar results. The found downscaling parameter for the *SW* term of the EBM was used as a translation for the novel extension from the ePDH into the eePDH. After having a factor for the temperature-independent term of the model, the factor for the temperature-dependent is calibrated with MC.

The newly formulated eePDH is generated, again solely for the first week, in another non-analytical way by calibrating both model parameters together with MC to have a comparison between the two approaches. The model is extended into the second week to be validated. Various approaches of validation aside from the used score *RMSD* which was used for calibration and validation are introduced. The model is put to the test.

While the calibration seems to have been a success, it is difficult to validate the model due to various shortcomings. The most major ones involve the lack of data to generate a fully physical EBM which could be used as a means of observed glacier ice surface melt. Next, the weather station did not function for the entirety of the measurement deployment which led to the necessity to use data from

a nearby weather station. Uncertainties arose due to those circumstances as well as others discussed in this thesis. The viability of such approaches to reduce glacier ice melt with synthetic covers is discussed briefly.

Overall, the theoretical approach to formulate a model which is capable of estimating glacier ice surface melt under two layers of geotextile can be considered viable. The execution, however, had shortcomings on various points. The overall result can serve as a base for further research to analyse the model approach in greater detail.

The thesis formulated two research questions:

1. How much glacier ice melt can be reduced when covering the glacier ice with two layers of geotextile?

This research question was fully answered with the field deployment measurements. The surface ice melt within the two weeks of measurement was reduced by **71.4 %**.

2. How much do the shortwave radiation factor and the positive degree hours temperature factor in the ePDH need to be reduced respectively to correspond to the actual melt of glacier ice under 2 layers of geotextile for a point scale location (eePDH)?

This research question was answered as well. The two reduction factors are:

$$f1 = 0.136102617 \ (SWRF) \tag{30}$$

$$ft = 0.822569907 \ (TF) \tag{31}$$

And while the results of this research question are given, they have to be regarded carefully. A lot of uncertainty, as mentioned afore, is involved in the generation of these results.

More work is needed to be able to get a more accurate and certain result to the second research question in particular. More research in this field is crucial since there is immense potential in these models to estimate melt accurately. With better models, more accurate estimates on the efficiency of glacier cover projects can be achieved to guarantee the best possible allocation of resources to protect glaciers from melting away completely, as this has widespread implications for humans and nature.

7. References

Braithwaite, R.J. (2009) 'Calculation of sensible-heat flux over a melting ice surface using simple climate data and daily measurements of ablation', Annals of Glaciology, 50(50), pp. 9–15. Available at: https://doi.org/10.3189/172756409787769726.

Brock, B.W. and Arnold, N.S. (2000) 'A spreadsheet-based (microsoft excel) point surface energy balance model for glacier and snow melt studies', Earth Surface Processes and Landforms, 25(6), pp. 649–658. Available at: https://doi.org/10.1002/1096-9837(200006)25:6<649::AID-ESP97>3.0.CO;2-U.

Carenzo, M. et al. (2009) 'Assessing the transferability and robustness of an enhanced temperature-index glacier-melt model', Journal of Glaciology, 55(190), pp. 258–274. Available at: https://doi.org/10.3189/002214309788608804.

Carenzo, M. et al. (2016) 'An enhanced temperature index model for debris-covered glaciers accounting for thickness effect', Advances in Water Resources, 94, pp. 457–469. Available at: https://doi.org/10.1016/j.advwatres.2016.05.001.

Cooper, M. (2010) 'Advanced Bash-Scripting Guide An in-depth exploration of the art of shell scripting Table of Contents', Okt 2005 Abrufbar uber httpwww tldp orgLDPabsabsguide pdf Zugriff 1112 2005, 2274(November 2008), pp. 2267–2274. Available at: https://doi.org/10.1002/hyp.

Fuchs, P., Asoaka, Y. and Kamaza, S. (2013) 'Estimation of Glacier Melt in the Tropical Zongo With an Enhanced Temperature-Index Model', Journal of Japan Society of Civil Engineers, Ser. B1 (Hydraulic Engineering), 69(4), p. I_187-I_192. Available at: https://doi.org/10.2208/jscejhe.69.i_187.

Geoproduct, S. (2021) 'Technische Daten SYTEC / Fiche technique SYTEC Geovlies / Géonontissé', p. 3176. Available at: https://shop.hug-baustoffe.ch/katalog/sytec-geovlies-nw-medium-200-gm-1302257?va=1291646.

Gupta, H. V. et al. (2009) 'Decomposition of the mean squared error and NSE performance criteria: Implications for improving hydrological modelling', Journal of Hydrology, 377(1–2), pp. 80–91. Available at: https://doi.org/10.1016/j.jhydrol.2009.08.003.

Hock, R. (2005) 'Glacier melt: A review of processes and their modelling', Progress in Physical Geography, 29(3), pp. 362–391. Available at: https://doi.org/10.1191/0309133305pp453ra.

Huss, M. et al. (2021) 'Quantifying the overall effect of artificial glacier melt reduction in Switzerland, 2005–2019', Cold Regions Science and Technology, 184(July 2020), p. 103237. Available at: https://doi.org/10.1016/j.coldregions.2021.103237.

Klok, E.J. and Oerlemans, J. (2002) 'Model study of the spatial distribution of the energy and mass balance of Morteratschgletscher, Switzerland', Journal of Glaciology, 48(163), pp. 505–518. Available at: https://doi.org/10.3189/172756502781831133.

Knoben, W.J.M., Freer, J.E. and Woods, R.A. (2019) 'Technical note: Inherent benchmark or not? Comparing Nash-Sutcliffe and Kling-Gupta efficiency scores', Hydrology and Earth System Sciences, 23(10), pp. 4323–4331. Available at: https://doi.org/10.5194/hess-23-4323-2019.

Lee, G. et al. (2019) 'Review of statistical model calibration and validation—from the perspective of uncertainty structures', Structural and Multidisciplinary Optimization, 60(4), pp. 1619–1644. Available at: https://doi.org/10.1007/s00158-019-02270-2.

Liu, S. et al. (2022) 'Quantifying the Artificial Reduction of Glacial Ice Melt in a Mountain Glacier (Urumqi Glacier No. 1, Tien Shan, China)', Remote Sensing, 14(12). Available at: https://doi.org/10.3390/rs14122802.

MacDougall, A.H. and Flowers, G.E. (2011) 'Spatial and temporal transferability of a distributed energy-balance glacier melt model', Journal of Climate, 24(5), pp. 1480–1498. Available at: https://doi.org/10.1175/2010JCLI3821.1.

MacDougall, A.H., Wheler, B.A. and Flowers, G.E. (2011) 'A preliminary assessment of glacier melt-model parameter sensitivity and transferability in a dry subarctic environment', Cryosphere, 5(4), pp. 1011–1028. Available at: https://doi.org/10.5194/tc-5-1011-2011.

Matthews, T. et al. (2015) 'Conditioning temperature-index model parameters on synoptic weather types for glacier melt simulations', Hydrological Processes, 29(6), pp. 1027–1045. Available at: https://doi.org/10.1002/hyp.10217.

MeteoSchweiz (2022) 'Bundesamt für Meteorologie und Klimatologie'. Available at: https://gate.meteoswiss.ch/idaweb/login.do;idaweb=wq2K-Gzuhb6Zj8U_7rfvTqfxCLench9pVIEjJ7UDlZ9QKwRuwukW!-1038120646.

Munro, D.S. (1989) 'Surface roughness and bulk heat transfer on a glacier: comparison with eddy correlation', Journal of Glaciology, 35(121), pp. 343–348. Available at: https://doi.org/10.1017/S0022143000009266.

Oerlemans, J. et al. (1998) 'Modelling the response of glaciers to climate warming', Climate Dynamics, 14(4), pp. 267–274. Available at: https://doi.org/10.1007/s003820050222.

Oerlemans, J. (2000) 'Analysis of a 3 year meteorological record from the ablation zone of morteratschgletscher, Switzerland: Energy and mass balance', Journal of Glaciology, 46(155), pp. 571–579. Available at: https://doi.org/10.3189/172756500781832657.

Oerlemans, J., Haag, M. and Keller, F. (2017) 'Slowing down the retreat of the Morteratsch glacier, Switzerland, by artificially produced summer snow: a feasibility study', Climatic Change, 145(1–2), pp. 189–203. Available at: https://doi.org/10.1007/s10584-017-2102-1.

Olefs, M. and Fischer, A. (2008) 'Comparative study of technical measures to reduce snow and ice ablation in Alpine glacier ski resorts', Cold Regions Science and Technology, 52(3), pp. 371–384. Available at: https://doi.org/10.1016/j.coldregions.2007.04.021.

Olson, M., Rupper, S. and Shean, D.E. (2019) 'Terrain Induced Biases in Clear-Sky Shortwave Radiation Due to Digital Elevation Model Resolution for Glaciers in Complex Terrain', Frontiers in Earth Science, 7(August), pp. 1–12. Available at: https://doi.org/10.3389/feart.2019.00216.

Pellicciotti, F. et al. (2005) 'An enhanced temperature-index glacier melt model including the shortwave radiation balance: Development and testing for Haut Glacier d'Arolla, Switzerland', Journal of Glaciology, 51(175), pp. 573–587. Available at: https://doi.org/10.3189/172756505781829124.

Pellicciotti, F. et al. (2014) 'Changes of glaciers in the Andes of Chile and priorities for future work', Science of the Total Environment, 493, pp. 1197–1210. Available at: https://doi.org/10.1016/j.scitotenv.2013.10.055.

Pool, S., Vis, M. and Seibert, J. (2021) 'Regionalization for Ungauged Catchments — Lessons Learned From a Comparative Large-Sample Study', Water Resources Research, 57(10), pp. 0–25. Available at: https://doi.org/10.1029/2021WR030437.

Saltelli, A. and Bolado, R. (1998) 'An alternative way to compute Fourier amplitude sensitivity test (FAST)', Computational Statistics and Data Analysis, 26(4), pp. 445–460. Available at: https://doi.org/10.1016/S0167-9473(97)00043-1.

Seguinot, J. (2013) 'Spatial and seasonal effects of temperature variability in a positive degree-day glacier surface mass-balance model', Journal of Glaciology, 59(218), pp. 1202–1204. Available at: https://doi.org/10.3189/2013JoG13J081.

Seibert, J. and Vis, M.J.P. (2012) 'Teaching hydrological modeling with a user-friendly catchment-runoff-model software package', Hydrology and Earth System Sciences, 16(9), pp. 3315–3325. Available at: https://doi.org/10.5194/hess-16-3315-2012.

Senese, A. et al. (2020) 'The non-woven geotextiles as strategies for mitigating the impacts of climate change on glaciers', Cold Regions Science and Technology, 173(January). Available at: https://doi.org/10.1016/j.coldregions.2020.103007.

Silwal, G. et al. (2023) 'Response of glacier modelling parameters to time, space, and model complexity: Examples from eastern slopes of Canadian Rocky Mountains', Science of the Total Environment, 872(October 2022), p. 162156. Available at: https://doi.org/10.1016/j.scitotenv.2023.162156.

Skogsberg, K. and Lundberg, A. (2005) 'Wood chips as thermal insulation of snow', Cold Regions Science and Technology, 43(3), pp. 207–218. Available at: https://doi.org/10.1016/j.coldregions.2005.06.001.

Swisstopo (2023) Bundesamt für Landtopographie. Available at: https://map.geo.admin.ch/?lang=de&topic=ech&bgLayer=ch.swisstopo.pixelkarte-farbe&E=2790172.57&N=1143026.43&zoom=5&catalogNodes=457,458&layers=ch.swisstopo.swissimage-product,ch.swisstopo.swisstlm3d-karte-grau,ch.swisstopo.pixelkarte-farbe-pk500.noscale,c.

UNEP (2023) Climate Change 2023: Synthesis Report | UNEP - UN Environment Programme. Available at: https://www.unep.org/resources/report/climate-change-2023-synthesis-report.

Xie, Y. et al. (2023) 'Applying Artificial Cover to Reduce Melting in Dagu Glacier in the Eastern Qinghai-Tibetan Plateau', Remote Sensing, 15(7), pp. 1–19. Available at: https://doi.org/10.3390/rs15071755.

Zekollari, H. et al. (2022) 'Ice-Dynamical Glacier Evolution Modeling—A Review', Reviews of Geophysics, 60(2). Available at: https://doi.org/10.1029/2021RG000754.

Zekollari, H., Fürst, J.J. and Huybrechts, P. (2014) 'Modelling the evolution of Vadret da Morteratsch, Switzerland, since the Little Ice Age and into the future', Journal of Glaciology, 60(224), pp. 1208–1220. Available at: https://doi.org/10.3189/2014JoG14J053.

Zekollari, H. and Huybrechts, P. (2018) 'Statistical modelling of the surface mass-balance variability of the Morteratsch glacier, Switzerland: Strong control of early melting season meteorological conditions', Journal of Glaciology, 64(244), pp. 275–288. Available at: https://doi.org/10.1017/jog.2018.18.

8. Appendix

Appendix A: Additional Plots & Figures
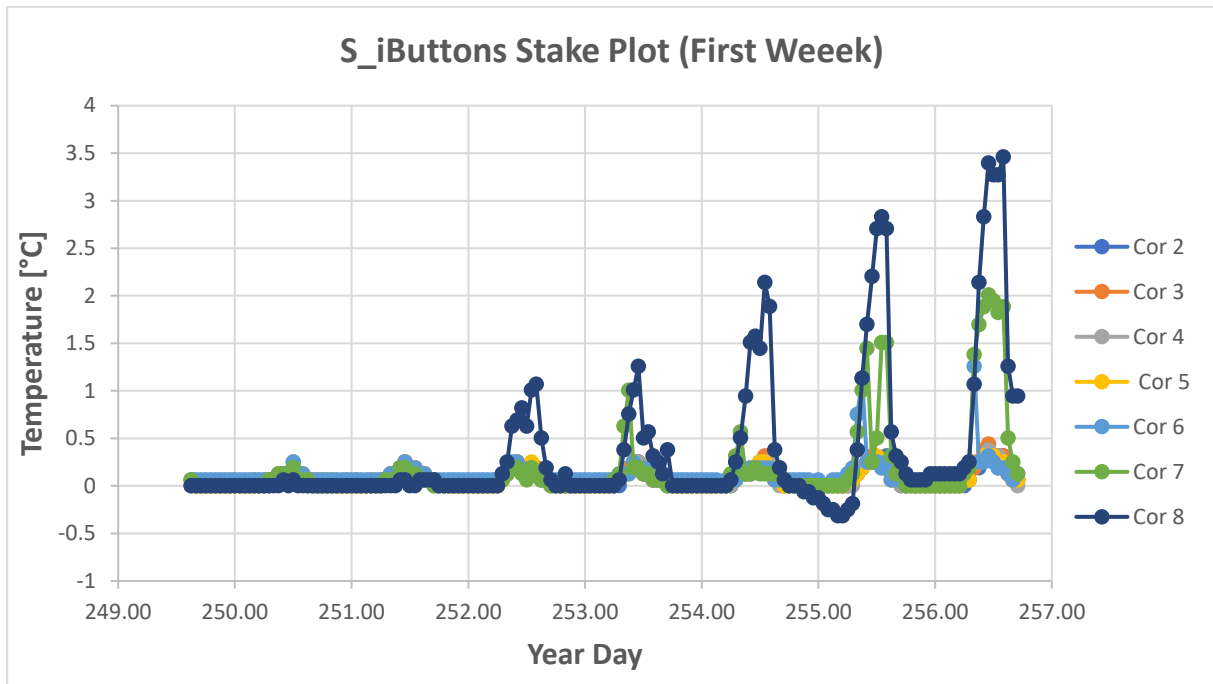
Figure 27: Temperature measurements of iButtons fixed on the ablation stake on S. Cor 8 is closest to the surface in the beginning, 2 is respectively furthest away from the surface deep in the glacier ice. As time passes, more melt occurs and the iButtons surface one after another experiencing daily temperature fluctuations.
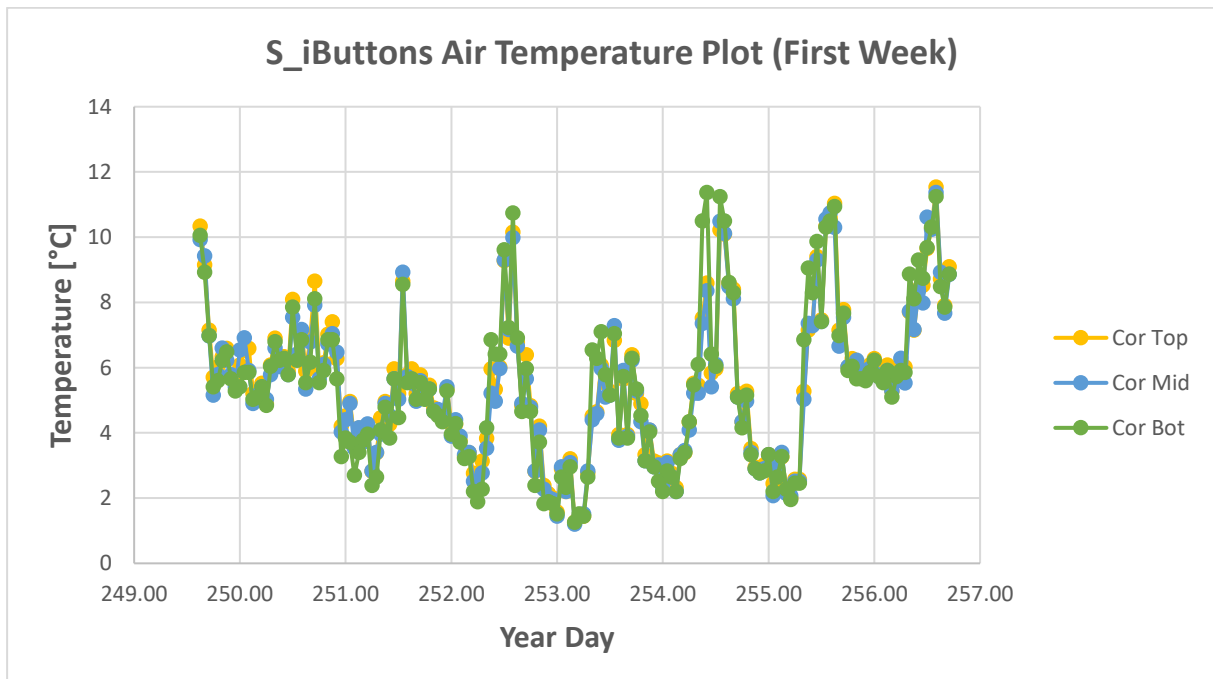
Figure 28: Radiation shield-protected iButtons on the ablation stake of S showing the daily temperature fluctuations at different altitudes.
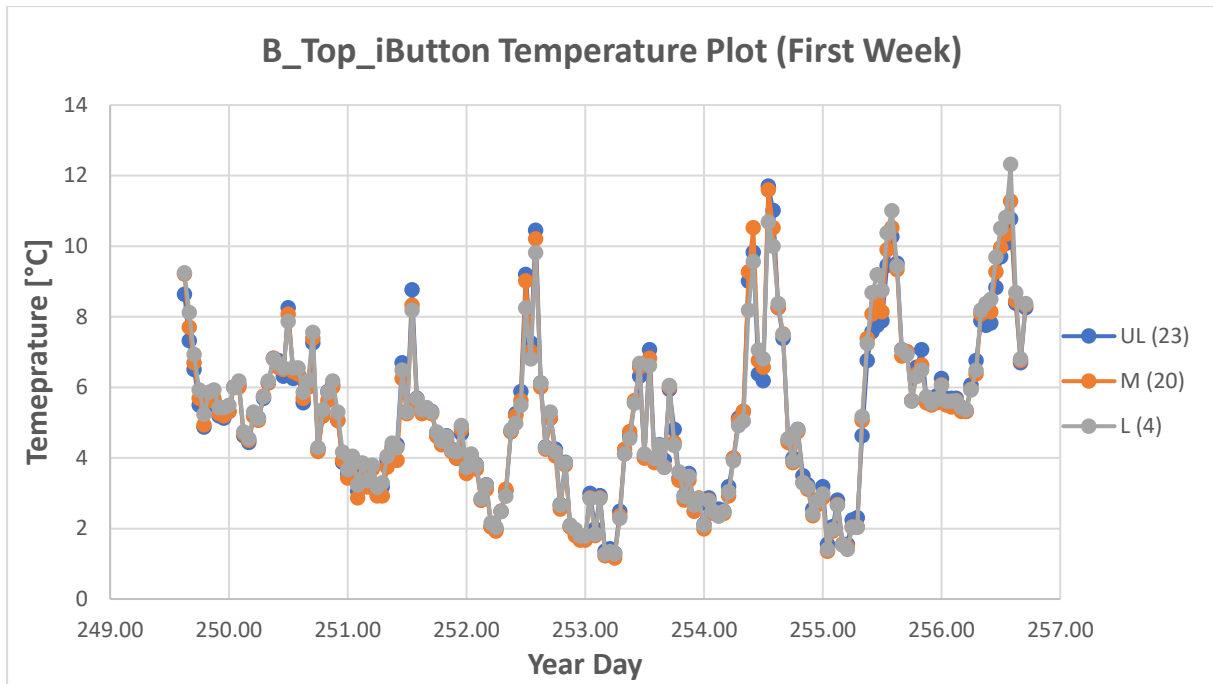
Figure 29: Temperature fluctuations measured by iButtons on B with the highest altitude protected by radiation shields.

Table 9: ANOVA of Figure 29 values. The null hypothesis that there is no difference in variance between the temperatures of the highest layer above B for a confidence interval of α=5 % is not rejected.

Number	sum	mean	variance
171	880.056	5.146526316	5.046326721
171	875.548	5.120163743	5.437585585
171	889.511	5.201818713	5.43286342

(SS)	(df)	(MS)	(F)	P-value	critical F-value
0.593926819	2	0.296963409	0.055971777	0.945571629	3.013398272
2705.851873	510	5.305591909			
2706.4458	512				
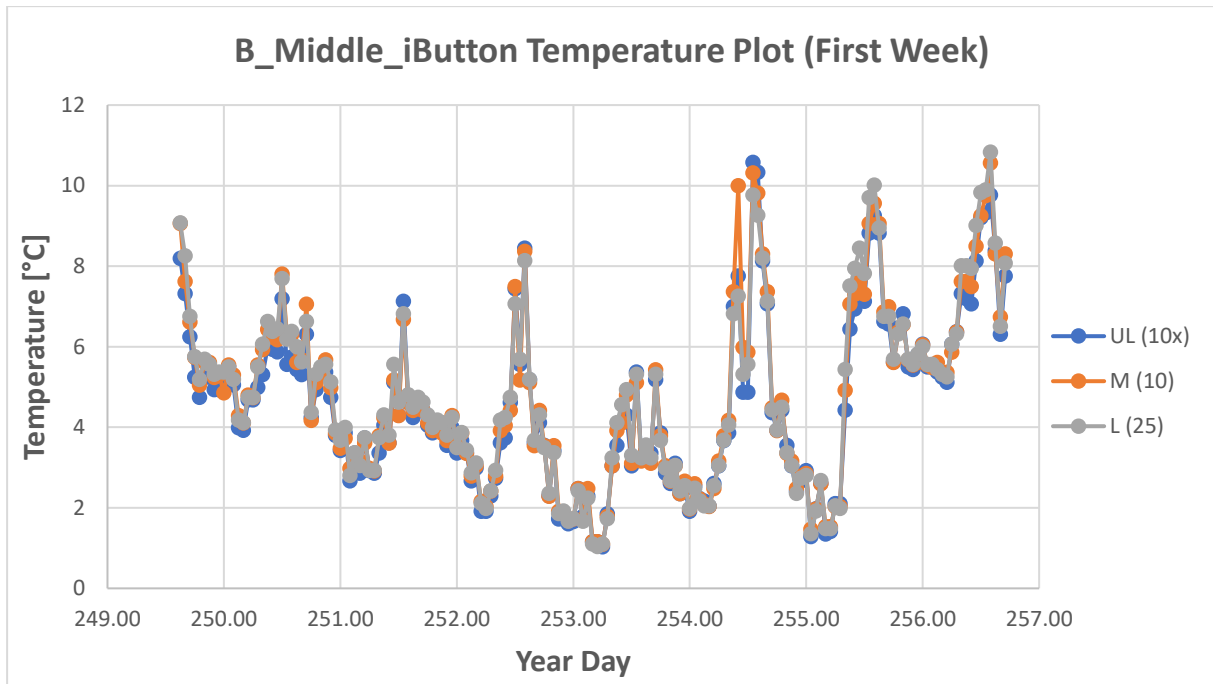
Figure 30: Temperature fluctuations measured by iButtons on B with the middle altitude protected by radiation shields.

Table 10: ANOVA of Figure 30 values. The null hypothesis that there is no difference in variance between the temperatures of the middle layer above B for a confidence interval of α=5 % is not rejected.

number	sum	mean	variance
171	784.553	4.58802924	4.25330737
171	812.158	4.749461988	4.662600215
171	818.691	4.787666667	4.727671847

(SS)	(df)	(MS)	(F)	P-value	critical F-value
3.840388222	2	1.920194111	0.422219284	0.655819211	3.013398272
2319.408503	510	4.547859811			
2323.248892	512				
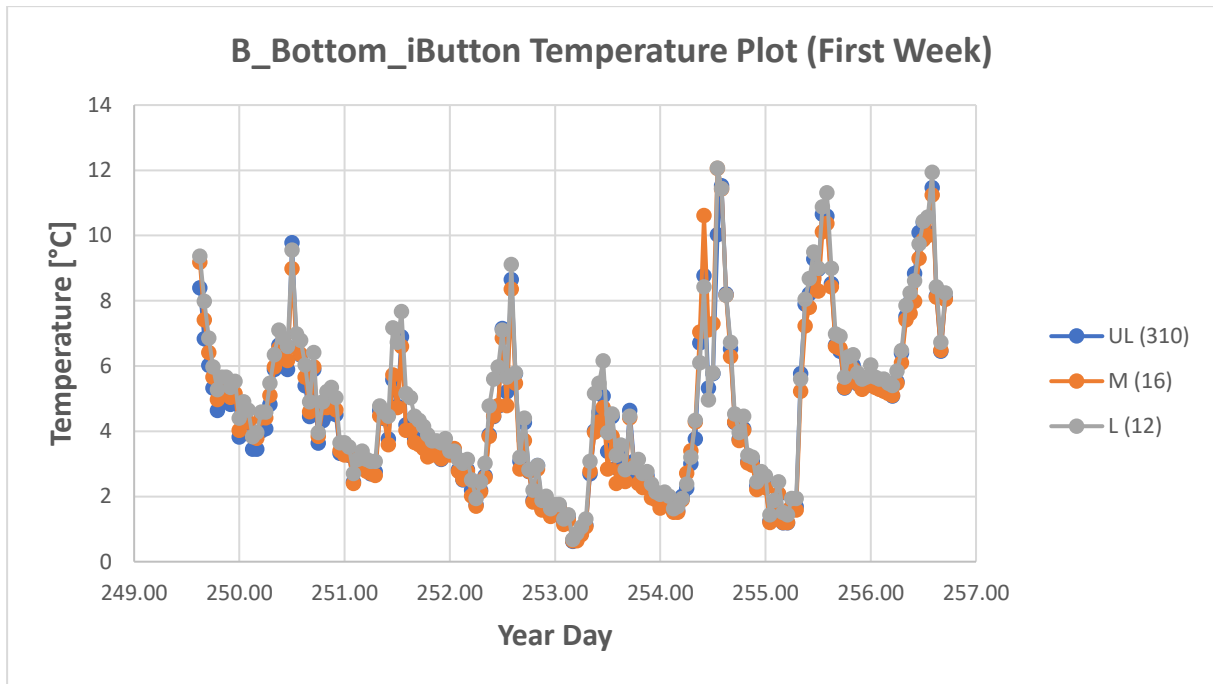
Figure 31: Temperature fluctuations measured by iButtons on B with the lowest altitude protected by radiation shields.

Table 11: ANOVA of Figure 31 values. The null hypothesis that there is no difference in variance between the temperatures of the lowest layer above B for a confidence interval of α=5 % is not rejected.

number	sum	mean	variance
171	774.921	4.531701754	5.883488846
171	771.939	4.514263158	6.004953995
171	835.084	4.883532164	6.177953027

(SS)	(df)	(MS)	(F)	P-value	critical F-value
14.8455554	2	7.422777698	1.232583037	0.292405524	3.013398272
3071.287298	510	6.022131956			
3086.132853	512				
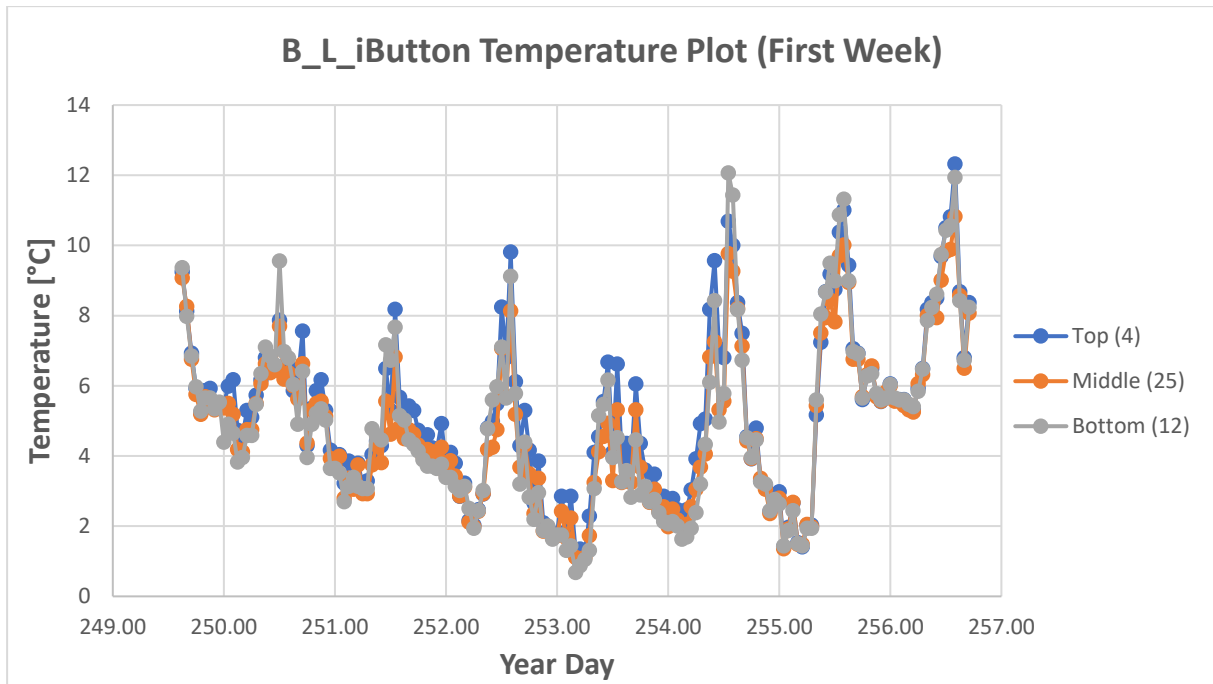
Figure 32: Temperature fluctuations measured by iButtons on B under the lower radiation shield (L).

Table 12: ANOVA of Figure 32 values. The null hypothesis that there is no difference in variance between the temperatures of the L on B for a confidence interval of α=5 % is not rejected.

Number	sum	mean	variance
171	889.511	5.201818713	5.43286342
171	818.691	4.787666667	4.727671847
171	835.084	4.883532164	6.177953027

(SS)	(df)	(MS)	(F)	P-value	critical F-value
16.07505103	2	8.037525515	1.475814415	0.22956704	3.013398272
2777.54301	510	5.446162765			
2793.618061	512				
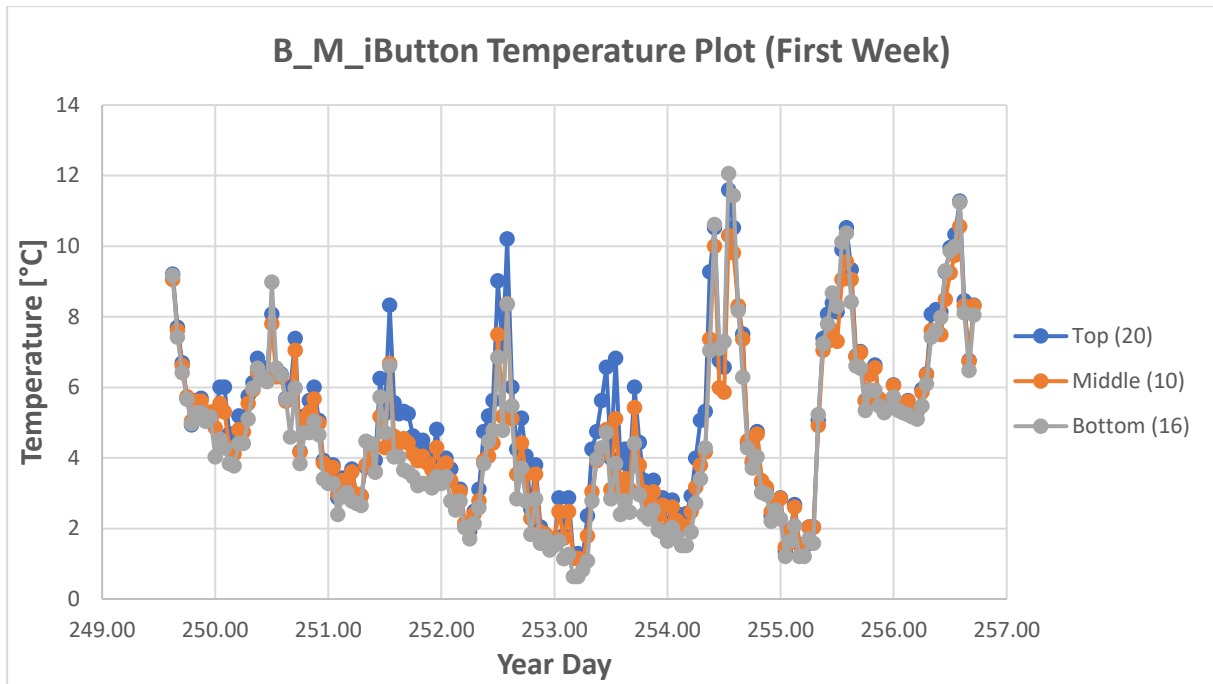
Figure 33: Temperature fluctuations measured by iButtons on B under the middle radiation shield (M).

Table 13: ANOVA of Figure 33 values. The null hypothesis that there is no difference in variance between the temperatures of the M on B for a confidence interval of α=5 % is not rejected.

number	sum	mean	variance
171	875.548	5.120163743	5.437585585
171	812.158	4.749461988	4.662600215
171	771.939	4.514263158	6.004953995

(SS)	(df)	(MS)	(F)	P-value	critical F-value
31.91166655	2	15.95583328	2.972187789	0.052078669	3.013398272
2737.873765	510	5.368379932			
2769.785432	512				
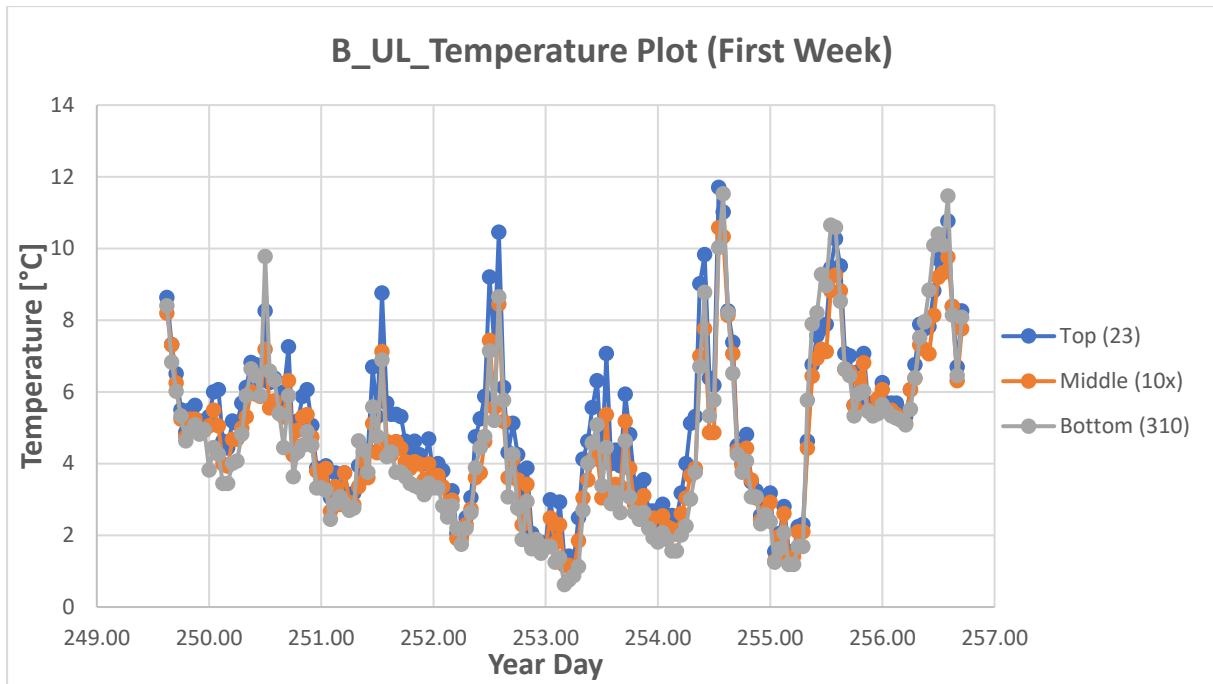
Figure 34: Temperature fluctuations measured by iButtons on B under the middle radiation shield (UL).

Table 14: ANOVA of Figure 34 values. The null hypothesis that there is no difference in variance between the temperatures of the UL on B for a confidence interval of α=5 % is not rejected.

Number	sum	mean	variance
171	880.056	5.146526316	5.046326721
171	784.553	4.58802924	4.25330737
171	774.921	4.531701754	5.883488846

(SS)	(df)	(MS)	(F)	P-value	critical F-value
39.50675762	2	19.75337881	3.903026846	0.020786359	3.013398272
2581.130899	510	5.061040979			
2620.637657	512				

Appendix B: Code for Monte Carlo simulation in VBA Excel for downscaling EBM

```vba
Option Explicit

'Define macro

Public Sub MonteCarlo_SW_sens_1rain(ByVal iterations As Long, _

                ByVal Swin_and_Swout As String, _

                ByVal Lwin_and_Lwout As String, _

                ByVal Qsens As String, _

                ByVal Qlat As String, _

                ByVal Qrain As String)

    'Define variables

    Dim ALT As Worksheet

    Dim DATA As Worksheet

    Dim lngCounter As Long

    Dim last_data_row As Long

    Dim new_row As Long

    Dim start_time As Single

    Dim end_time As Single

    Dim progress_counter As Long

    Unload ParametersForm_MC

    ProgressBar.Show vbModeless

    'Set start time

    start_time = Timer()

    Application.ScreenUpdating = False

    'Set workbook references

    Set ALT = ThisWorkbook.Worksheets("Alternative for weighting")

    Set DATA = ThisWorkbook.Worksheets("MC test")

    'Find last data row

    last_data_row = DATA.Range("A" & Rows.Count).End(xlUp).Row

    new_row = last_data_row + 1

    progress_counter = 1

    'Loop for set number of iterations
```

```vba
For lngCounter = new_row To new_row + iterations - 1

    'Set random value between 0 & 1 to respective weigthing cells

    'With ALT

    '   .Range("B1:B2").Value = Rnd()

    '   .Range("B3:B4").Value = 0

    '   .Range("B5").Value = Rnd()

    '   .Range("B6").Value = 0

    '   .Range("B7").Value = 1

    'End With

    'Debug.Print lngCounter

    'Set values for parameters

    If Swin_and_Swout = "RND" Then

        ALT.Range("B1:B2").Value = Rnd()

    Else

        ALT.Range("B1:B2").Value = Cint(Swin_and_Swout)

    End If

    If Lwin_and_Lwout = "RND" Then

        ALT.Range("B3:B4").Value = Rnd()

    Else

        ALT.Range("B3:B4").Value = Cint(Lwin_and_Lwout)

    End If

    If Qsens = "RND" Then

        ALT.Range("B5").Value = Rnd()

    Else

        ALT.Range("B5").Value = Cint(Qsens)

    End If

    If Qlat = "RND" Then

        ALT.Range("B6").Value = Rnd()

    Else

        ALT.Range("B6").Value = Cint(Qlat)

    End If
```

l

```vba
        If Qrain = "RND" Then

            ALT.Range("B7").Value = Rnd()

        Else

            ALT.Range("B7").Value = Cint(Qrain)

        End If

        'ALT.Range("B1:B2").Value = Rnd()

        'ALT.Range("B3:B4").Value = 0

        'ALT.Range("B5").Value = Rnd()

        'ALT.Range("B6").Value = 0

        'ALT.Range("B7").Value = 1

        'Add new row to data from current iteration results

        DATA.Range("A" & new_row).Value = lngCounter - 1

        DATA.Range("B" & new_row & ":H" & new_row).Value =
WorksheetFunction.Transpose(ALT.Range("B1:B7"))

        DATA.Range("I" & new_row).Value = ALT.Range("B10").Value

        'Iterate last row and progress counter

        new_row = new_row + 1

        progress_counter = progress_counter + 1

        'Update progress bar

        Call UpdateProgressBar(progress_counter, iterations)

    'Move to next iteration

    Next lngCounter

end_time = Timer() - start_time

Application.ScreenUpdating = True

Unload ProgressBar

'Notify user calculations are complete and time it took to complete

MsgBox iterations & " iterations were completed in: " & end_time & " seconds."

'End macro

End Sub

Sub TurnOnScreenUpdating()

    Application.ScreenUpdating = True

End Sub
```

J

```vba
'Define macro

Sub MonteCarlo_all()

'Define iterations

Dim lngCounter As Long

For lngCounter = 1 To 10

'Choose correct worksheet

Worksheets("Alternative for weighting").Select

'Set random value between 0 & 1 to respective weigthing cells

Range("B1:B2").Value = Rnd()

Range("B3:B4").Value = Rnd()

Range("B5").Value = Rnd()

Range("B6").Value = Rnd()

Range("B7").Value = Rnd()

'Select the worksheet with the results

Sheets("Alternative for weighting").Select

'Select the required cells to copy

Range("A1:D7").Select

'Copy the selected cells

Range(Selection, Selection.End(xlDown)).Copy

'Select the worksheet with the simulation results

Sheets("Monte Carlo (all)").Select

'Paste the latest values into respective cells

Range("A" & Rows.Count).End(xlUp).Offset(1).PasteSpecial xlPasteValues

'Move to next iteration

Next lngCounter

'End macro

End Sub
```

K

Appendix C: Code for GAP simulation in VBA Excel for downscaling EBM

```vba
Option Explicit

'Define macro

Public Sub MonteCarlo_SW_sens_1rain(ByVal iterations_per_subset As Long, _

                    ByVal total_subsets As Long, _

                    ByVal allowed_variance As Double, _

                    ByVal Swin_and_Swout As String, _

                    ByVal Lwin_and_Lwout As String, _

                    ByVal Qsens As String, _

                    ByVal Qlat As String, _

                    ByVal Qrain As String)

    'Define variables

    Dim ALT As Worksheet

    Dim DATA As Worksheet

    Dim lngCounter As Long

    Dim last_data_row As Long

    Dim new_row As Long

    Dim start_time As Single

    Dim end_time As Single

    Dim progress_counter As Long

    Dim iterations As Long

    Dim initial_subset_flag As Boolean

    Dim current_subset As Long

    Dim minimum_RMSD As Double

    Dim row_match As Long

    Dim constrained_random_number As Double

    Unload ParametersForm_GAP

    ProgressBar.Show vbModeless

    'Set start time

    start_time = Timer()

    Application.ScreenUpdating = False
```

```vba
    iterations = iterations_per_subset * total_subsets

    allowed_variance = allowed_variance / 100

    'Set workbook references

    Set ALT = ThisWorkbook.Worksheets("Alternative for weighting")

    Set DATA = ThisWorkbook.Worksheets("GAP")

    'Find last data row

    last_data_row = DATA.Range("A" & Rows.Count).End(xlUp).Row

    new_row = last_data_row + 1

    progress_counter = 0

    current_subset = 1

    initial_subset_flag = True

    'Loop for set number of iterations

    For lngCounter = new_row To new_row + iterations - 1

        If progress_counter Mod iterations_per_subset = 0 And progress_counter > 0 Then

            initial_subset_flag = False

            current_subset = current_subset + 1

            allowed_variance = allowed_variance * (10 ^ (2 - current_subset))

            minimum_RMSD = WorksheetFunction.Min(DATA.Range("I" & new_row - (iterations_per_subset * (current_subset - 1)) & ":I" & lngCounter))

            row_match = DATA.Range("I" & new_row - (iterations_per_subset * (current_subset - 1)) & ":I" & lngCounter).Find(minimum_RMSD).Row

        End If

        If initial_subset_flag = True Then

            'Set values for parameters

            If Swin_and_Swout = "RND" Then

                ALT.Range("B1:B2").Value = Rnd()

            Else

                ALT.Range("B1:B2").Value = Cint(Swin_and_Swout)

            End If

            If Lwin_and_Lwout = "RND" Then

                ALT.Range("B3:B4").Value = Rnd()

            Else
```

```vba
            ALT.Range("B3:B4").Value = Cint(Lwin_and_Lwout)

        End If

        If Qsens = "RND" Then

            ALT.Range("B5").Value = Rnd()

        Else

            ALT.Range("B5").Value = Cint(Qsens)

        End If

        If Qlat = "RND" Then

            ALT.Range("B6").Value = Rnd()

        Else

            ALT.Range("B6").Value = Cint(Qlat)

        End If

        If Qrain = "RND" Then

            ALT.Range("B7").Value = Rnd()

        Else

            ALT.Range("B7").Value = Cint(Qrain)

        End If

        'Add new row to data from current iteration results

        DATA.Range("A" & new_row).Value = lngCounter - 1

        DATA.Range("B" & new_row & ":H" & new_row).Value =
WorksheetFunction.Transpose(ALT.Range("B1:B7"))

        DATA.Range("I" & new_row).Value = ALT.Range("B10").Value

    Else

        'Set values for parameters with constraints

        If Swin_and_Swout = "RND" Then

            constrained_random_number = (Rnd() * allowed_variance) - (allowed_variance / 2) +
DATA.Range("B" & row_match).Value

            If constrained_random_number < 0 Then

                constrained_random_number = 0

            ElseIf constrained_random_number > 1 Then

                constrained_random_number = 1

            End If
```

```
            ALT.Range("B1:B2").Value = constrained_random_number

        Else

            ALT.Range("B1:B2").Value = Cint(Swin_and_Swout)

        End If

        If Lwin_and_Lwout = "RND" Then

            constrained_random_number = (Rnd() * allowed_variance) - (allowed_variance / 2) +
    DATA.Range("D" & row_match).Value

            If constrained_random_number < 0 Then

                constrained_random_number = 0

            ElseIf constrained_random_number > 1 Then

                constrained_random_number = 1

            End If

            ALT.Range("B3:B4").Value = constrained_random_number

        Else

            ALT.Range("B3:B4").Value = Cint(Lwin_and_Lwout)

        End If

        If Qsens = "RND" Then

            constrained_random_number = (Rnd() * allowed_variance) - (allowed_variance / 2) +
    DATA.Range("F" & row_match).Value

            If constrained_random_number < 0 Then

                constrained_random_number = 0

            ElseIf constrained_random_number > 1 Then

                constrained_random_number = 1

            End If

            ALT.Range("B5").Value = constrained_random_number

        Else

            ALT.Range("B5").Value = Cint(Qsens)

        End If

        If Qlat = "RND" Then

            constrained_random_number = (Rnd() * allowed_variance) - (allowed_variance / 2) +
    DATA.Range("G" & row_match).Value

            If constrained_random_number < 0 Then
```

```vba
            constrained_random_number = 0

        ElseIf constrained_random_number > 1 Then

            constrained_random_number = 1

        End If

        ALT.Range("B6").Value = constrained_random_number

    Else

        ALT.Range("B6").Value = Cint(Qlat)

    End If

    If Qrain = "RND" Then

        constrained_random_number = (Rnd() * allowed_variance) - (allowed_variance / 2) +
DATA.Range("H" & row_match).Value

        If constrained_random_number < 0 Then

            constrained_random_number = 0

        ElseIf constrained_random_number > 1 Then

            constrained_random_number = 1

        End If

        ALT.Range("B7").Value = constrained_random_number

    Else

        ALT.Range("B7").Value = Cint(Qrain)

    End If

    'Add new row to data from current iteration results

    DATA.Range("A" & new_row).Value = lngCounter - 1

    DATA.Range("B" & new_row & ":H" & new_row).Value =
WorksheetFunction.Transpose(ALT.Range("B1:B7"))

    DATA.Range("I" & new_row).Value = ALT.Range("B10").Value

    End If

    'Iterate last row and progress counter

    new_row = new_row + 1

    progress_counter = progress_counter + 1

    'Update progress bar

    Call UpdateProgressBar(progress_counter, iterations)

  'Move to next iteration
```

```vba
    Next lngCounter

end_time = Timer() - start_time

Application.ScreenUpdating = True

Unload ProgressBar

'Notify user calculations are complete and time it took to complete

MsgBox iterations & " iterations were completed in: " & end_time & " seconds."

'End macro

End Sub
```

Appendix D: Calculation for the Sun Irradiation Angle onto the Glacier Surface
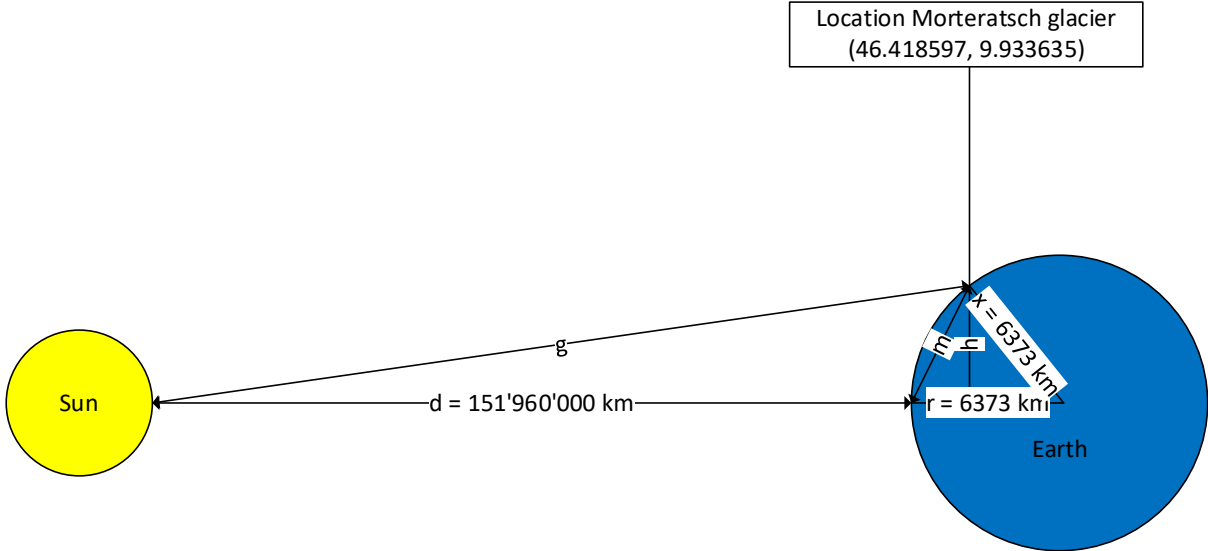
Location Morteratsch glacier
(46.418597, 9.933635)

Figure 35: Simplified visual representation of the sun and earth and the respective required distances necessary to be able to calculate the Icf.

First of all, a few assumptions need to be stated. Those involve the following. For this calculation, the distance from the sun to the earth (=d) was assumed to be 151'960'000 km. In reality, this can vary since Earth's orbit around the sun is not perfectly round and additionally as well as thus, the distance between the sun and Earth varies. Next, the radius of the earth at the equator (=r) was assumed to be 6'373 km. The location was measured in longitude and latitude. Due to it being pinpointed through aerial imagery, it is an approximation. However, it will do suffice since the deviation is so small it is neglectable for this entire approximative calculation. The chosen radius for the earth consists of the assumption that the average radius of the earth, which is mostly located around 45° of longitude, is 6'371 km. The additional two kilometres come from the elevation of the location which is about 2'168 m.a.s.l. That altitude was rounded to two kilometres and added to the average radius of the earth. Thus, r and x are assumed to be the same. Of course, that would be the case for a perfect sphere. The earth is not a perfect sphere, but rather a geoid. However, the difference is also minimal and thus neglectable.

Next, the exact date of measurement can lead to huge differences in the result due to the angle of the earth towards the sun varying with seasons. In that aspect, it is noteworthy that the measurement period for this thesis was from 06.09.2022 until 20.09.2022. That being said, it is close to one of two dates being most in the middle between the longest and shortest day of the year (maximum possible sunlight). That one of the two dates would be 21.09.2022 which is exactly in the middle between the longest (21.06.2022) and the shortest day (21.12.2022) of the year. Thus, the deviation is small and also neglectable for this calculation. Daily variations of irradiance were not included in this calculation.

It is noteworthy, that all these assumptions and the following calculations could be done way more accurately. However, this is not necessary for the purpose of this thesis. Plus, it would go beyond the intended scope of this thesis.

Now, to the calculation path to receive the specific irradiation angle on the glacier for noon.

There is the angle between the distances r and x (see Figure 35), that being the longitude of 46.418597°. We also do have the lengths of those two distances. With those, one can calculate via the law of sine the other angles and the missing distance m. For clarification, the angles will be named as

well. Those were not included in the figure due to space and thus visibility issues. The angle between r and x is going to be β. The angle between m and x is going to be α and the last one in that triangle is going to be γ.

In the following two equations, the path to calculate the missing three values of this triangle will be displayed.

$$m = \frac{r}{\sin\left(\frac{180-\beta}{2}\right)} * \sin(\beta) = 5'023.08 \; km \tag{32}$$

$$\alpha = \gamma = \frac{180-\beta}{2} = 66.79° \tag{33}$$

Having those values, the next step is to calculate the angle between d and m. It is called δ. This is a simple calculation as shown below.

$$\delta = 180 - \gamma = 113.21° \tag{34}$$

Now, having the angle δ, the next steps are to find the following values of g, the angle between d and g, let it be ε and the angle between m and g, let it be φ. Then g can be calculated via the law of cosine. This is done in the following equation.

$$\sqrt{d^2 + m^2 - 2dm * \cos(\delta)} = 151'961'979.6 \; km \tag{35}$$

Now, having g, via the manipulation of the law of sine ε is obtainable as displayed in the next equation.

$$\varepsilon = \sin^{-1}\left(\frac{\frac{1}{g}}{\frac{\sin(\delta)}{m}}\right) = 8.17 * 10^{-11} \tag{36}$$

With that, calculating φ is one additional simple step as shown below.

$$\varphi = 180 - \delta - \varepsilon = 66.79° \tag{37}$$

Having solved everything for the triangle d-m-g, the next triangle which is m-h-r can be calculated. Two out of three angles are known in this triangle which are γ and the angle between r and h which is per definition 90°. The last angle, let it be ζ, is calculated as follows.

$$\zeta = 180 - 90 - \gamma = 23.21° \tag{38}$$

Having also that angle, the angle between g and x, let it be θ, can be calculated. This is done as displayed below.

$$\theta = \varphi + \alpha - \zeta = 110.37° \tag{39}$$

Subtracting 90° from will result in an angle between g and an imaginary tangent on the earth surface at the measurement location on the glacier. That angle is ι. Having that angle, one can subtract it from 90°. This is done due to the following reasons. It is attempted to find out at what angle the sunlight hits the surface of the earth at the measurement location assuming that the surface there is flat (which it is not, but that will be of concern later).

To give an analogy, picture the situation at the equator. The tangent to the equator would be 90° to the direction of the incoming sunlight. Subtracting that from 90° itself would result in 0°. Now, if you put that angle of 0° into cosine, the result will be 1, or rather 100 %. That is the amount of energy that can be absorbed by the surface, again assuming it's flat and assuming it is a perfect black body.

Now back to the measurement location, the sunlight does not hit vertically onto the surface. Since sunlight does not hit vertically, but the incoming angle is deviated by ι, this angle is put into cosine to

S

receive the percentage of potentially maximum absorption, assuming a flat-surfaced, perfect black body. This results in the percentage of 93.745 %.

Now, the surface at hand is not perfectly flat. The glacier has a slope. The median measured slope of all the measurement locations is 8° as is the slope for the spot where the covered glacier ablation was measured. Thus, you need to add those 8° to the degrees of ι. This results in the latest angle κ, which is 28.37°. Putting κ into cosine results in an absorption percentage of 87.988 %. That, however, is based on the assumption that the glacier is exposed as much away from the sunlight as possible. And since the site is located in the northern hemisphere, that direction would be north. However, that is also not quite the case here at this site. The azimuth or exposition of the slope is tilted slightly westwards. If facing north is 0° and each additional degree rotates clockwise, then the mean exposition of all measurement spots is 336.5° and the median exposition as well as the exposition where the covered glacier ablation was measured is 334°. This is a deviation of -26° of the north. This also needs to be corrected.

The aforementioned correction requires some explanation. As stated above, having a slope facing perfectly north-wards would have the lowest effect of the sun on it given the stated circumstances at hand (longitude, slope gradient, location). Oppositely, the sun would have the maximum possible effect given the stated circumstances. Now, to calculate the actual percentage of the sun irradiation effect for the site, both sine and cosine are required. To figure out the maximum irradiation percentage, you have to go the opposite way that was gone to get κ. Thus, one can define a new angle λ. This one is the opposite of κ meaning that instead of adding our 8° of slope gradient to the ι, you subtract those from it. Figuratively speaking, κ is the glacier facing perfectly north and λ is the glacier facing perfectly south. The afore-calculated angle ι would be the equivalent of the glacier facing perfectly either eastwards or westwards

If you calculate the percentage of irradiation being absorbed for north, south, and east or west glacier variants, you get the following results.

$$\cos(\kappa) = 87.988\ \% \tag{40}$$

$$\cos(\lambda) = 97.678\ \% \tag{41}$$

$$\cos(\iota) = 93.745\ \% \tag{42}$$

So, this is the cosine of the maximum, minimum, and middle value. Now, in the real case, the location is somewhere in between those two extrema. And where exactly that is will be explained next. As mentioned before, the glacier's exposition, while north was 0°, is 334°. The question now is, how the base will be defined, meaning the 0° angle. In this case, it can be argued that the 0° angle can be west. It would work with any other orientation, but this one is arguably the simplest one to understand. As stated above, from the northern perspective, the glacier location is facing 334° if angles are measured counterclockwise. If you change the base from north to west, then the new angle is 334°-270°=64°, let this one be μ. Now, sine will be used. The sine of 0 is 0 and the sine of 90 is 1. If you take the sine of μ, you get 89.879 %. In this case with this sort of base and rotation, 100 % would be the equivalent of 87.988 % or cos(κ). And 0 % is 93.745 % or cos(ι). Thus, the required value, let it be *Icf* (irradiation correction factor), is between that two sin (μ) or 89.879 % along the way from cos(ι) to cos(κ). Calculating the final step of the irradiation factor for the site results in the following formula.

$$icf = (\cos(\iota) * 100 - ((\cos(\iota) - \cos(\kappa)) * 100 * \sin(64)))/100 = 88.571\ \% \tag{43}$$

This is the maximum potential amount a perfect black body could absorb irradiation for 21.09.2022 given the circumstances at hand with the made assumptions and simplifications for the site.

Appendix E: Top 40 MC Results for Downscaling of EBM

Table 15: Top 40 lowest MC-based RMSD (S) scores in EBM to downscale EBM from clean ice to fit covered cumulative vertical ice melt.

Iteration	SWin	SWout	LWin	LWout	Qsens	Qlatent	Qrain	RMSD (S)
9373	0.136102617	0.136102617	0.766905189	0.766905189	0.053635657	0.093529701	0.96109122	0.318853160538206
20004	0.163546562	0.163546562	0.729556262	0.729556262	0.093233705	0.004581749	0.700896502	0.318862446356696
61163	0.105936348	0.105936348	0.65269208	0.65269208	0.385410726	0.005797267	0.876510203	0.323482798720477
76769	0.059869945	0.059869945	0.890378594	0.890378594	0.248889267	0.060747385	0.650502622	0.324833379710307
43373	0.089958608	0.089958608	0.911684871	0.911684871	0.100253642	0.010804653	0.537879646	0.324905227180458
72004	0.089886665	0.089886665	0.804051578	0.804051578	0.309200883	0.038320839	0.554757357	0.325439761399611
89998	0.087772012	0.087772012	0.75631839	0.75631839	0.239631891	0.010333478	0.973802447	0.326599622421522
68328	0.053028345	0.053028345	0.925612867	0.925612867	0.161158032	0.080126345	0.88270998	0.326680157998759
82828	0.136443615	0.136443615	0.659009635	0.659009635	0.260439992	0.136263669	0.9059484	0.328262073394767
76319	0.124679148	0.124679148	0.886746883	0.886746883	0.062396705	0.087388158	0.544091046	0.328424929476763
41963	0.034479439	0.034479439	0.945187807	0.945187807	0.273548543	0.044508815	0.651000559	0.328528293217149
97447	0.154914916	0.154914916	0.546527863	0.546527863	0.331588924	0.034206033	0.940453827	0.329412189460927
32585	0.133915603	0.133915603	0.686308026	0.686308026	0.306901753	0.049307585	0.697029054	0.329728812950477
71179	0.061733544	0.061733544	0.927878618	0.927878618	0.132116735	0.048882365	0.897645533	0.331266115092483
88619	0.115873635	0.115873635	0.86116147	0.86116147	0.045158803	0.171084285	0.947055399	0.331536703595797
24815	0.055981219	0.055981219	0.761785984	0.761785984	0.430443466	0.003755689	0.733465016	0.331806381988901
41413	0.143272817	0.143272817	0.845492244	0.845492244	0.017581522	0.102571011	0.731330574	0.331985607353645
8670	0.168011308	0.168011308	0.633764565	0.633764565	0.25280118	0.034302175	0.71146667	0.331995508260871
16894	0.08138144	0.08138144	0.965919793	0.965919793	0.039538622	0.324480474	0.889759898	0.332303229475057
17369	0.088323295	0.088323295	0.964686513	0.964686513	0.046961606	0.103542089	0.711083353	0.332852069813274
96804	0.131258965	0.131258965	0.763919055	0.763919055	0.177645326	0.188846886	0.835601091	0.333985755277602
86406	0.080384374	0.080384374	0.643227398	0.643227398	0.484666586	0.057944238	0.982825637	0.334229974957352
35090	0.05332458	0.05332458	0.839397013	0.839397013	0.301187038	0.14329499	0.872037053	0.334447020502843
97598	0.208033204	0.208033204	0.589870751	0.589870751	0.155966997	0.010351598	0.726677775	0.335045287557411
98687	0.089238703	0.089238703	0.920802593	0.920802593	0.177026451	0.093108296	0.478102505	0.335278766601384
93066	0.21518743	0.21518743	0.531054556	0.531054556	0.194476128	0.058642566	0.840349793	0.335570896108299
66413	0.121779382	0.121779382	0.533507705	0.533507705	0.582929671	0.018342972	0.648565471	0.335708437167504
14326	0.190906644	0.190906644	0.720840275	0.720840275	0.024288893	0.121694505	0.743723273	0.336239406209165
67125	0.038932264	0.038932264	0.985662341	0.985662341	0.115625918	0.252773762	0.947714508	0.336271837819158
48035	0.117124379	0.117124379	0.724108458	0.724108458	0.356220186	0.038193107	0.444850028	0.336649371926450
25579	0.033502877	0.033502877	0.948117495	0.948117495	0.264759481	0.070876002	0.571898997	0.337109152210876
4532	0.071723938	0.071723938	0.619281948	0.619281948	0.581283212	0.068753541	0.923420191	0.337304204525509
72577	0.046360195	0.046360195	0.87817347	0.87817347	0.443707764	0.00168252	0.251525342	0.337404530886613
63414	0.032013059	0.032013059	0.927989781	0.927989781	0.211434126	0.134477556	0.982717872	0.337918320097240
87107	0.092414677	0.092414677	0.776753187	0.776753187	0.262739122	0.125276923	0.763676703	0.338040378959062
58919	0.116119444	0.116119444	0.811351776	0.811351776	0.091804683	0.089496255	0.766770661	0.338775917695393
46748	0.113155842	0.113155842	0.897818267	0.897818267	0.037178159	0.326556981	0.773545027	0.338810436216812
69177	0.080562294	0.080562294	0.759453893	0.759453893	0.348206341	0.143167257	0.762129724	0.338939472861858
36788	0.130897522	0.130897522	0.535511196	0.535511196	0.551345468	0.002316773	0.591480494	0.339022867338137
22398	0.04774344	0.04774344	0.996521294	0.996521294	0.158671618	0.334268987	0.758831859	0.339056725457657

Appendix F: Top 40 GAP Results for Downscaling of EBM

Table 16: Top 40 lowest GAP-based RMSD (S) scores in EBM to downscale EBM from clean ice to fit covered cumulative vertical ice melt.

Iteration	SWin	SWout	LWin	LWout	Qsens	Qlatent	Qrain	RMSD (S)
90345	0.145675183762	0.145675183762	0.573390981372	0.573390981372	0.355885246545	0.000000000000	0.890425557607	0.321623221414
89884	0.145675183771	0.145675183771	0.573390978104	0.573390978104	0.355885247321	0.000000000000	0.890425595857	0.321623221472
86991	0.145675182517	0.145675182517	0.573390980604	0.573390980604	0.355885249861	0.000000000729	0.890425568196	0.321623221523
87760	0.145675183337	0.145675183337	0.573390999742	0.573390999742	0.355885246396	0.000000000000	0.890425614340	0.321623221534
87484	0.145675184147	0.145675184147	0.573390977172	0.573390977172	0.355885249529	0.000000000000	0.890425605183	0.321623221580
87221	0.145675182491	0.145675182491	0.573391045805	0.573391045805	0.355885246385	0.000000000000	0.890425557685	0.321623221633
91936	0.145675184764	0.145675184764	0.573391014309	0.573391014309	0.355885246151	0.000000000000	0.890425594363	0.321623221639
93831	0.145675186500	0.145675186500	0.573391000245	0.573391000245	0.355885246163	0.000000000000	0.890425578957	0.321623221646
97347	0.145675183330	0.145675183330	0.573390982974	0.573390982974	0.355885253321	0.000000000000	0.890425564618	0.321623221661
98646	0.145675184776	0.145675184776	0.573391020364	0.573391020364	0.355885247214	0.000000000000	0.890425562493	0.321623221671
93154	0.145675184658	0.145675184658	0.573390982217	0.573390982217	0.355885252157	0.000000000000	0.890425561033	0.321623221677
87842	0.145675183096	0.145675183096	0.573391018544	0.573391018544	0.355885248254	0.000000000000	0.890425617314	0.321623221680
85953	0.145675184183	0.145675184183	0.573391022444	0.573391022444	0.355885246325	0.000000000000	0.890425619599	0.321623221682
92712	0.145675182485	0.145675182485	0.573391025687	0.573391025687	0.355885248394	0.000000000000	0.890425619331	0.321623221689
98415	0.145675182978	0.145675182978	0.573391030195	0.573391030195	0.355885248158	0.000000000000	0.890425600130	0.321623221703
92441	0.145675184517	0.145675184517	0.573391012994	0.573391012994	0.355885250018	0.000000000000	0.890425558983	0.321623221725
92350	0.145675183920	0.145675183920	0.573391012824	0.573391012824	0.355885250154	0.000000000000	0.890425584761	0.321623221729
86185	0.145675184363	0.145675184363	0.573391013554	0.573391013554	0.355885248046	0.000000000000	0.890425635961	0.321623221734
99119	0.145675183489	0.145675183489	0.573390995460	0.573390995460	0.355885251974	0.000000000000	0.890425627442	0.321623221746
82534	0.145675186049	0.145675186049	0.573390984220	0.573390984220	0.355885252616	0.000000000000	0.890425556627	0.321623221768
94856	0.145675184546	0.145675184546	0.573391039621	0.573391039621	0.355885246242	0.000000000000	0.890425613637	0.321623221768
84137	0.145675187183	0.145675187183	0.573390992594	0.573390992594	0.355885248424	0.000000000000	0.890425614367	0.321623221772
87553	0.145675182651	0.145675182651	0.573390989929	0.573390989929	0.355885255197	0.000000000000	0.890425603352	0.321623221773
95710	0.145675189297	0.145675189297	0.573391005483	0.573391005483	0.355885245810	0.000000000000	0.890425571049	0.321623221788
81282	0.145675187741	0.145675187741	0.573390995040	0.573390995040	0.355885247477	0.000000000000	0.890425627119	0.321623221790
97097	0.145675183413	0.145675183413	0.573390997067	0.573390997067	0.355885255514	0.000000000000	0.890425547319	0.321623221791
99850	0.145675183307	0.145675183307	0.573390974992	0.573390974992	0.355885257669	0.000000000000	0.890425569726	0.321623221793
86368	0.145675187903	0.145675187903	0.573390975595	0.573390975595	0.355885250184	0.000000000000	0.890425612694	0.321623221795
98767	0.145675185663	0.145675185663	0.573391043040	0.573391043040	0.355885246929	0.000000000000	0.890425560551	0.321623221804
89312	0.145675183041	0.145675183041	0.573390998775	0.573390998775	0.355885254862	0.000000000000	0.890425590729	0.321623221805
90848	0.145675186041	0.145675186041	0.573391011651	0.573391011651	0.355885250611	0.000000000000	0.890425571219	0.321623221832
96766	0.145675187378	0.145675187378	0.573391024716	0.573391024716	0.355885247683	0.000000000000	0.890425560174	0.321623221836
91974	0.145675185809	0.145675185809	0.573390985528	0.573390985528	0.355885246936	0.000000005214	0.890425573864	0.321623221848
80856	0.145675184269	0.145675184269	0.573390988989	0.573390988989	0.355885252533	0.000000002987	0.890425549354	0.321623221848
88839	0.145675188411	0.145675188411	0.573391014042	0.573391014042	0.355885246176	0.000000000000	0.890425624386	0.321623221857
90705	0.145675187393	0.145675187393	0.573390983223	0.573390983223	0.355885252759	0.000000000000	0.890425575357	0.321623221858
93314	0.145675183363	0.145675183363	0.573391000361	0.573391000361	0.355885254952	0.000000000000	0.890425616272	0.321623221861
85999	0.145675183478	0.145675183478	0.573390977915	0.573390977915	0.355885257343	0.000000000000	0.890425624983	0.321623221865
98784	0.145675184092	0.145675184092	0.573390997184	0.573390997184	0.355885254949	0.000000000000	0.890425607137	0.321623221873
87640	0.145675187272	0.145675187272	0.573391018259	0.573391018259	0.355885249878	0.000000000000	0.890425558278	0.321623221882

9. Personal Declaration of Independent Work

I hereby declare that the submitted thesis is the result of my own, independent work. All external sources are explicitly acknowledged in the thesis.

Zürich, 14 September 2023   Bogdan Dukic